NASA CONTRACTOR
REPORT

NASA CR-120513

(NASA-CR-120513) DISCIPLINE REPORT ON THERMAL ANALYSES OF M551, M552, AND M553 EXPERIMENTS (Massachusetts Inst. of Tech.) 84 p HC $4.75 CSCL 13H

N75-10962

Unclas
G3/12 02825

DISCIPLINE REPORT ON THERMAL ANALYSES OF M551, M552, and M553 EXPERIMENTS

By T. Muraki and K. Masubuchi
Massachusetts Institute of Technology
Department of Ocean Engineering
Cambridge, Massachusetts

November 1974

Prepared for

NASA-GEORGE C. MARSHALL SPACE FLIGHT CENTER
Marshall Space Flight Center, Alabama 35812

TECHNICAL REPORT STANDARD TITLE PAGE

1. REPORT NO.	2. GOVERNMENT ACCESSION NO.	3. RECIPIENT'S CATALOG NO.
NASA CR-120513		

4. TITLE AND SUBTITLE
Discipline Report on Thermal Analyses of M551, M552, and M553 Experiments

5. REPORT DATE
November 1974

6. PERFORMING ORGANIZATION CODE

7. AUTHOR(S)
T. Muraki and K. Masubuchi

8. PERFORMING ORGANIZATION REPORT #

9. PERFORMING ORGANIZATION NAME AND ADDRESS
Massachusetts Institute of Technology
Department of Ocean Engineering
Cambridge, Massachusetts

10. WORK UNIT NO.

11. CONTRACT OR GRANT NO.
NAS 8-28732

12. SPONSORING AGENCY NAME AND ADDRESS
National Aeronautics and Space Administration
Washington, D. C. 20546

13. TYPE OF REPORT & PERIOD COVERED
Contractor Report

14. SPONSORING AGENCY CODE

15. SUPPLEMENTARY NOTES

16. ABSTRACT

M551 Experiment. Reduced gravity does not significantly affect the thermal histories in the M551 specimen, even if molten metal flow pattern is different from that in terrestrial conditions. Thermal histories corresponding to terrestrial experimental conditions were calculated by use of the computer programs developed by M.I.T. and Lockheed independently. The analytical results showed fairly good agreement with the ground-base results.

M552 Experiment. Heat conduction through brazing alloy is improved in the Skylab conditions, because of the increased extent, rate and uniformity of braze spreading in space. Quantitative evaluation on heat flow under the Skylab condition was not made. The thermal histories obtained analytically showed good agreements with the ground-base results.

M553 Experiment. Effects of reduced gravity on heat flow in the M553 specimen are insignificant, because convection effects appear instantaneously and conduction is a governing factor on the heat flow.

The predicted temperature histories compared very closely to ground-base results.

17. KEY WORDS	18. DISTRIBUTION STATEMENT
	Unclassified - Unlimited

19. SECURITY CLASSIF. (of this report)	20. SECURITY CLASSIF. (of this page)	21. NO. OF PAGES	22. PRICE
Unclassified	Unclassified	82	NTIS

TABLE OF CONTENTS

LIST OF ILLUSTRATIONS

Table

SECTION I: INTRODUCTION

Skylab Experiments of M551 metals melting, M552 exothermic brazing, and M553 sphere forming were conducted by the NASA-Marshall Space Flight Center. Their objectives are to study the effects of reduced gravity on the melting and solidification of metals and to evaluate the techniques applicable to assembly and repair of hardware in space.

For the preceding Skylab experiments, the only significant difference between space and earth processings is the lack of gravity. The maximum gravity level experienced during operation of the M551, M552, and M553 experiments aboard Skylab II was

$7 \times 10^{-4}\ g_E (g_E = 9.8\ m/sec^2)$.

This report summarizes the thermal analyses of the M551, the M552, and the M553 experiments. Contributions to the thermal study, including the corresponding ground-base experiments, were made as follows:

Contributor	Analysis	Experiment
M.I.T.	M551, M552	M552
Lockheed	M551, M553	
Arthur D. Little		M553
(NASA)		(M551)

Details of the preceding thermal study are presented in individual final reports [1], [2], [3], and [4]. Qualitative evaluations on fluid and heat flow needed are cited from [5]and [6].

SECTION II: M551 EXPERIMENT

A. INTRODUCTION

The primary objective of this experiment is to study the melting and solidification of metals in reduced gravity. A secondary objective is to evaluate the electron beam (eb) process as a joining and cutting technique applicable to assembly and repair of structures in space.

The M551 experiment consisted of a rotating metal disk mounted perpendicular to an electron beam heat source with the eb impingement point located 6 cm from the center of rotation. The thickness of materials varies with angular position around the disk. The

velocity of the beam relative to the impingement point was 1.61 cm/sec. The continuous weld was followed by 15 second duration in the thickest portion.

The three materials listed below were used in the experiment:

2219 Aluminum
321 Stainless steel
Tantalum

Thermal analysis was conducted both by M.I.T. and Lockheed using finite-element and finite-difference computer programs developed independently. Particular attention was given to the study of reduced gravity effects on heat flow.

B. M551 THERMAL ANALYSIS

1. Electron Beam Characterization. A constant heat designed for the M551 experiment is generated by electron beam (eb) with 20 kilovolts and 50 milliamperes.

The distribution of eb power can be described by the following equation:

$$\dot{q}_{supplied} = \dot{q}_v + \dot{q}_c + \dot{q}_r + \dot{q}_i + \dot{q}_u$$

where

$\dot{q}_v$ = power loss due to vaporization

$\dot{q}_c$ = power supplied for conduction

$\dot{q}_r$ = power loss due to radiation

$\dot{q}_i$ = power loss due to ionization and excitation of evaporation atoms

$\dot{q}_u$ = power loss due to uncertainty

These mechanisms of eb power are shown schematically in Figure 1. The power losses due to vaporization, radiation and ionization and excitation can be estimated by using the corresponding theories and the appropriate values. In estimating the power losses, it is important to choose the proper characteristic values. It should be noted that the power loss due to uncertainty factors cannot be avoided in estimating.

The uncertainty factors will be caused by the difference between the chosen and the actual values and also by experimental conditions. Therefore, in practice, the efficiency of the electron beam is assumed for the thermal calculations. As the eb diameter, 0.15 cm and 0.318 cm (0.125 inch) were adopted in [1] and [3], respectively.

2. Heat Transfer Modes. In the M551 experiment, the following modes govern heat transfer:

- conduction
- radiation
- convection
- vaporization

Conduction is a governing factor. On the other hand, radiation affects the temperature history at the cooling stage in the specimen. Both convection and vaporization are restricted to the molten metal region. It is predicted that the effects of convection upon the temperature histories are subtle, although vaporization affects the magnitude of temperature in the specimen. This prediction is drawn from the following:

- the molten metal region is small compared with a whole specimen
- the materials used have high thermal diffusivity via thermal characteristics due to fluid motion, and
- the electron beam power loss due to vaporization occurs.

3. Effects of Reduced Gravity. The effects of reduced gravity on heat flow occur as a result of different fluid motion. In other words, the flow pattern is different in the Skylab versus ground processings.

From the characteristics of the M551 experiment, in the case where the molten metal region is small and cools rapidly after a heat source passes, it is seen that reduced gravity only slightly affects the heat flow, if at all. As pointed out in [3], it should also be noted that since all fluid mechanic phenomena require a finite time to occur (due to inertia considerations) an effect due to gravity during the weld portion of the experiment may not occur (except for a more spherical bead when beading occurs) as large cooling rates are available via conduction.

4. Temperature History Results. Detailed temperature histories in the M551 specimens were analyzed by both Lockheed and M.I.T. independently. For the thermal analysis, Lockheed and M.I.T. developed computer programs based on the finite-difference and the finite-element methods, respectively.

a. Lockheed Study. Thermal histories corresponding to the experimental test conducted at NASA-MSFC with the M512 Facility have been calculated. The stainless steel disk was discretely divided into 289 nodal points shown schematically in Figure 2. The operating procedure consisted of the weld beginning at node 4 and continuing around the weld circle through all four quadrants. The weld portion ends at a time of approximately 19 seconds

with the dwell beginning on node 316 at 19.5 seconds and continuing until 34.5 seconds (15-second duration). The input power was 1 kW with a 75% conversion efficiency assumed for the calculations. Table 1 defines the eb location as a function of time for both the weld and dwell modes of operation.

Figure 3 shows the nodes on the weld circle for the entire quadrant of the thin section (0.02-inch thickness). This result indicates that full penetration will occur with an average of 500°C superheat. Notice also as the dwell is begun at 20 seconds, no effect is seen at this location. Figure 4 shows the radial distribution of temperature corresponding to the center of the quadrant. Note that the nodes surrounding the weld circle do not melt as the maximum temperature is 800°C. Also a nearly symmetric radial temperature gradient about the weld circle is seen to exist. Figure 5 gives the weld circle distribution of temperature through the entire quadrant of 0.05-inch thickness. Again, full penetration is predicted with 300°C of superheat. Figure 6 reveals the same results as those for the thin section, namely no melting except on the weld circle and again near symmetry existing.

The situation in the third quadrant consisting of a 0.125-inch thickness section is shown in Figure 7. For this beam power (1 kW) these results indicate that melting is confined to near the surface. In fact, the average temperature over one third of the thickness is below the melt temperature indicating that less than one-third penetration occurs. Figure 9 shows the profiles just below the surface node as shown in the previous figure. Exactly the same trend is observed with lower maximum temperatures. The radial profile for the bottom layer is shown in Figure 9, indicating precisely the same trend as before. The thickest quadrant results are shown in Figure 10 for the upper surface where again, melting is seen to occur only near the surface. Here, an asymmetric situation develops about the weld circle with a substantial difference in temperature in the positive and negative radial directions. As the center of this quadrant is reached, the dwell portion of the cycle is initiated as depicted in Figures 11 and 12. It is seen that nearly full penetration is predicted (no allowance for eb cavity) and a substantial melt region is outlined. Within a few seconds of eb cutoff, nearly isothermal conditions result near the dwell region as indicated by the temperatures at 40 seconds.

A comparison between these calculated results and those obtained by experiment are shown in Table 2 where the maximum temperatures are given in each case. The calculated results in the weld case are consistently lower than the corresponding experimental values. As previously stated, a 1 kW beam power (50 mA and 20 kV) was assumed with an efficiency of 75% giving rise to an input power of 0.75 kW. If the actual input power was slightly higher, this could explain the trend. Also, some of the maximum temperatures for the dwell occur after 40 seconds. This accounts for

the dwell temperatures in the table being listed as greater than some level (i.e., >50). This means that the maximum temperature will occur later in time than the cutoff of the plot. In general, however, agreement is fairly good. Temperature histories were also calculated for aluminum and tantalum disks, and the results are given in Reference [3].

b. M.I.T. Study. To analyze various heat transfer phenomena involved in the M551 experiment, mathematical models based on the finite-element method were developed. The computer program by use of the mathematical models was also developed.

Sample Specimen - As described in the preceding section, three types of materials were used for this experiment. The emphasis of the M.I.T. analysis was placed on one of the materials--Stainless steel. The sample specimen used is described as follows

- a circular disk of 6.5 inches in diameter
- it consists of four quadrants with different thicknesses of 0.020, 0.050, 0.125, and 0.250 inches

Thermophysical Properties - The following values of the 321 stainless steel are adopted as thermophysical properties of the specimen.

Thermal conductivity	= 12.9 Btu/hr/ft/^{o}F
Specific heat	= 0.14 Btu/lb/^{o}F
Density	= 494 lb/ft^{3}
Melting point	= 2600^{o}F
Latent heat of fusion	= 117 Btu/lb

The above properties are the average values of the 321 stainless steel for the temperature range of interest.

Experimental Conditions - The following experimental conditions are used for the analysis

- 80% is the efficiency of the electron beam with 20 kilovolts and 50 milliamperes
- The electron beam diameter is 0.125 inch
- The disk is heated along a 4.5-inch diameter circle.
- The disk rotates clockwise at a speed of 37 inches/min. relative to the electron beam through three quadrants and then dwells for 30 seconds at the middle point on the weld circle in the 0.25-inch thick quadrant.

Analytical Model - As shown in Figure 13, three-dimensional finite-elements were used combined with two-dimensional elements. The three-dimensional element was used for the region near the heat source and the two-dimensional element for the rest of the above region.

A mesh pattern an typical nodal names used are shown in Figure 13. The model contains 448 nodes and 336 elements.

In the analysis, the following assumptions are adopted:

a. Temperature in the thickness direction is three-dimensional in the region of a band of 0.5-inch width along the weld circle through Quadrants 2 to 4.

b. In the rest of the above region, temperature is uniform in the thickness direction.

c. Thermophysical properties are invaliant with temperature.*

d. The heat exchange due to the radiation between the disk and the surroundings is not considered.*

e. The effect of metal melting and solidification is not considered.

f. The initial temperature of the disk is uniform at $78^{\circ}F$.

g. The heat source in uniformly distributee over the region of 0.125-inch width band on the upper surface of the disk.

Analytical Results - Results obtained by the three-dimensional analysis are shown in Figures 14 to 17. Temperature history curves in the figures denote the average of the temperatures at the nodes shown in the parentheses.

The following results are shown in the figures:

a. The temperature histories at points on the weld circle in Quadrants 1 to 3 (Figures 14 to 16).

b. The temperature histories at the point where the electron beam dwells and at two other points in Quadrant 4 (Figure 17).

c. The temperature histories of nodes located outside of the weld circle in Quadrants 1 to 3 (Figures 18 to 21).

d. The temperature histories in the thickness direction in Quadrants 1 to 3 (Figures 16,17,20 and 21).

The following items are observed from the figures:

a. The temperature difference between the upper and the lower surfaces of the disk disappears in a few seconds after the heat source passes over.

b. The melting occurs along the weld circle in Quadrant 1 and at the point where the heat source dwells in Quadrant 4.

c. The maximum temperature obtained is about $4,500^{\circ}F$ in Quadrant 1.

Discussion -

a. It is enough to use three-dimensional finite elements to a limited region close to the heat source in Quadrants 3 and 4.

b. Even in the region in Quadrant 3 mentioned above, temperature becomes uniform in the thickness direction of the disc in a few seconds after the heat source passes over.

c. The temperature difference of the points close to the heat source in Quadrant 4 keeps almost constant value while heat is supplied.

* The computer program is available for the analysis considering these effects.

d. The heat radiation should be considered in the analysis as the next step because of considering the effect of the surroundings of the disk.

SECTION III: M552 EXPERIMENT

A. INTRODUCTION

The primary objectives of this experiment are to evaluate a tube joining technique for the assembly and repair of hardware in space and to demonstrate the feasibility of exothermic reaction in space.

The exothermic brazing unit used in the experiment is shown in Figure 22. Both stainless steel and nickel assemblies with a uniform clearance and a taper clearance are brazed with a Ag-28Cu-0.2Li alloy. The heat required to melt or flow a brazing alloy is generated by the exothermic reactant mixture which consisted of metals and metal oxides. When matched to the heat sink characteristics of the tubing, sixty grams of this exothermic material produces 650 $\pm$ 30 calories/gram. Application of 24 volts d.c. current to the igniter leads heats the tungsten filament in the igniter pyrotechnic material sufficiently to cause combustion.

The heat generated from this reaction in turn, ignites the primary exothermic charge. This heat transferred through the coupling of the sleeve and the tube liquifies the two concentric rings of brazing alloy. The alloy then flows the length of the brazing alloy cavity until it is contained by the interference fit at the ends of coupling.

The emphasis of the M.I.T. study was placed on heat flow in the tube and the sleeve, especially during a period from ignition to the time when brazing alloy solidifies. For this purpose, analytical models were developed by use of the general-purpose, three-dimensional, finite-element heat flow program developed for the M551 experiment.

Analytical study was also made to examine how reduced gravity could affect heat flow in the exothermic brazing unit. To improve the analytical models, experiments were made of three specimens tested in the ground-base laboratory.

B. EXPERIMENTAL RESULTS

Ground-base experiments on heat flow were conducted of three specimens of stainless steel at M.I.T. Based on the experimental data, analytical models were developed.

In Skylab specimens, quantitative evaluations of thermal

history were not made experimentally. Qualitative information of the thermal history was obtained by use of radioisotope mapping conducted by Oak Ridge National Laboratory [6].

The ground-base experiment results are shown in Figures 23 to 31 with those of locations of thermocouples in the specimens tested.

A summary of the important findings obtained through the experiments are as follows:

a. The maximum temperature of the inner wall of the tube is between 1900 and 2000°F.

b. The center of the tube is nearly the hottest point.

c. The temperature distribution of the inner wall of the tube is almost symmetric for the middle point of the tube length.

d. The center of the inner wall of the tube starts cooling down around 60 seconds from ignition.

e. The temperature distribution is almost axisymmetric.

f. Temperature of the brazing alloy cools down below the melting point (1390°F) after about 240 seconds from ignition.

The preceding findings were made from Figures 24 to 31. The findings gave a basis to simplify the analytical models.

C. M552 THERMAL ANALYSIS

1. Heat Transfer Modes. In the M552 experiment, the following modes govern heat transfer:

- conduction
- radiation
- convection

Conduction is a governing factor. Radiation occurs in both the gap between the sleeve and the tube and the outer parts of the brazing unit. In the outer parts of the unit, radiation affects the temperature history. In other words, as far as the heat flow in the sleeve and portions of the tube surrounded by the sleeve during the period from ignition to the time when brazing alloy solidifies is concerned, radiation does not affect the temperature history significantly.

Convection in the M552 specimen is closely associated with capillary flow which occurs in the gap between the tube and the sleeve.

2. Effects of Reduced Gravity. Gravity has no direct effect on conduction and radiation. Indirect effect of gravity is exhibited in convection. For the M552 experiment, convection is associated with capillary flow. The results of the capillary flow analysis [51 include the increased extent, rate, and uniformity of braze spreading in space. Those results indicate better heat conduction through brazing alloy in space than on the ground.

Quantitative results have not been obtained on the difference of heat flow because of lack of basic information needed.

3. Temperature History Results. In the analysis of heat flow in the M552 experiment, the following questions need to be answered:

a. How much heat is actually produced by the exotherm material?
b. What are the rate and the distribution of heat supplied to materials which surround the exotherm material?
c. What are the thermophysical properties of the material used for insulation?
d. How much effect does radiation have upon the temperature distribution of the unit?
e. How does the gap between the sleeve and the tube in conveying heat?
f. How much effect do melting and solidification of the braze alloy have upon the temperature distribution of the sleeve and the tube?

Quantitative evaluations concerning the preceding questions are difficult because of lack of data needed. Since the temperature distribution in the sleeve and portions of the tube surrounded by the sleeve during the period from ignition to the time when brazing alloy solidifies is most important in the thermal analysis. Many unknowns involved in the above questions can be reduced to estimate the heat supplied to the outer wall of the sleeve by use of the ground-base experiment results. From the same reason, the analysis is made for 120 seconds.

The thermal analysis was performed of two models. One is the tube and the sleeve and the other the precending parts plus the outer shell. The first model is shown in Figure 32. The distribution and the rate of heat intensity used in the analysis are shown in Figures 32(a) and (b), respectively. In Figure 32(b), Capitals A and B correspond to the heat distribution type shown in Figure 32(a). Parts with no capital letter indicate Type C of uniform heat distribution.

Figure 32(c) shows the mesh pattern used for the finite-element analysis.

The following values are adopted as thermophysical properties of 347 stainless steel.

Specific heat	= 0.12 Btu/lb/^{o}F
Thermal Conductivity	= 0.278 x 10^{-3}Btu/sec/inch/^{o}F
Density	= 0.29 lb/inch^{3}

Results obtained are given in Figures 33 to 36. Figures 33 to 35 show the comparisons between the experimental and the analytical results. Figure 36 shows the temperature distribution of the

joint of the sleeve and the tube at times 30, 40, 60, and 120 seconds from ignition.

The analytical results at thermocouples 1 and 4 show good agreement with the experimental results. On the other hand, some discrepancy is seen at thermocouple 7 which is located almost at the end of the tube. This discrepancy can be explained by the effect of radiation.

For the second model, which consists of the tube, the sleeve, and the outer shell, the analytical results were not necessarily improved as compared with those obtained in the first model. Therefore, further description of the second model is not given in this report.

SECTION IV: M553 EXPERIMENT

A. INTRODUCTION

The basic objective of the sphere forming experiment is to determine the effects of reduced gravity on fundamental solidification phenomena. The experiment consisted of twenty-eight 6.35 mm diameter spherical specimens which were cast using the electron beam gun as a heat source. The specimens were initially supported on two wheels by a sting. After melt was completed, the spheres were expected to be separated from their stings and allowed to solidify while free-floating in the vacuum chamber. Specimens consisted of the following materials: pure nickel; Ni-1%Ag; Ni-30%Cu; and Ni-12%Sn.

B. EXPERIMENTAL RESULTS

Ground-base experiments were conducted to obtain the temperature distribution of the specimens during and after the melting process [4]. These data were required for determining vaporization losses, estimating surface tension effects, and understanding the release and movement of the specimens.

The objectives of this work were to obtain an indication of maximum and average surface temperature of the various M553 experiment specimens during the melting process and to determine the initial cooling rates of the specimens when the electron beam was turned off. The temperature measurements were of secondary importance to the preparation of ground based specimens and had to be conducted on a non-interfering basis. Thus, optimum temperature measurement techniques could not be used; rather, they were more of an expedient and exploratory nature.

Specimen "Average" Temperatures. Table 3 presents the "average" specimen temperatures measured as soon as possible after turnoff of the electron beam. The values given include the corrections for all the temperature measurement errors other than the specimen emittance error.

Cooling Rate. Average cooling rates were measured for the majority of the specimens. The values obtained should be subject to smaller errors than the absolute measurements because some of the errors (window, pyrometer, and emittance) tend to cancel.

$$\frac{dT}{dt} = \frac{T^{(1)}-T^{(2)}}{t} = \frac{1}{t}\,(T^{(1)}_{measured}-T^{(2)}_{measured}-(E^{(1)}_{pyro}-E^{(2)}_{pyro})$$
$$-(E^{(1)}_{WM}-E^{(2)}_{WM})-(E^{(1)}_{film}-E^{(2)}_{film}))$$

where

E_{pyro} = error in pyrometer instrument temperature measurement

E_{window} = error caused by optical absorption of the window

E_{mirror} = error caused by incomplete reflection and absorption of the mirror

E_{film} = error caused by absorption of the film on the window

The cooling rates indicated on Table 4 represents an average cooling rate, i.e., we measured the time required for a sample to cool from some temperature which was above or near the melting point to a temperature several hundred degrees lower. Thus, this cooling rate includes some surface solidification and cooldown.

C. M553 THERMAL ANALYSIS

1. Heat Transfer Modes. In the M553 experiment, the following modes govern heat transfer:

- conduction
- radiation
- convection
- vaporization

From the feature of this experiment, it is seen that the last three modes have much more effects on the temperature history in the specimen than that in the M551 and M552 experiments. Radiation and vaporization significantly affect the cooling rate of the specimen because of the extent of the surface area. The effect of convection on the thermal history appears for a short period

because the sphere reaches isothermal superheat conditions in approximately a second.

2. Effects of Reduced Gravity. As far as the thermal analysis is concerned, reduced gravity in space has significant effects on convection within the molten region of the specimen. According to the convection analysis by Lockheed [5], convection is governed by the following forces:

in ground tests,
- surface tension
- gravity

for Skylab condition,
- surface tension

The surface tension driving force considered above is a surface tension gradient caused by radial and lateral temperature gradients. The gravity driven convection occurs when thermal or concentration gradients exist in the fluid.

In the report [5], it is concluded that no significant difference in magnitude of convection occurred between Skylab, KC-135 and ground processing, which reinforces the theory of surface tension as the dominating force for fluid motion in the M553 experiment.

Flow patterns between terrestrial and space processing of the M553 experiment are predicted, as shown in Figure 37. Considering the preceding discussions, the difference of the fluid motion in the molten metal between Skylab and ground processing affects the temperature distribution in the specimen.

However, as pointed out in the preceding section, the effect of convection on the thermal history appears instantaneously. From this consideration, it is concluded that the convection effect is insignificant on the thermal history of the M553 specimen.

3. Temperature History Resules. This subsection presents the results of calculation for the M553 materials of interest. First, consider the time required for the material to become superheated and cool to the melt temperature for the operating procedures used in the actual Skylab mission. This time can be determined from the temperature history calculated by the Lockheed Thermal Analyzer, which includes allowances for:

- A three-dimensional network
- Conduction heat loss
- Radiation heat loss
- Vaporization heat loss
- Variable properties (with temperature and phase), and
- Variable heat source

The spheres are discretely modeled by 69 nodal points with each

of the corresponding nodal temperature histories computed. Allowances are included for sting melting and automatic electron beam cutoff. The nodal arrangement is shown for the inner layer in Figure 38, with the outer layer and electron beam impingement location given in Figure 39.

The thermal history for pure nickel is shown in Figures 40 through 43. It is seen that in less than one second after eb cutoff, the sphere is nearly isothermal in each layer. The time corresponding to the onset of solidification is shown in Figure 40 and is approximately 10.5 seconds. This time must be added to the time needed for solidification to determine the necessary free-float time for containerless solidification. The corresponding temperature histories for Ni-12% Sn, Ni-1% Ag and Ni-30% Cu are shown in Figures 44, through 47, 48 through 51, and 52 through 55, respectively. The essential features of these results are as follows:

- Vaporization forces can be computed
- Time above melt temperature can be determined, and
- Superheat can be determined.

These items either affect the free-float time directly or the time duration needed for solidification. The solidification time including both vaporization and radiation losses for all four materials has been computed. These results are summarized in Table 5 for the M553 materials. These calculations indicate that from 32 to 48 seconds are necessary for complete solidification to occur.

Unfortunately, provision was not made during the Skylab flight tests for temperature measurements. Ground test measurements were made, however, and reported in References [4], [7]. The measured temperatures represent a spatial average over the observed sphere surface (near the impingement point) and a time average for a period on the order of one or two seconds after electron beam cutoff. For the pure nickel specimens, the maximum measured temperature was about 1500°C for the sting-type specimens and about 1450°C for the release specimens. Figures 40 and 41 show predicted "average" temperatures of about 1600°C for the one or two second time period after beam cutoff. An emittance correction for the sample could have raised the measured temperature by about 100°C, thus giving good agreement between the predicted and measured results [4], [7]. The maximum measured temperature for the nickel-12% tin specimens was about 1400°C, which after emittance corrections could be increased to about 1500°C. This is about 100°C less than the 1600°C predicted average indicated in Figures 44 through 48. The maximum measured temperature for the nickel-1% silver specimens was also about 1400°C with possible emittance correction to 1500°C, and this also compares to a predicted value of about 1600°C indicated in Figures 48 through 51. For the nickel-30%

copper specimens, a maximum measured value of about 1350°C compares to a predicted value (from Figures 52 through 55) of about 1425°C, thus giving good agreement if emittance corrections increased the measured values by 50 to 100°C.

SECTION V: CONCLUSIONS - SUMMARY

The thermal analyses of M551 (metals melting), M552 (exothermic brazing), and M553 (sphere forming) experiments were conducted by M.I.T. and Lockheed. The corresponding ground-base experiments were performed by M.I.T., Arthur D. Little, and NASA.

From data obtained to date, it is concluded that no significant difference of thermal histories exists between ground-base and space experiments of M551, M552, and M553 specimens, although no quantitative results of the thermal histories have been obtained from the Skylab specimens.

Conclusions reached in each experiment are as follows:

M551 Experiment. Reduced gravity does not significantly affect the thermal histories in the M551 specimen, even if molten metal flow pattern is different from that in terrestrial conditions. Thermal histories corresponding to terrestrial experimental conditions were calculated by use of the computer programs developed by M.I.T. and Lockheed independently. The analytical results showed fairly good agreement with the ground-base results.

M552 Experiment. Heat conduction through brazing alloy is improved in the Skylab conditions, because of the increased extent, rate and uniformity of braze spreading in space. Quantitative evaluation on heat flow under the Skylab condition was not made. The thermal histories obtained analytically showed good agreements with the ground-base results.

M553 Experiment. Effects of reduced gravity on heat flow in the M553 specimen are insignificant, because convection effects appear instantaneously and conduction is a governing factor on the heat flow.

The predicted temperature histories compared very closely to ground-base results.

SECTION VI: REFERENCES

1. Muraki, T. and Masubuchi, K., "Final Report on Thermal Analysis of M551 Experiment for Materials Processing in Space," NASA-MSFC, Contractor Report, M.I.T., December 5, 1973.

2. Muraki, T. and Masubuchi, K., "Final Report on Thermal Analysis of M552 Experiment for Materials Processing in Space," NASA-MSFC, Contractor Report, M.I.T., December 5, 1973.

3. Brashears, M. R. and Robertson, S. J., "Research Study on Materials Processing in Space Experiment, M512, Final Report," LMSC-HREC TR D306954, Lockheed Missiles & Space Co., December 1, 1973.

4. Johnson, P. C. and Peters, E. T., "M553 Sphere Forming Experiment, Phase C Report," Arthur D. Little, Inc., December, 1973.

5. Bourgeois, S. V., "Convection Effects on Skylab Experiments M551, M552 and M553, Phase C Report," LMSC-HREC TR D306955, Lockheed Missiles & Space Co., December 1, 1973.

6. Braski, D. N., Adair, H. L. and Kobisk, E. H., "Radioisotope Tracer Studies in the NASA Skylab Exothermic Brazing Experiment M552," Oak Ridge National Laboratory.

7. Johnson, P. C., Peters, C. T. and Wechsler, A. E., "M553 Sphere Forming Experiment, Phase B Report," Contract NAS8-28723, Arthur D. Little, Inc., July, 1973.

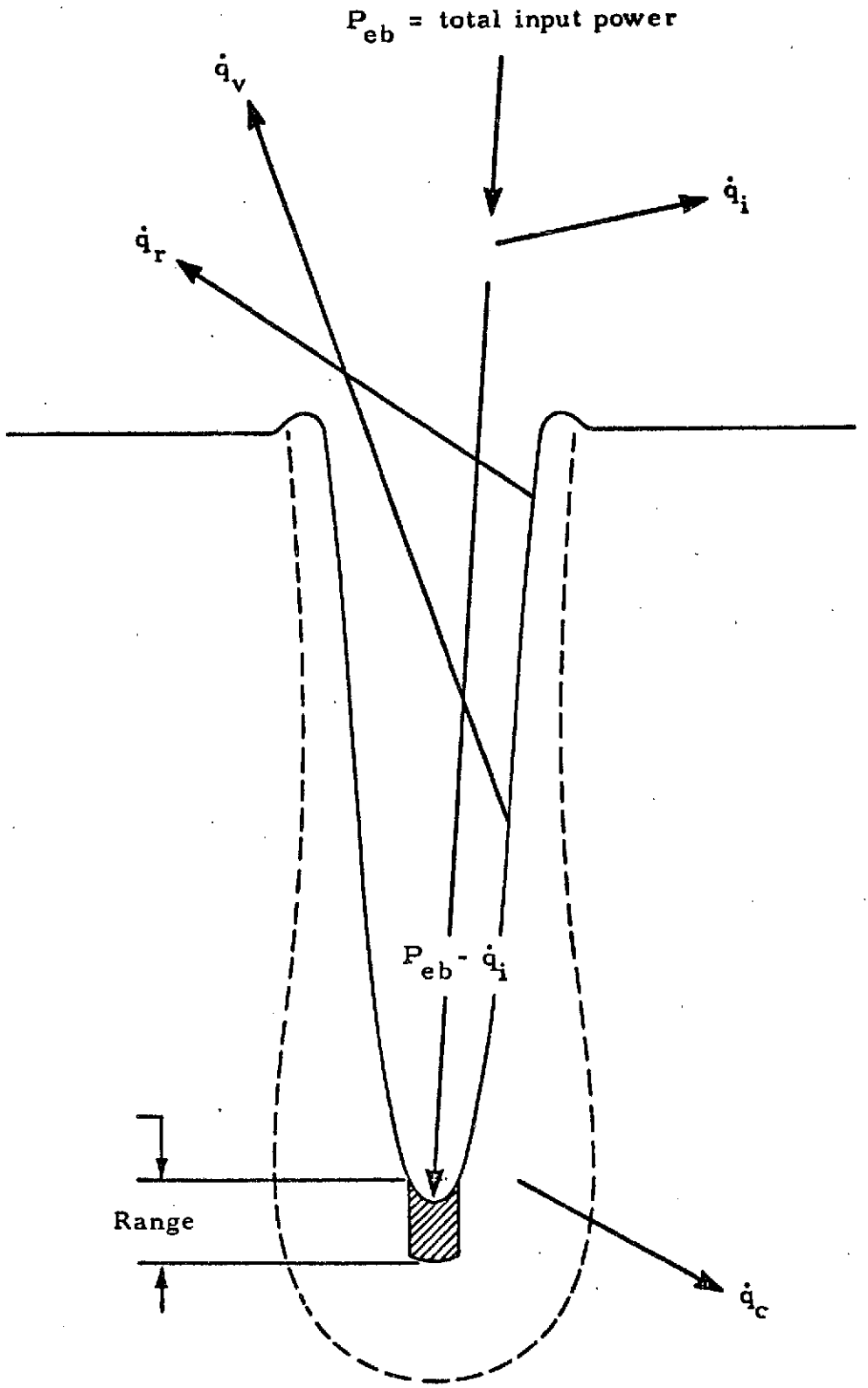

FIGURE 1. THERMAL MECHANISMS

Table 1

ELECTRON BEAM POSITION VERSUS TIME (DISK ROTATION)

Node	Time (sec)	Node	Time (sec)	Node	Time (sec)	Node	Time (sec)
4	0	104	5.5805	204	11.161	304	17.237
10	0.62005	110	6.2005	204	11.657	310	18.454
16	1.2401	116	6.8206	210	12.773	316	19.570
22	1.8602	122	7.4406	216	13.889	316	34.570
28	2.4802	128	8.0607	222	15.005		
34	3.1003	134	8.6807	228	16.121		
40	3.7203	140	9.3008				
46	4.3404	146	9.9208				
52	4.9604	152	10.541				

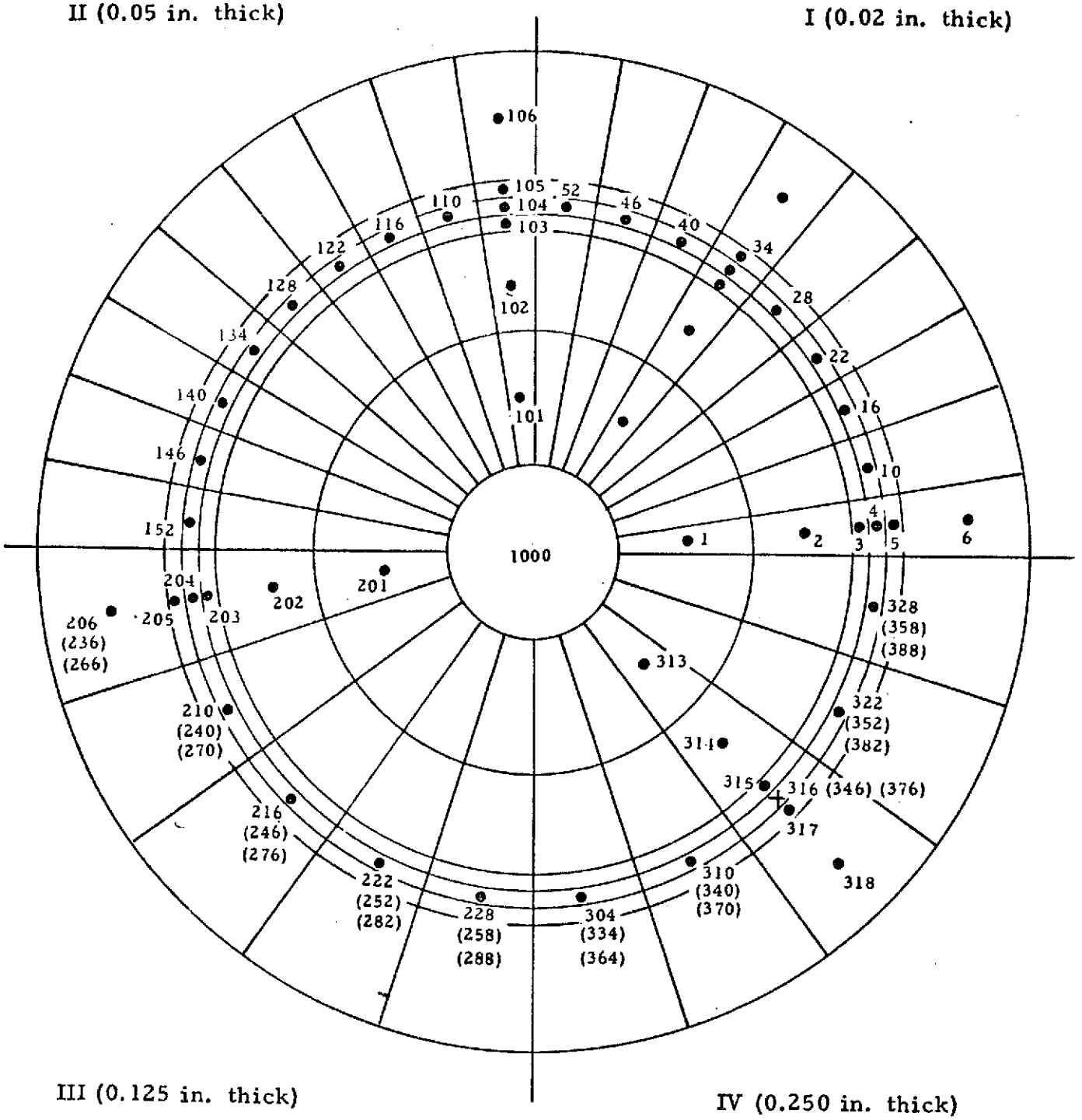

FIGURE 2 NODAL POINT ARRANGEMENT FOR THERMAL CALCULATIONS

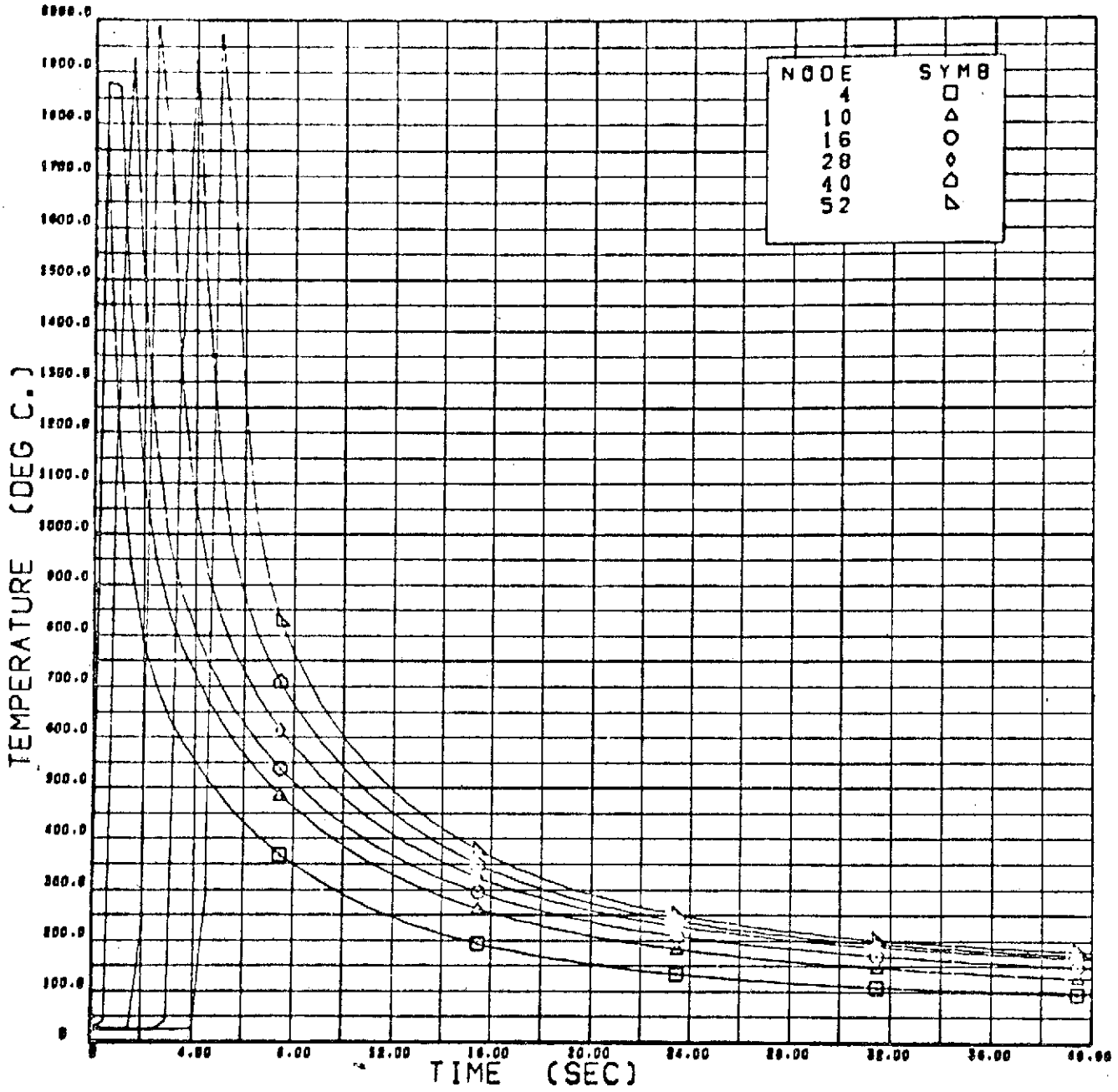

FIGURE 3 THERMAL HISTORY FOR 0.02-INCH STAINLESS STEEL DISK (NODES 4, 10, 16, 28, 40 AND 52)

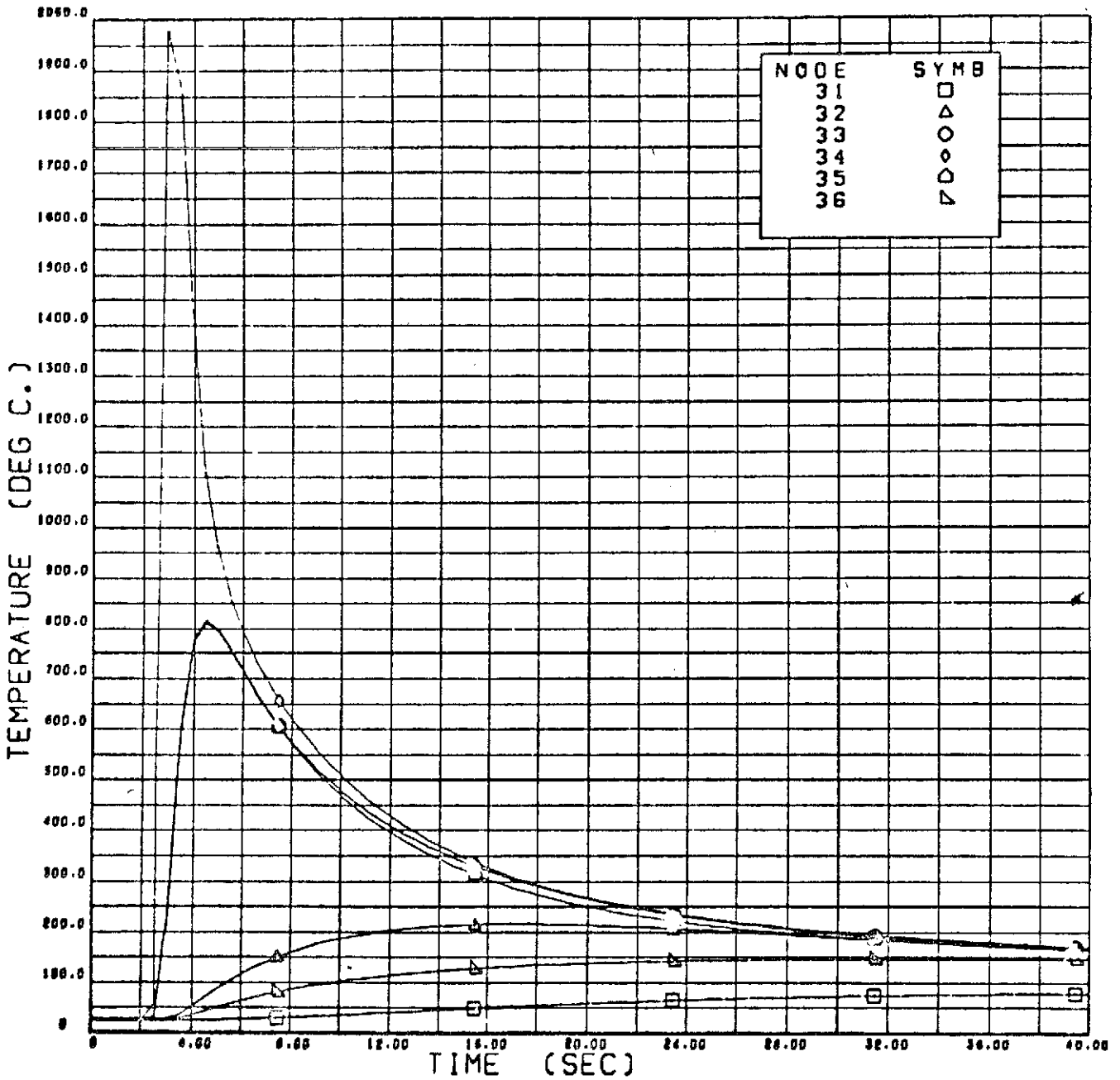

FIGURE 4 THERMAL HISTORY FOR 0.02-INCH STAINLESS STEEL DISK (NODES 31 THROUGH 36)

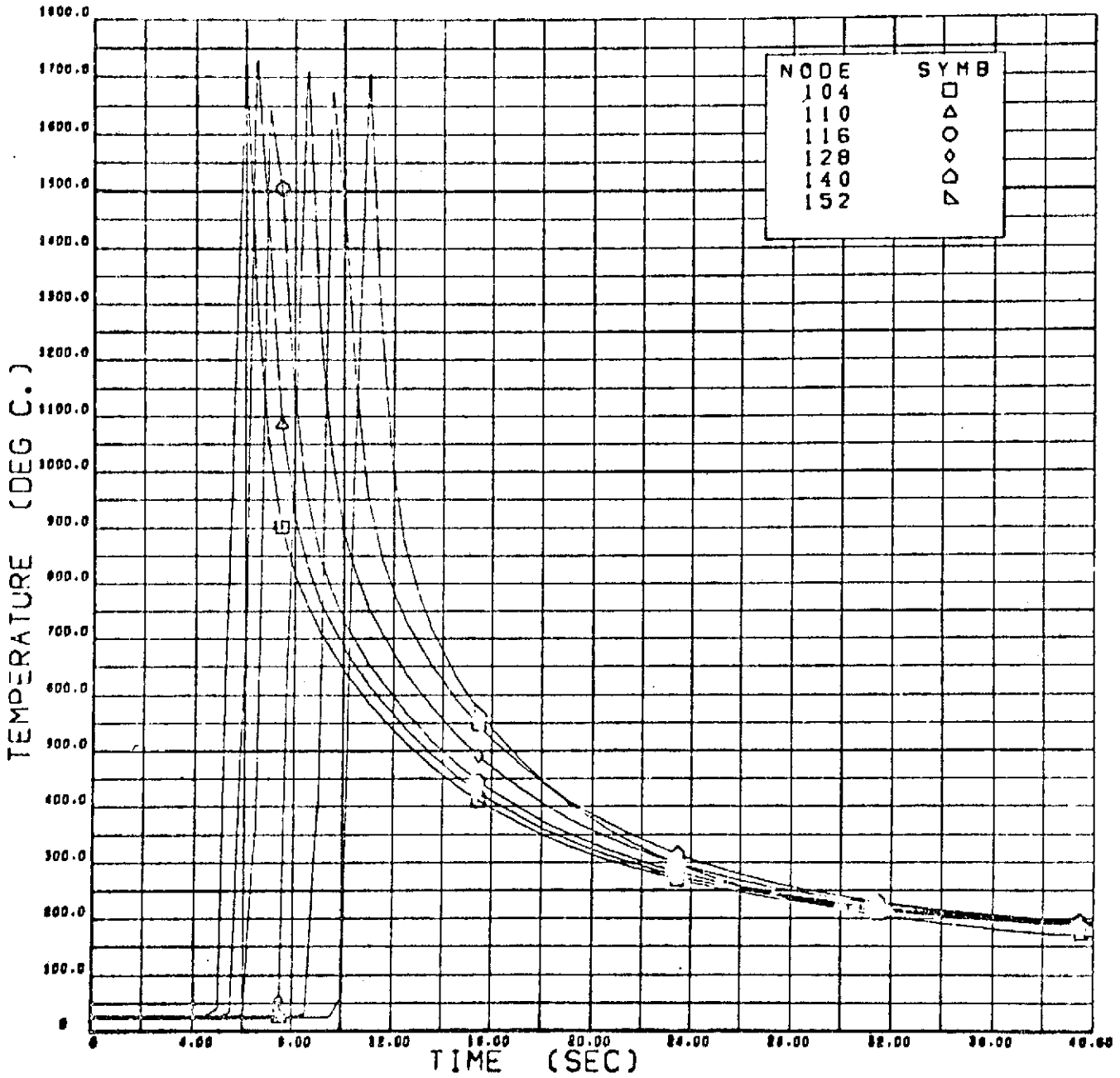

FIGURE 5 THERMAL HISTORY FOR 0.05-INCH STAINLESS STEEL DISK (NODES 104, 110, 116, 128, 140 AND 152)

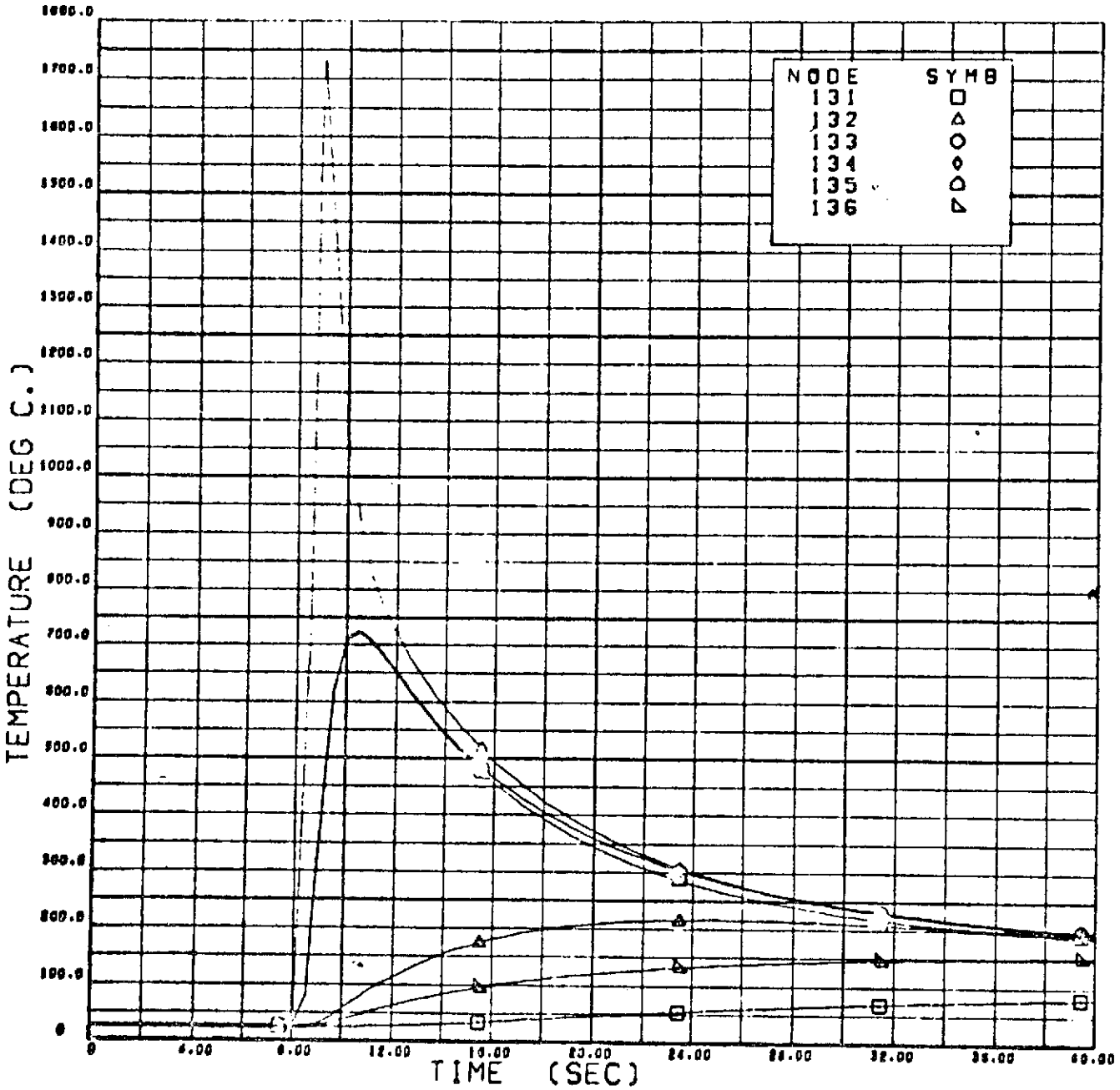

FIGURE 6 THERMAL HISTORY FOR 0.05-INCH STAINLESS STEEL DISK (NODES 131 THROUGH 136)

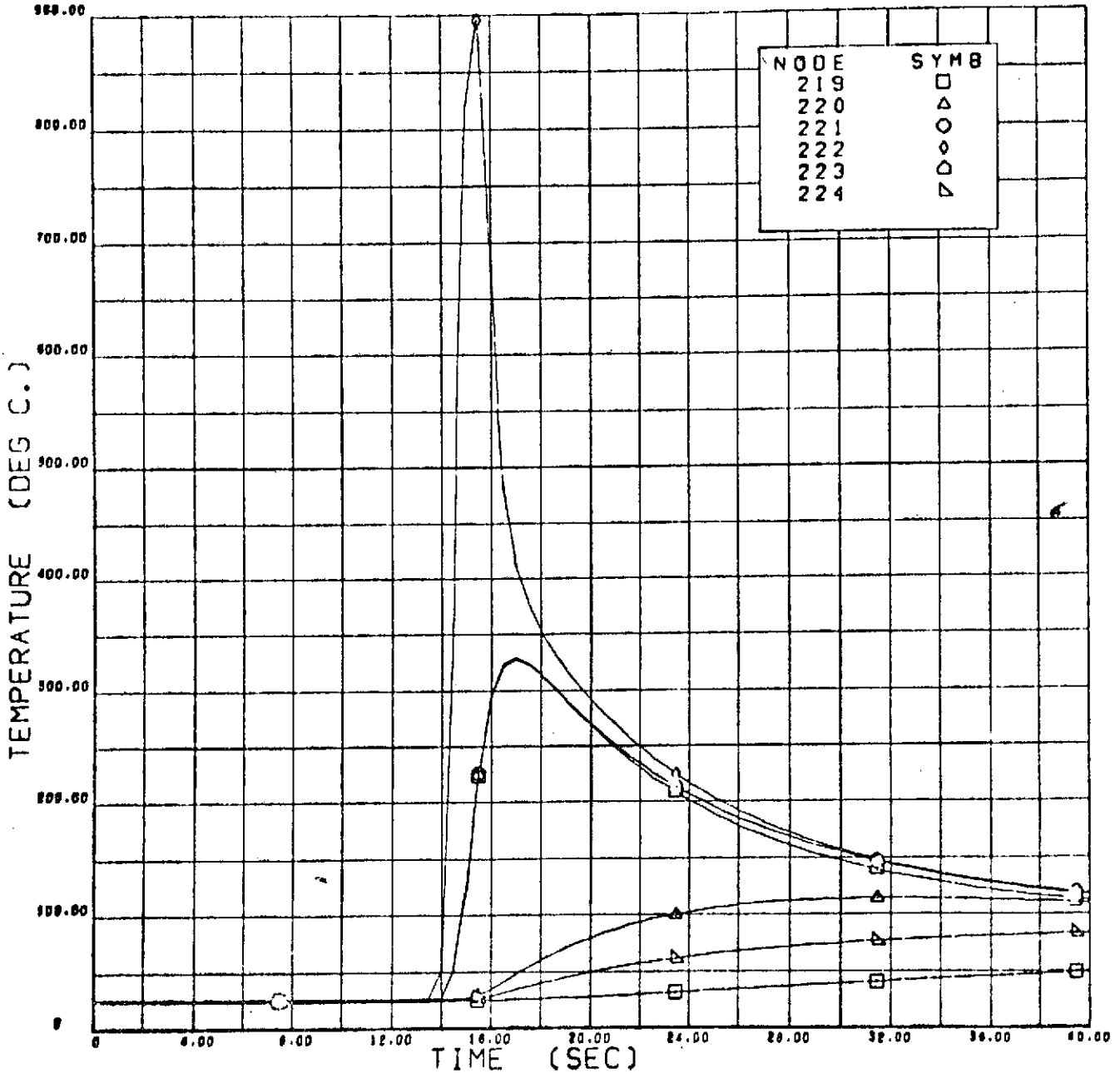

FIGURE 7 THERMAL HISTORY FOR 0.125-INCH STAINLESS STEEL DISK (NODES 219 THROUGH 224)

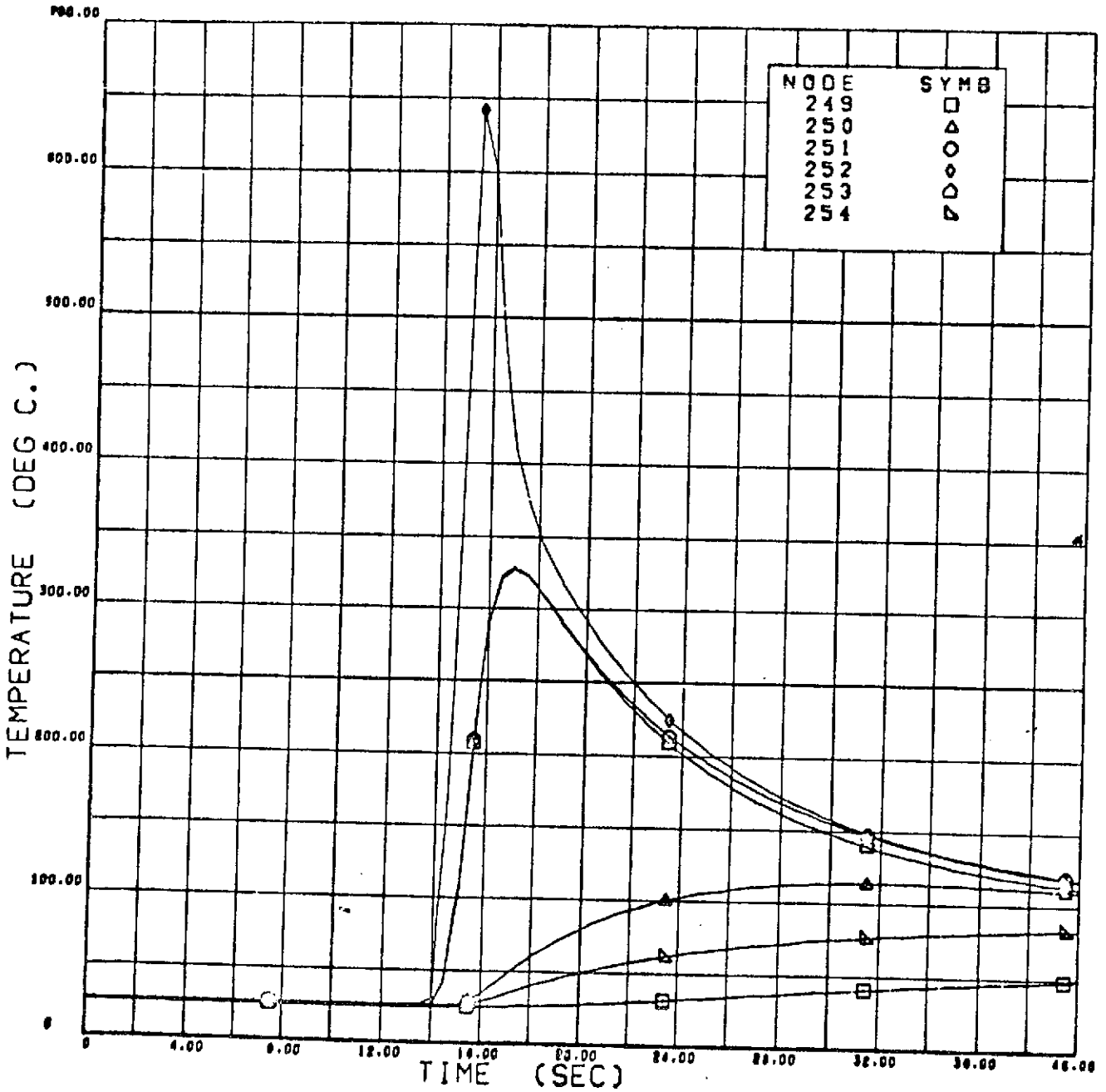

FIGURE 8 THERMAL HISTORY FOR 0.125-INCH STAINLESS STEEL DISK (NODES 249 THROUGH 254)

Table 2

COMPARISON OF CALCULATED AND EXPERIMENTAL MAXIMUM TEMPERATURES

Node No.	Thermocouple No.	Weld		Dwell	
		Calculated Max. Temp. (°C)	Experimental Max. Temp. (°C)	Calculated Max. Temp. (°C)	Experimental Max. Temp. (°C)
317	1	322	387	1430	638
315	2	236	349	1105	1160
223	4	330	515	112	—
221	5	332	404	118	171
219	6	37	97	>50	171
135	7	725	871	187	—
133	8	725	815	196	121
131	9	41	102	>80	118
35	10	818	1093	165	—
33	11	819	599	169	163
31	12	58	91	>80	106

TABLE 3

MAXIMUM "AVERAGE" SPECIMEN TEMPERATURES

Specimen No.	Specimen Material	Specimen Type	Temperature (°C) Expected Melting Range	Pinwheel No. 1	Pinwheel No. 2
1	Tungsten	Sting	--	--	--
2	Nickel	Sting	1450	1500	1500
3	Nickel-12% Tin	Sting	1220-1370	1410	<1555
4	Nickel-1% Silver	Sting	1450	1380	----
5	Nickel	Release	1450	1415	1380
6	Nickel	Release	1450	1445	1390
7	Nickel-12% Tin	Release	1220-1370	1390	1350
8	Nickel-1% Silver	Release	1450	1270	1425
9	Nickel-30% Copper	Release	1330-1380	1260	1355
10	Nickel-30% Copper	Release	1330-1380	1180	1315
11	Nickel-1% Silver	Release	1450	1320	1390
12	Nickel-12% Tin	Release	1220-1370	1280	1390
13	Nickel	Release	1450	1325	1400
14	Nickel-12% Tin	Release	1220-1370	1330	1340
15	Nickel-1% Silver	Release	1450	1375	1410

Note: ---- indicates when viewing window was cleaned

TABLE 4

"AVERAGE" COOLING RATES

Material	Specimen No.	Initial & Second Temperatures (°C)		Time Between Temperature Measurements (sec)	Cooling Rate (°C/sec)
Nickel	1-6	1445	1030	14	30
Nickel	1-13	1325	925	8	50
Nickel	2-2	1500	1140	10	36
Nickel	2-5	1380	980	15	27
Nickel	2-13	1400	1150	10	25
Nickel-1% Silver	1-15	1375	1095	12	23
Nickel-1% Silver	2-8	1425	1310	10	12
Nickel-1% Silver	2-11	1390	1210	7.5	24
Nickel-1% Silver	2-15	1410	1270	7	20
Nickel-12% Tin	1-12	1280	865	20	21
Nickel-12% Tin	1-14	1330	1060	18	15
Nickel-12% Tin	2-3	<1555	1075	17	<28
Nickel-12% Tin	2-7	1350	1170	15	12
Nickel-12% Tin	2-12	1390	1130	13	20
Nickel-12% Tin	2-14	1340	1165	14	13
Nickel-30% Copper	1-9	1260	905	12	30
Nickel-30% Copper	2-9	1355	1105	11	23
Nickel-30% Copper	2-10	1315	1005	9.5	33

Table 5

THERMAL SUMMARY

Material	eb Time (sec)	T_{melt} (^{o}C)	Maximum Superheat (^{o}C)	Average Superheat (^{o}C)	Solidification Initialization (sec)	Solidification Time (sec)	Total Time (sec)
Ni	2.98	1455	228	91	10.7	25	36
Ni-12% Sn	2.65	1370	330	132	12.0	36	48
Ni-1% Ag	3.01	1454	210	84	9.3	23	32
Ni-30% Cu	2.30	1357	98	39	7.3	30	38

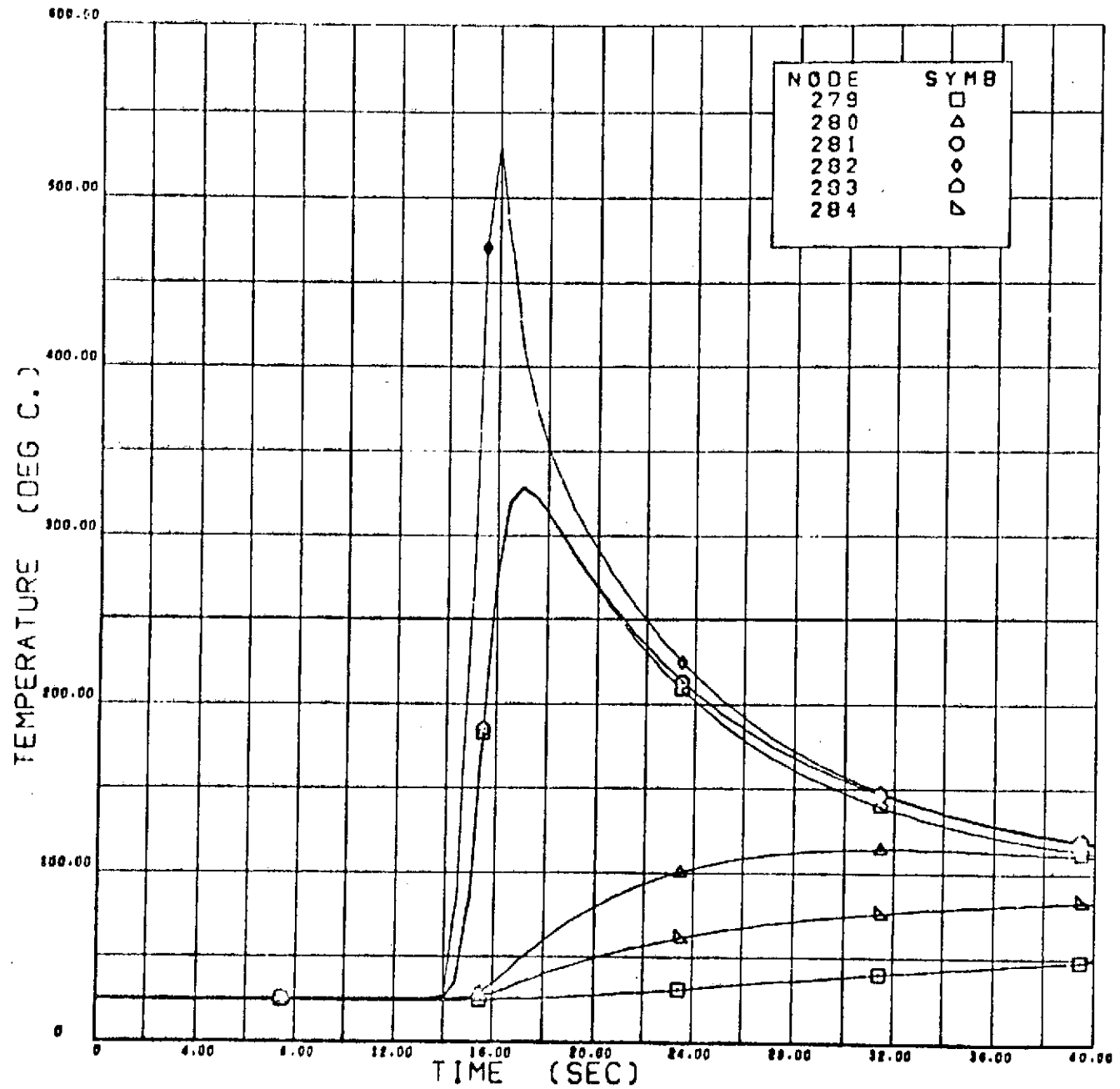

FIGURE 9 THERMAL HISTORY FOR 0.125-INCH STAINLESS STEEL DISK (NODES 279 THROUGH 284)

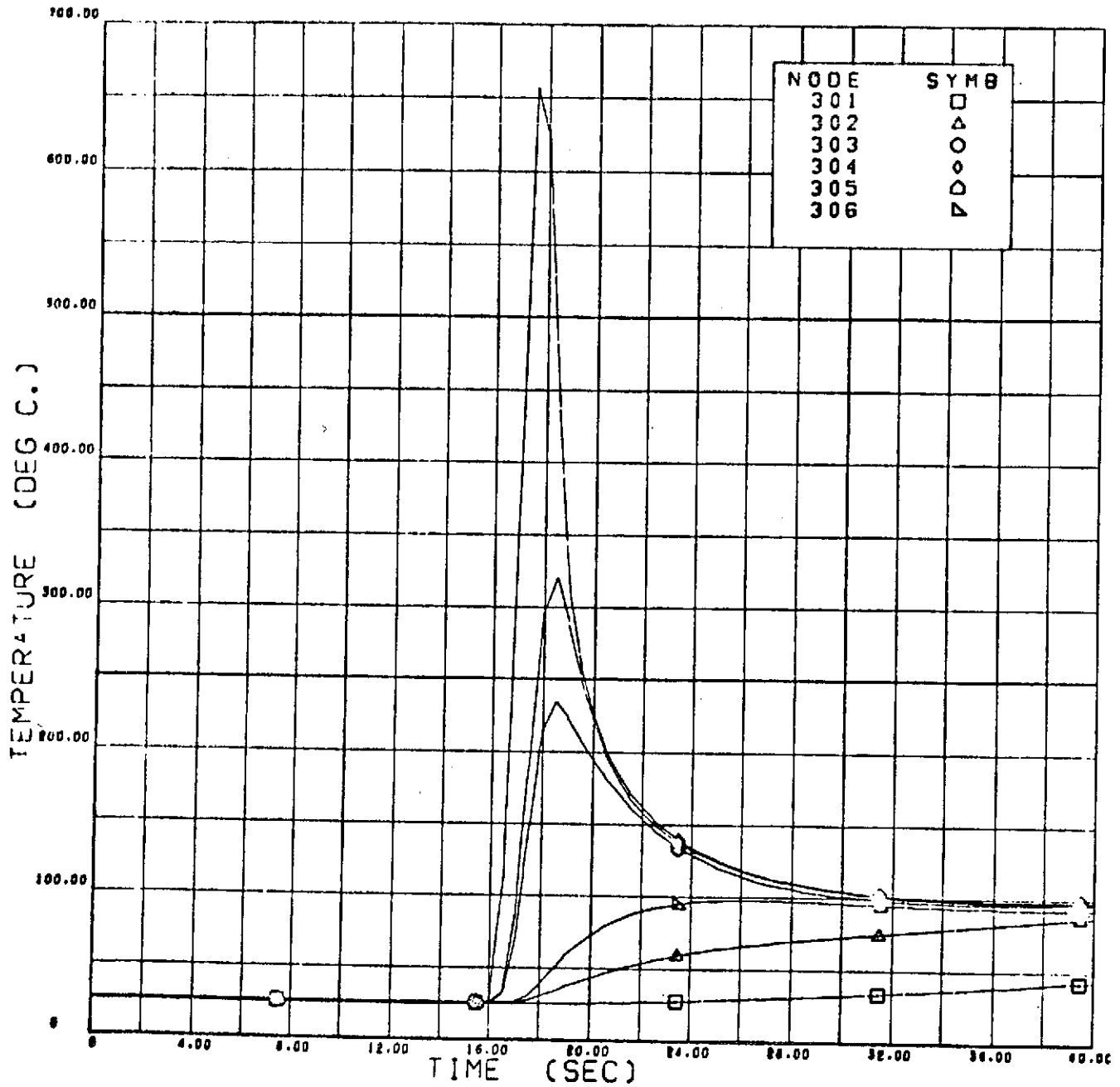

FIGURE 10 THERMAL HISTORY FOR 0.25-INCH STAINLESS STEEL DISK (NODES 301 THROUGH 306)

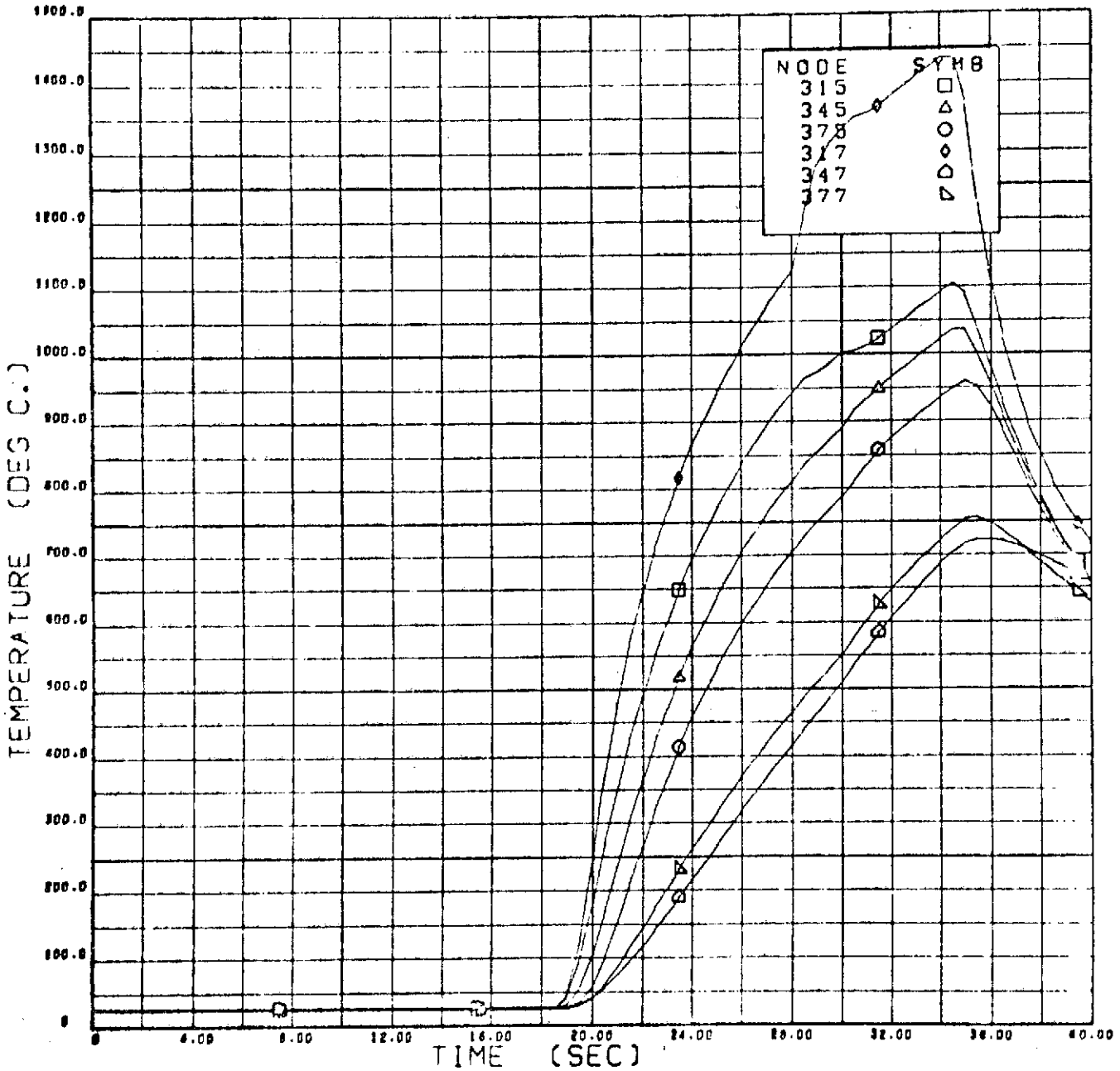

FIGURE 11 THERMAL HISTORY FOR 0.25-INCH STAINLESS STEEL DISK (NODES 315, 345, 375, 317, 347 AND 377)

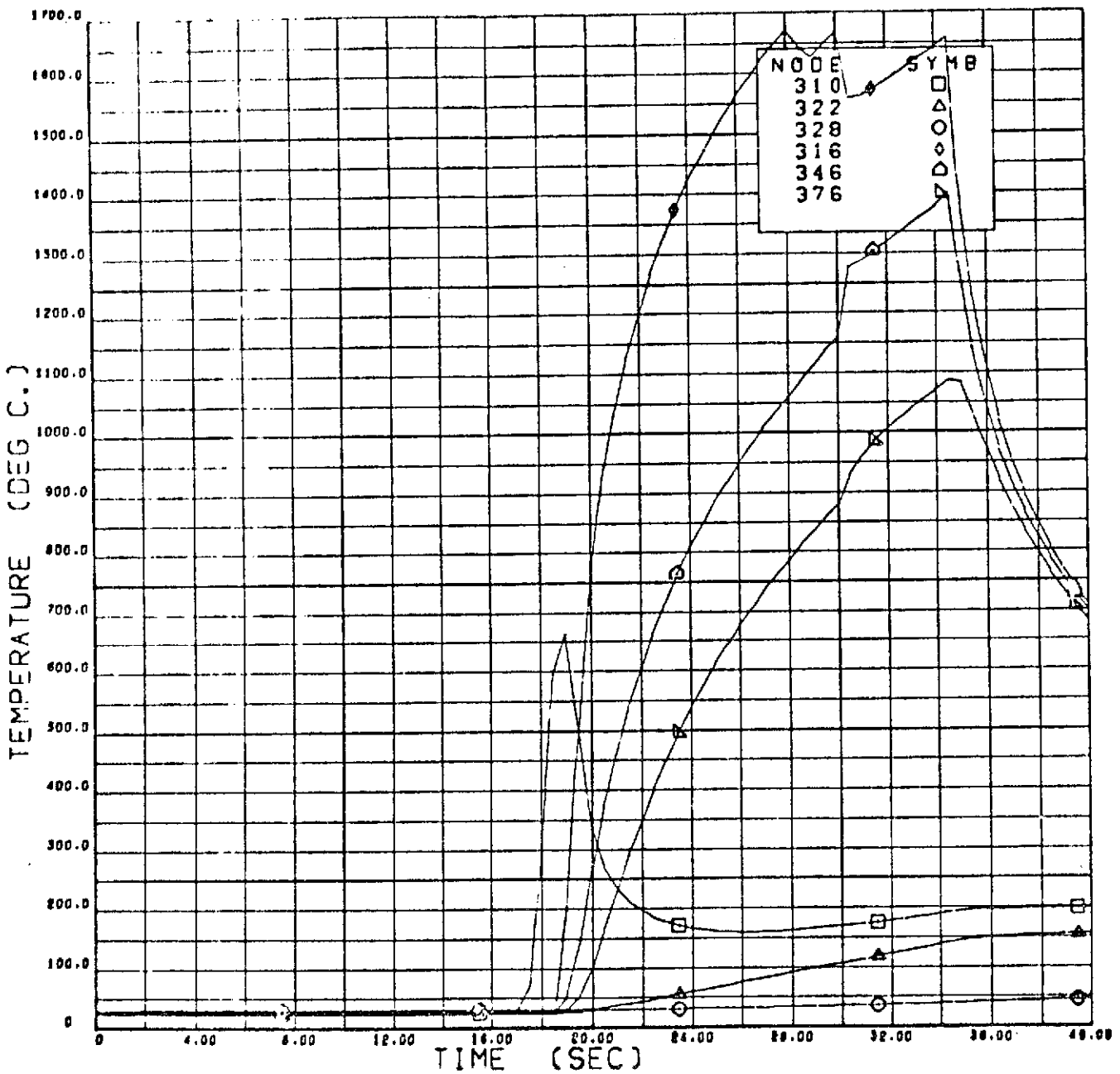

FIGURE 12 THERMAL HISTORY FOR 0.25-INCH STAINLESS STEEL DISK (NODES 310, 322, 328, 316, 346 AND 376)

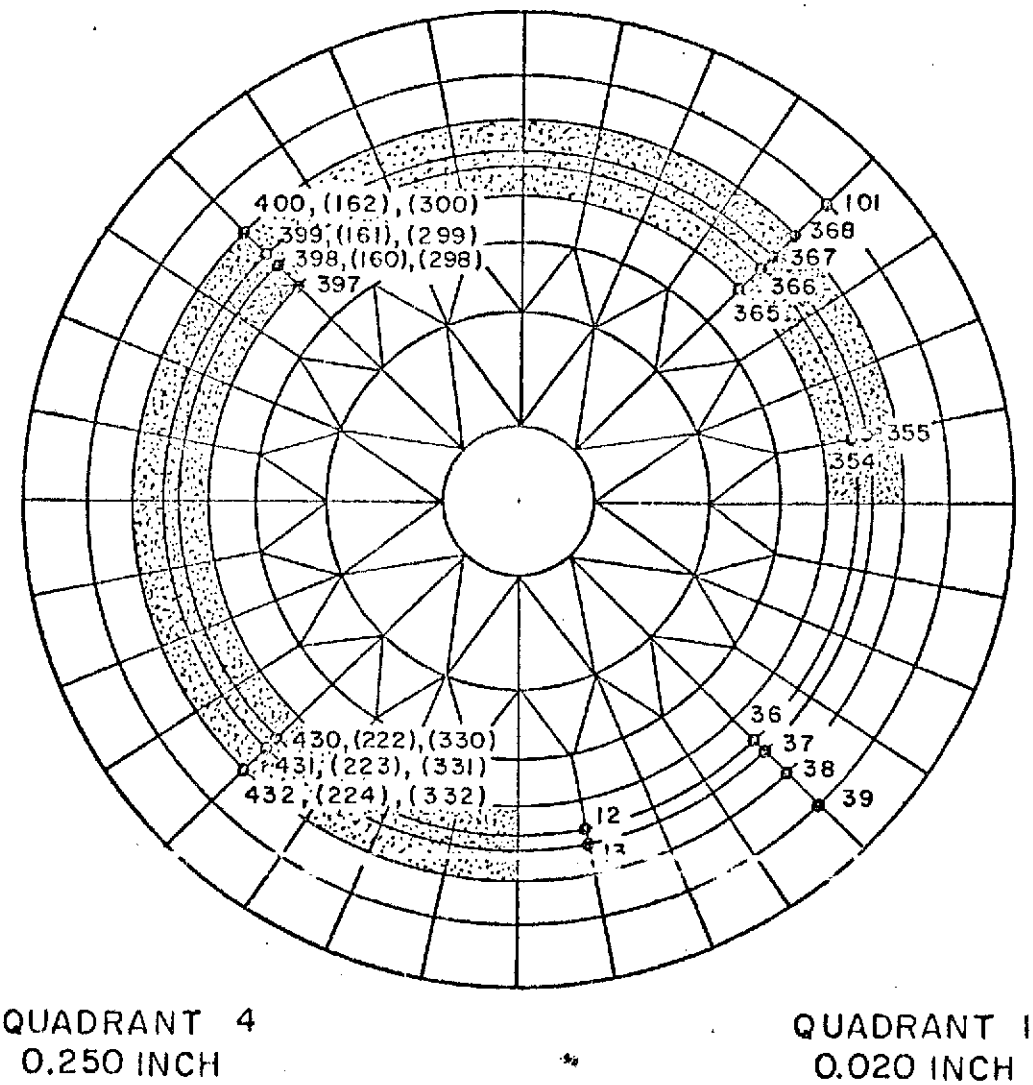

a = 432
b = 224
c = 332

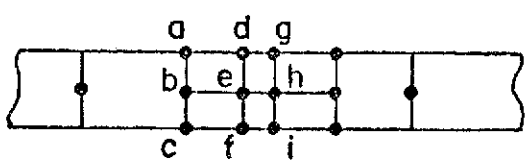

d = 431 g = 430
e = 223 h = 222
f = 331 i = 330

Note: Dotted portions consist of three-dimensional elements. Numbers in parentheses denote subsurfaces and an example is shown in the above enlarged figure of a section in Quadrant 4.

FIGURE 13 Mesh Pattern and Node Arrangement for Finite Element Analysis of Disc

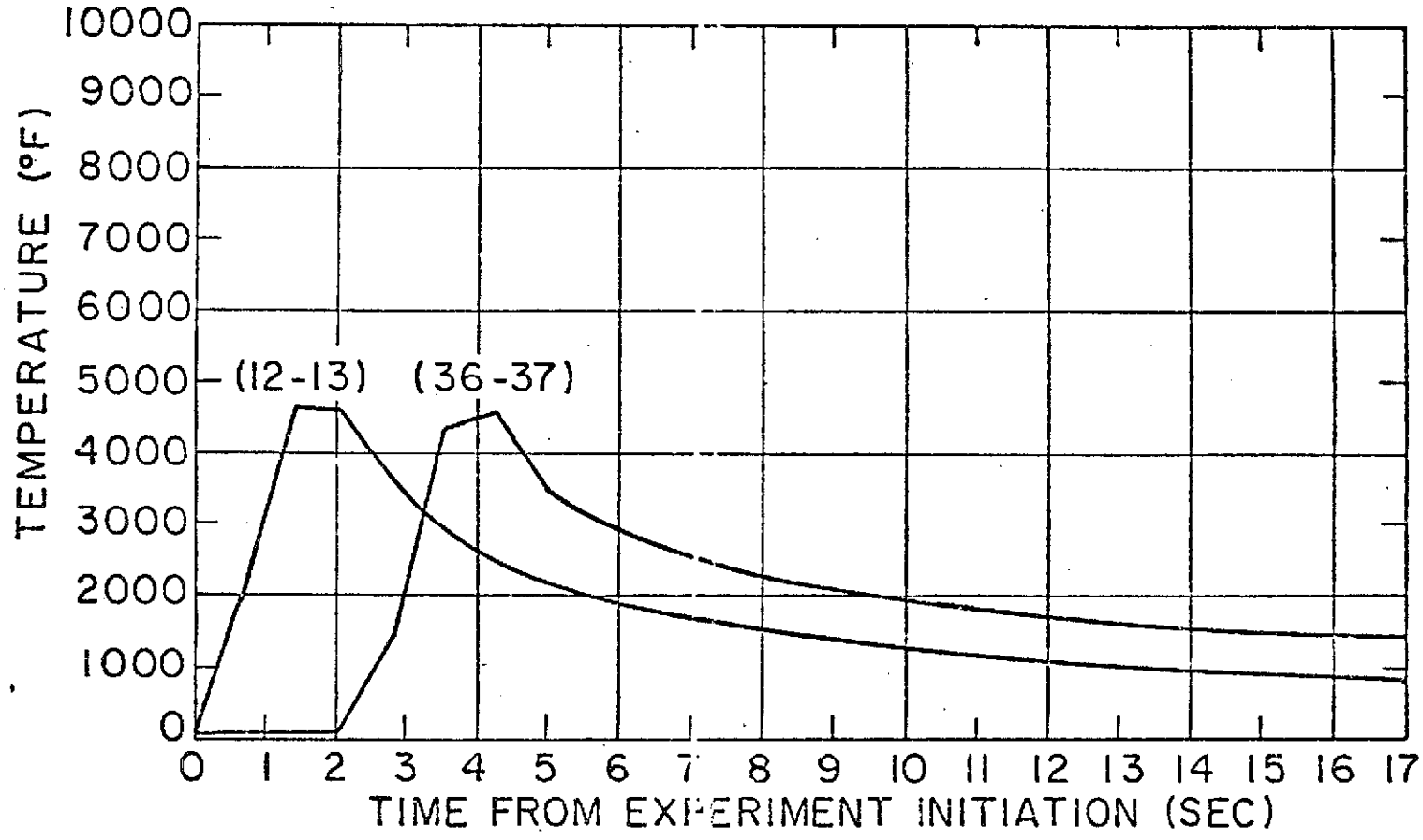

Note: Curves denote the average temperatures of nodes in the parentheses

Figure 14 Calculated Temperature Histories of Points on Weld Circle in Quadrant 1

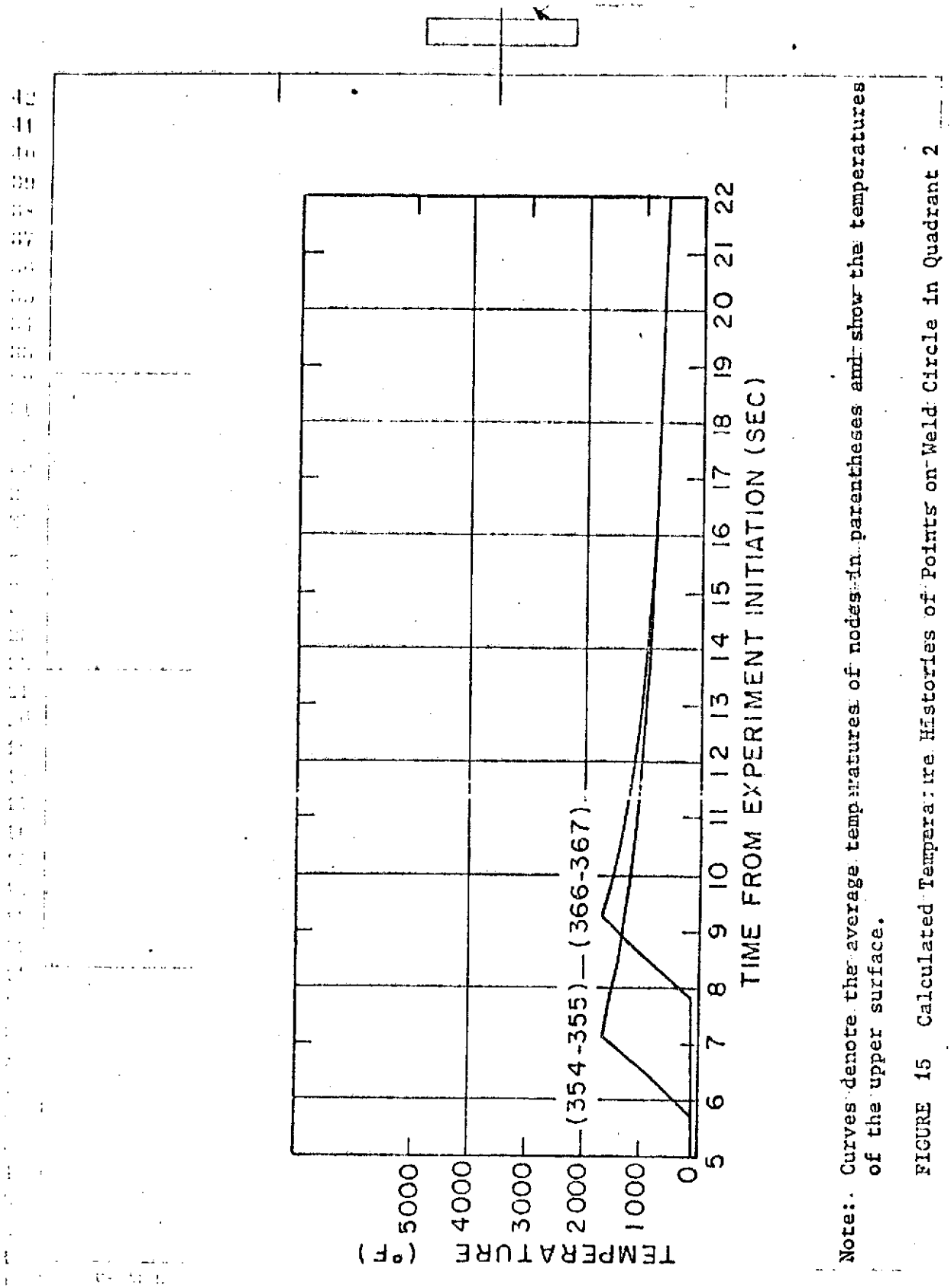

Note: Curves denote the average temperatures of nodes in parentheses and show the temperatures of the upper surface.

FIGURE 15 Calculated Temperature Histories of Points on Weld Circle in Quadrant 2

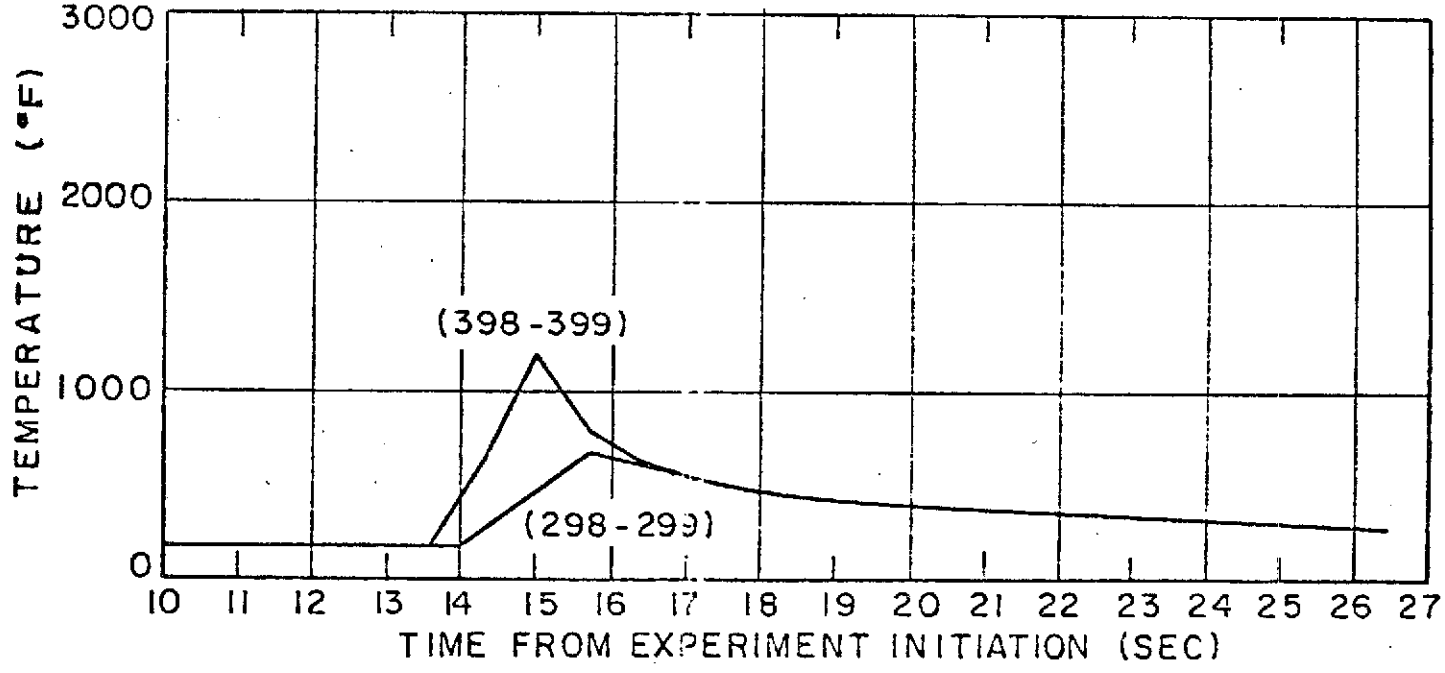

Note: Curves denote the average temperatures of nodes in parentheses and also show the comparison between temperatures of the upper and the lower surfaces.

FIGURE 16 Calculated Temperature Histories of Points on Weld Circle in Quadrant 3

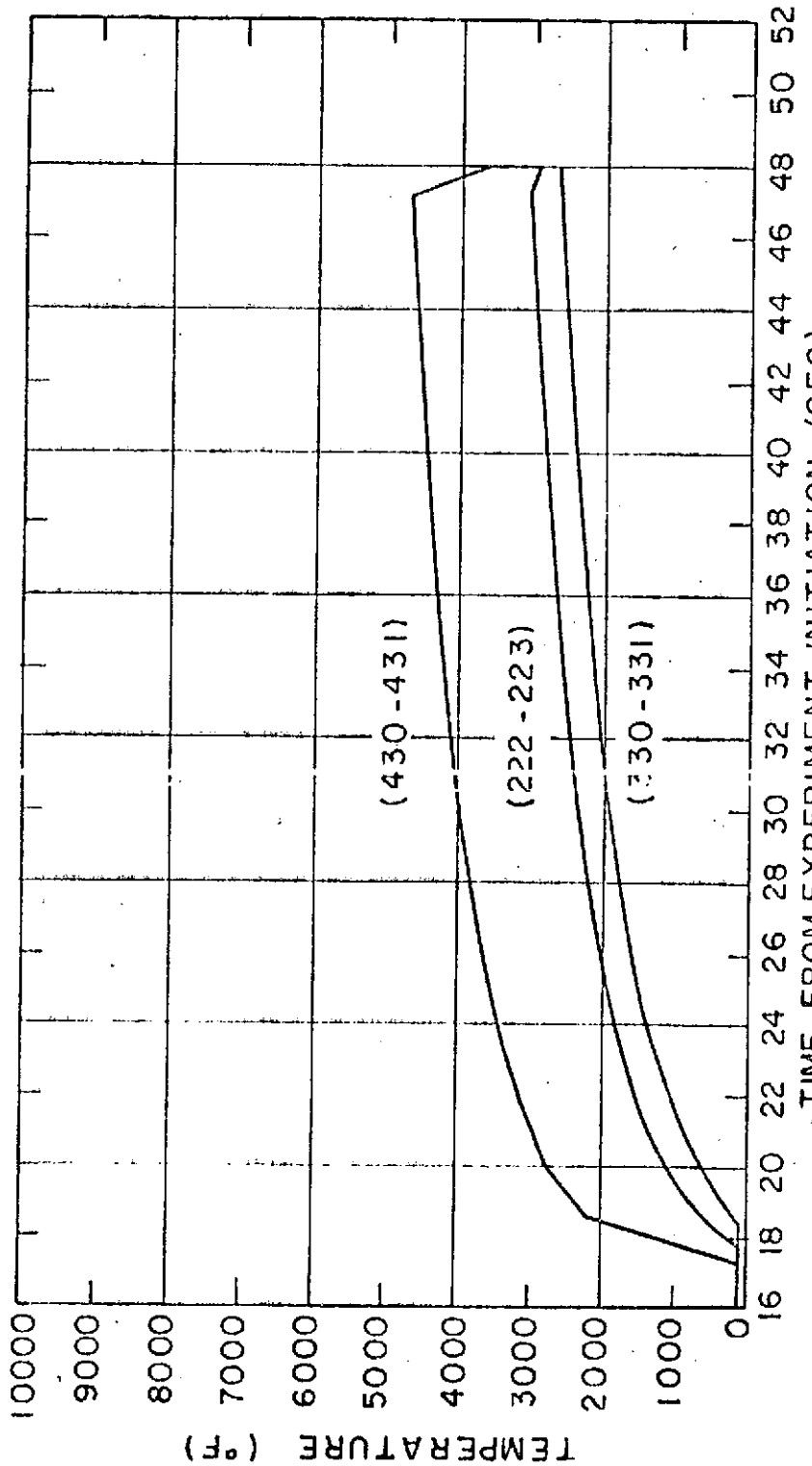

Note: Curves denote the average temperatures of nodes in parentheses and also show the comparison among temperatures of the upper, the middle, and the lower surfaces.

FIGURE 17 Calculated Temperature Histories at Point where Heat Source Dwells

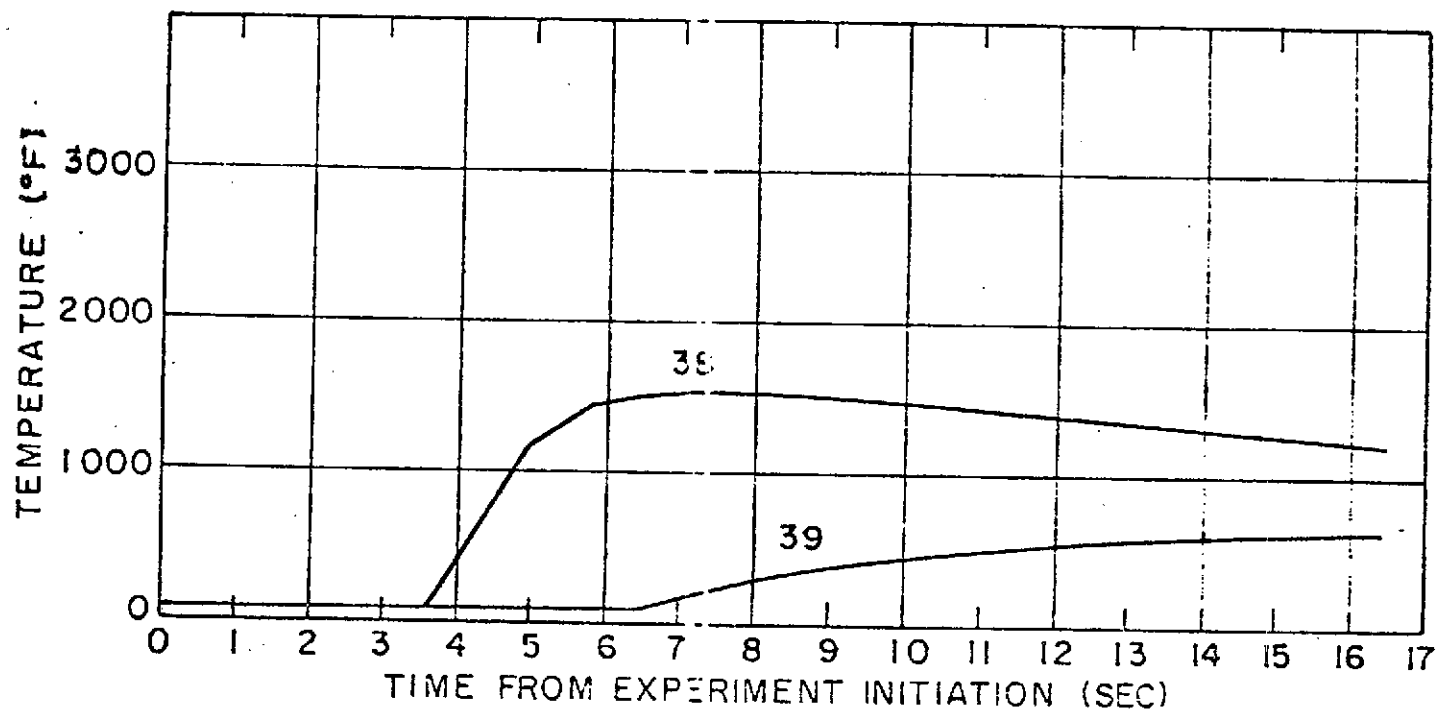

Figure 18 Calculated Temperature Histories of Nodes outside of Weld Circle in Quadrant 1

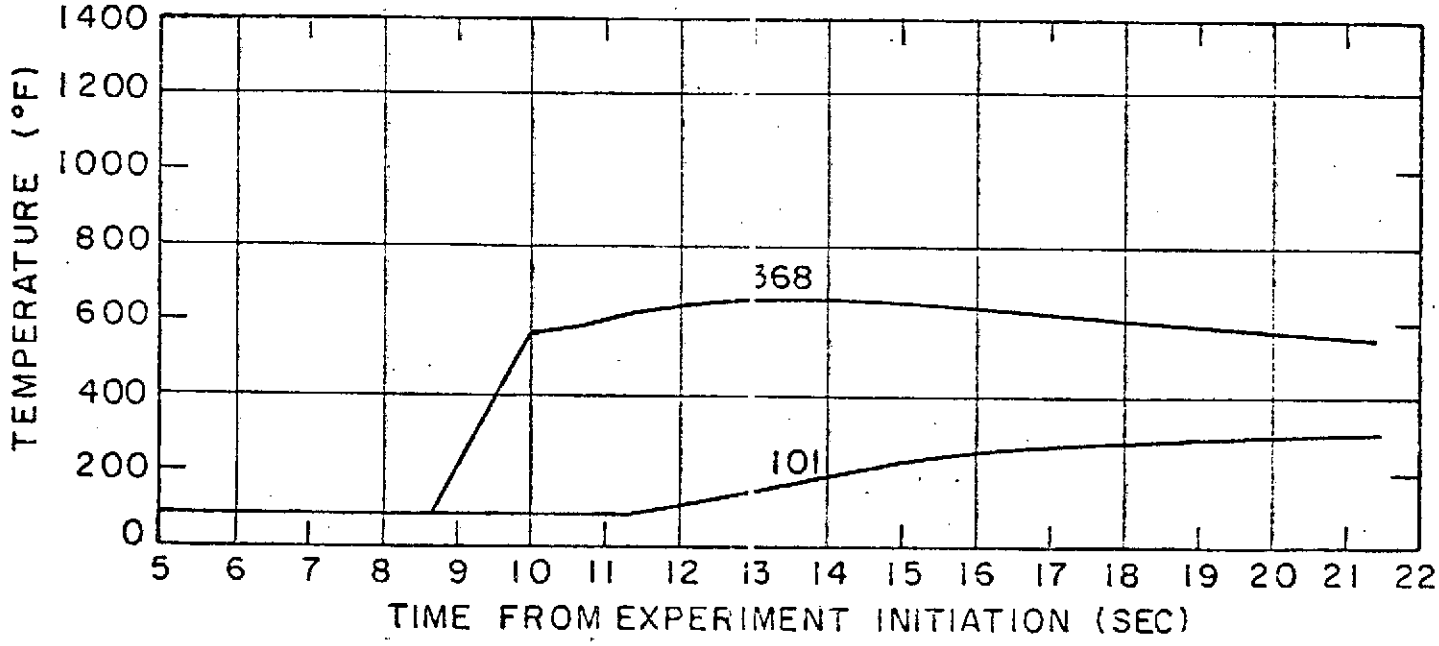

Figure 19 Calculated Temperature Histories of Nodes outside of Weld Circle in Quadrant 2

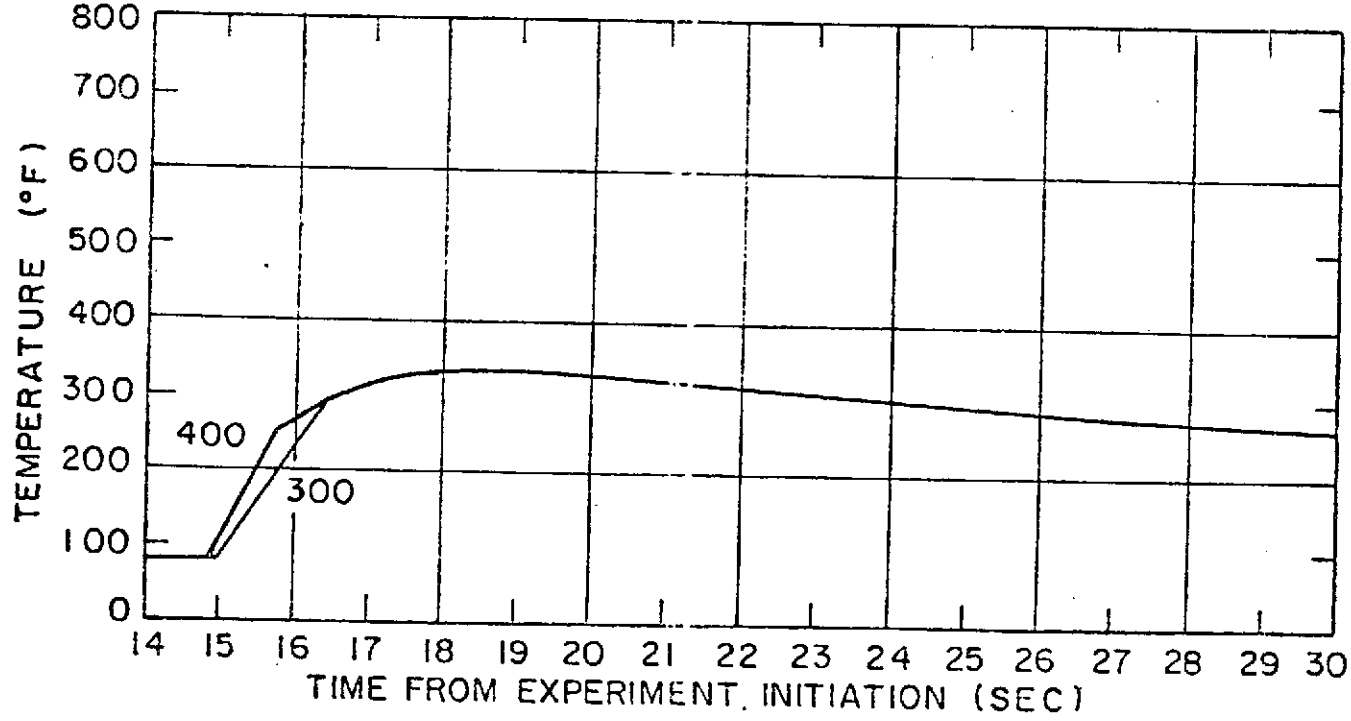

Note: Curves show the comparison between temperatures of the upper and the lower surfaces.

FIGURE 20 Calculated Temperature Histories of Nodes outside of Weld Circle in Quadrant 3

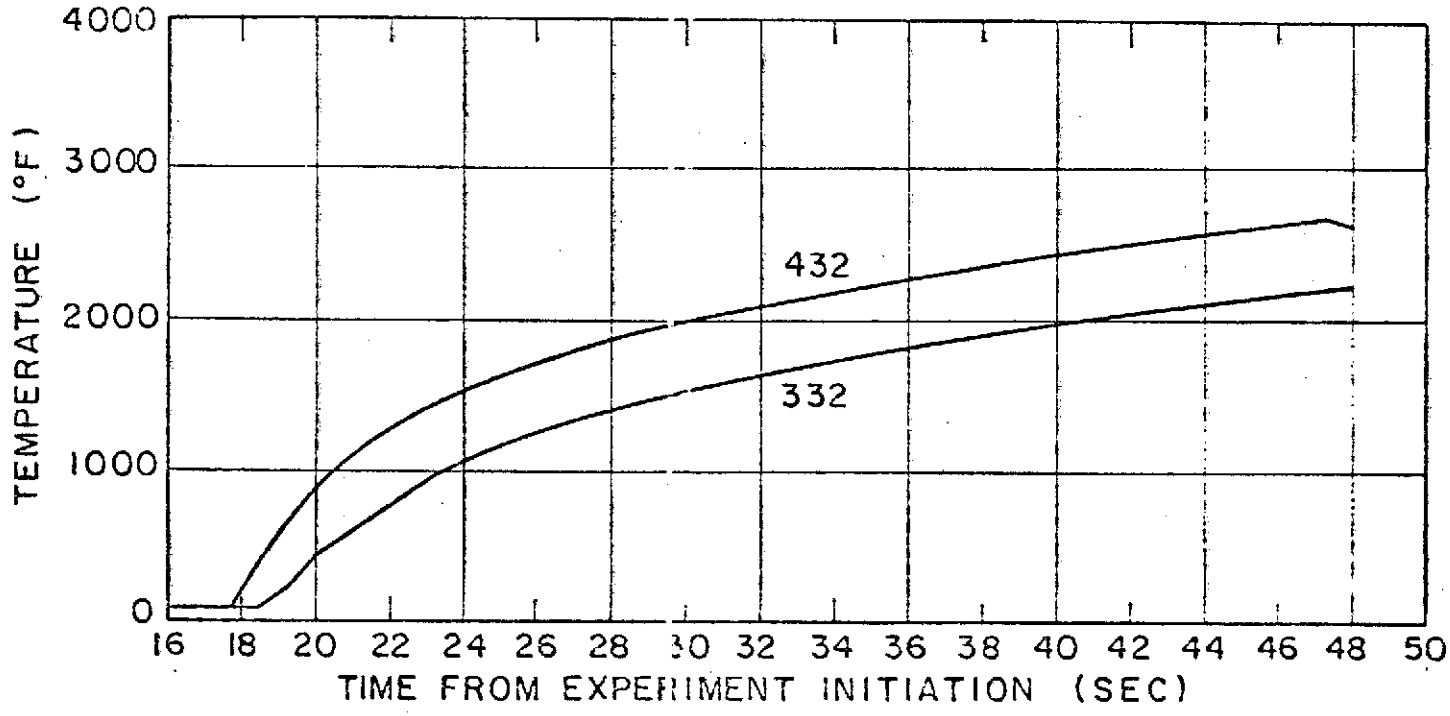

Note: Curves show the comparison between temperatures of the upper and the lower surfaces.

FIGURE 21. Calculated Temperature Histories of Nodes Near Dwelling Heat Source

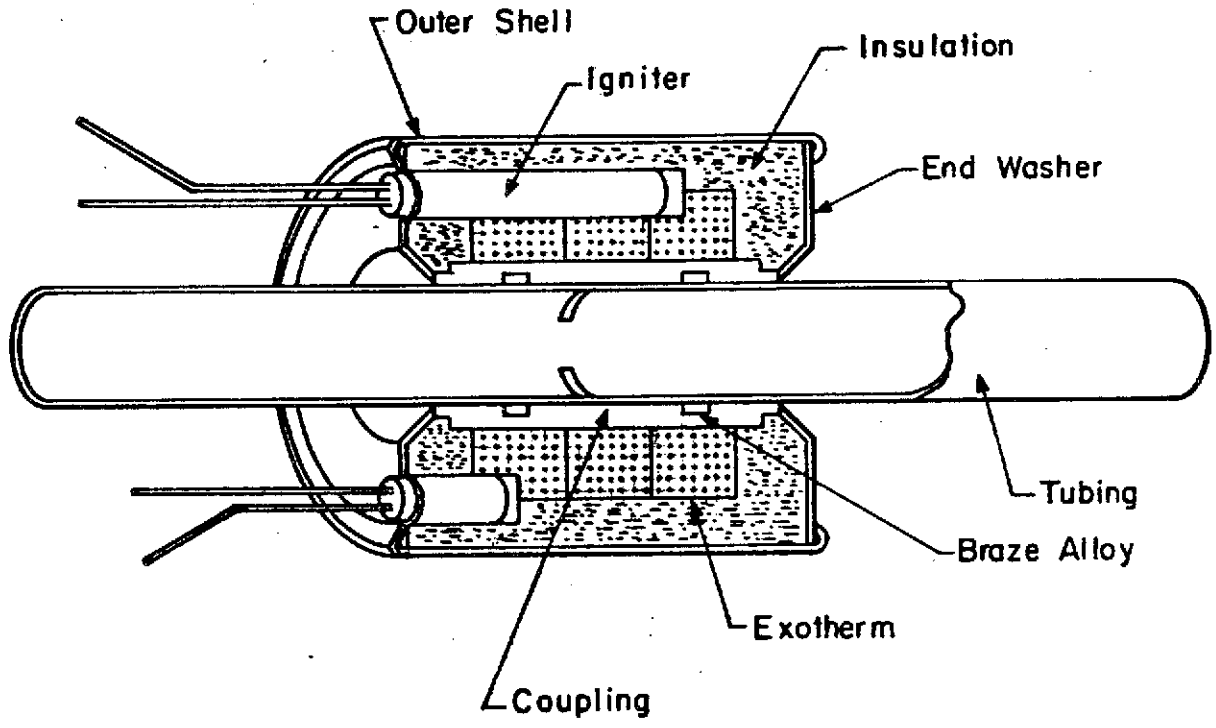

FIGURE 22 Cross Section of Exothermic Braze Unit

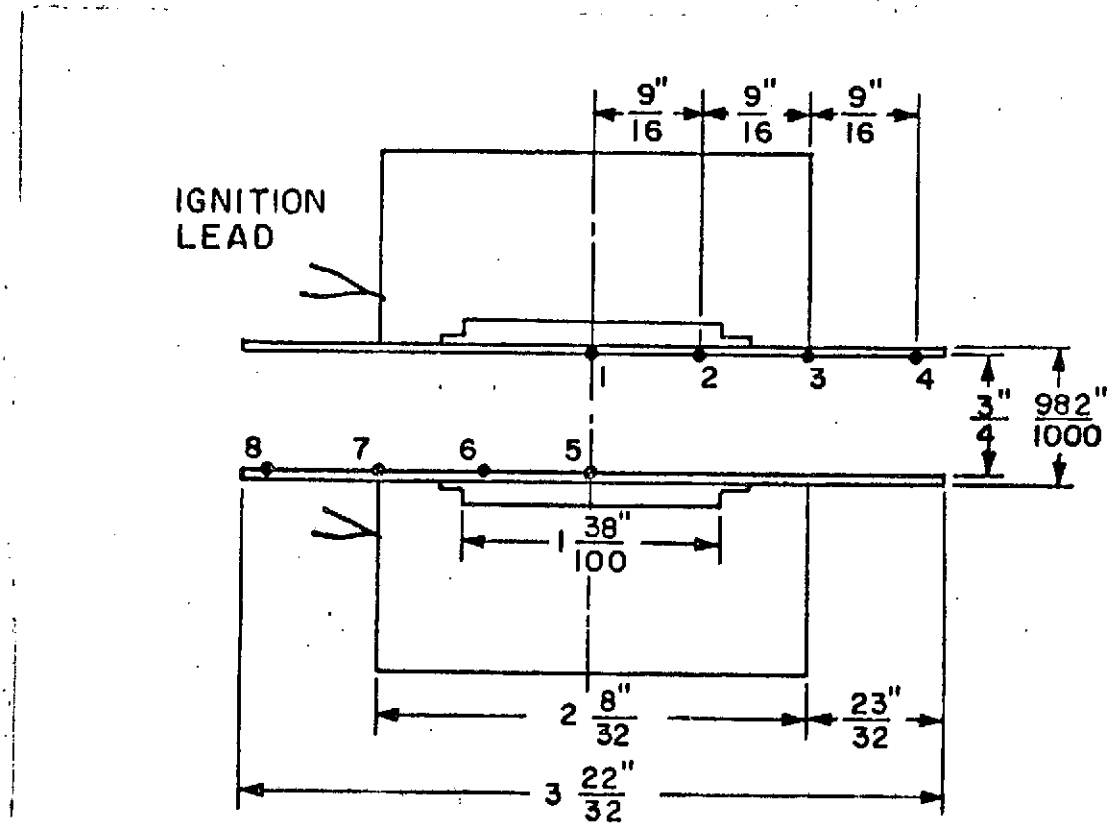

EXPERIMENT 1

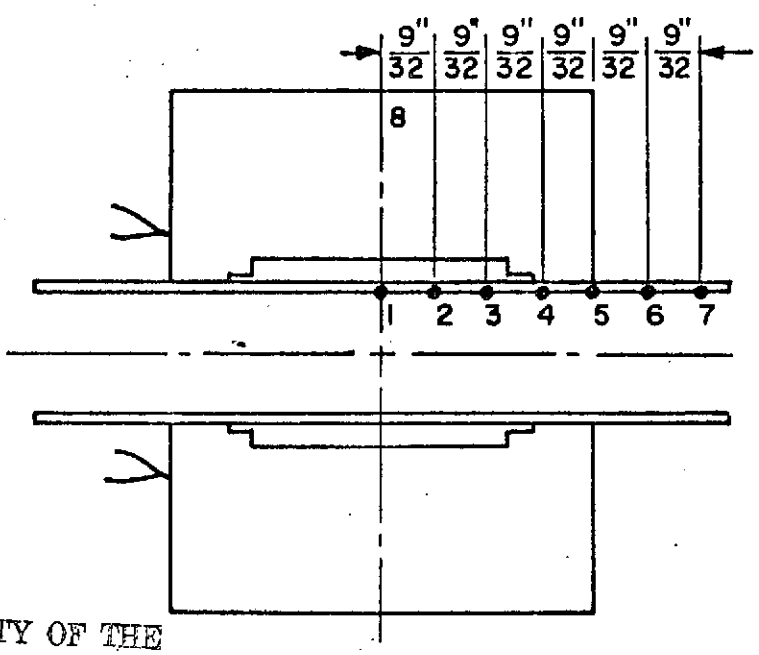

EXPERIMENT 2

FIGURE 23 Locations of Thermocouples in Specimens Tested

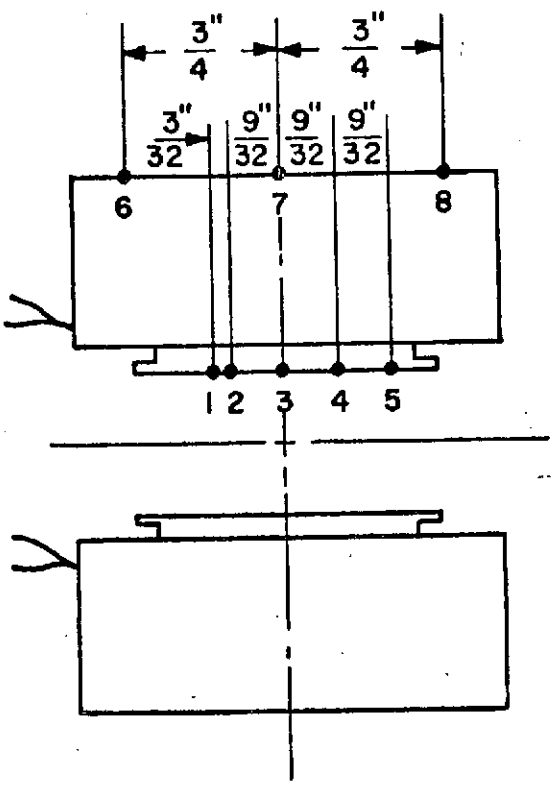

FIGURE 23 Locations of Thermocouples in Specimens Tested (cont.)

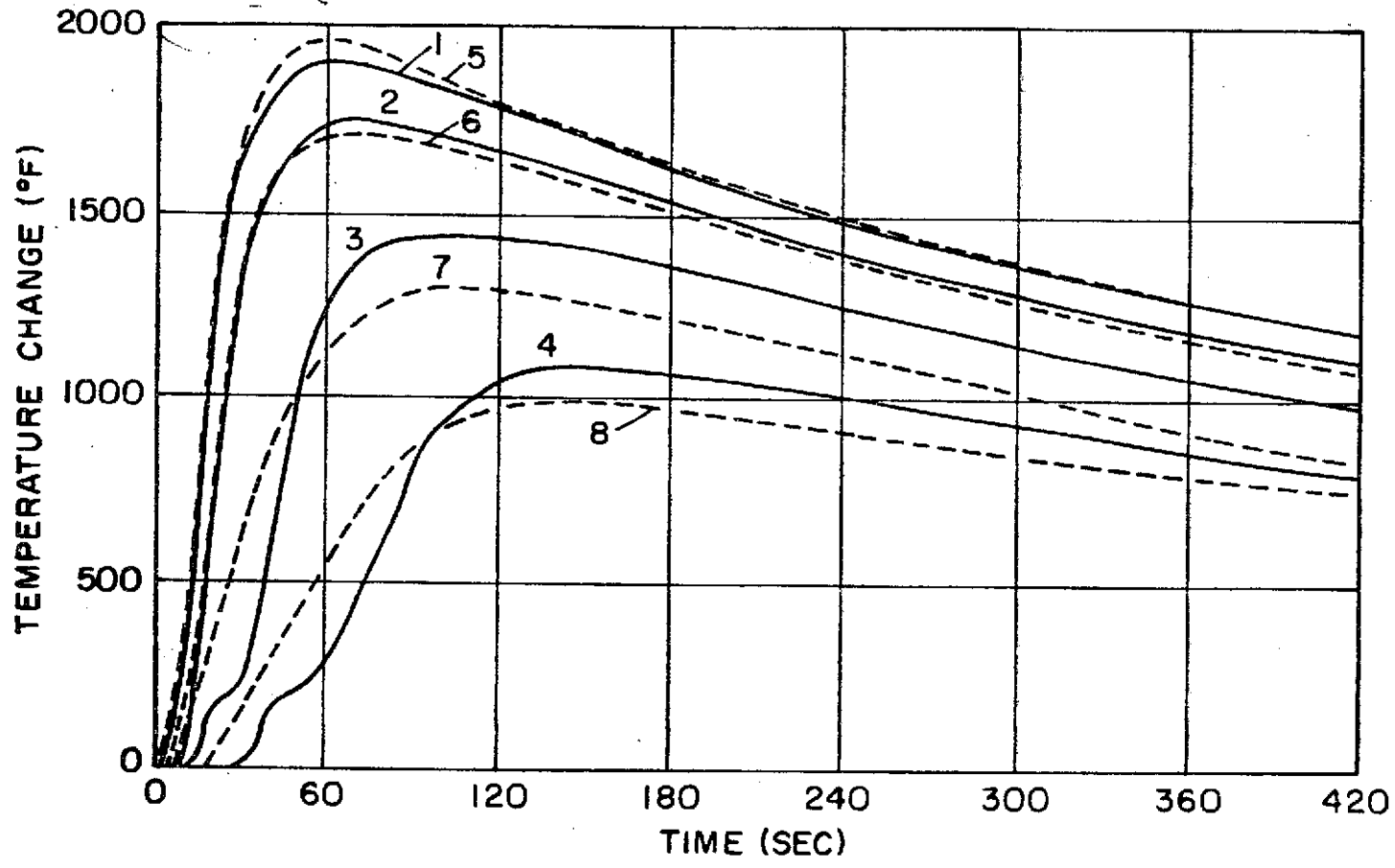

Note: Numbers on Curves Denote Thermocouple Numbers

FIGURE 24 Temperature Change Measured in Experiment 1

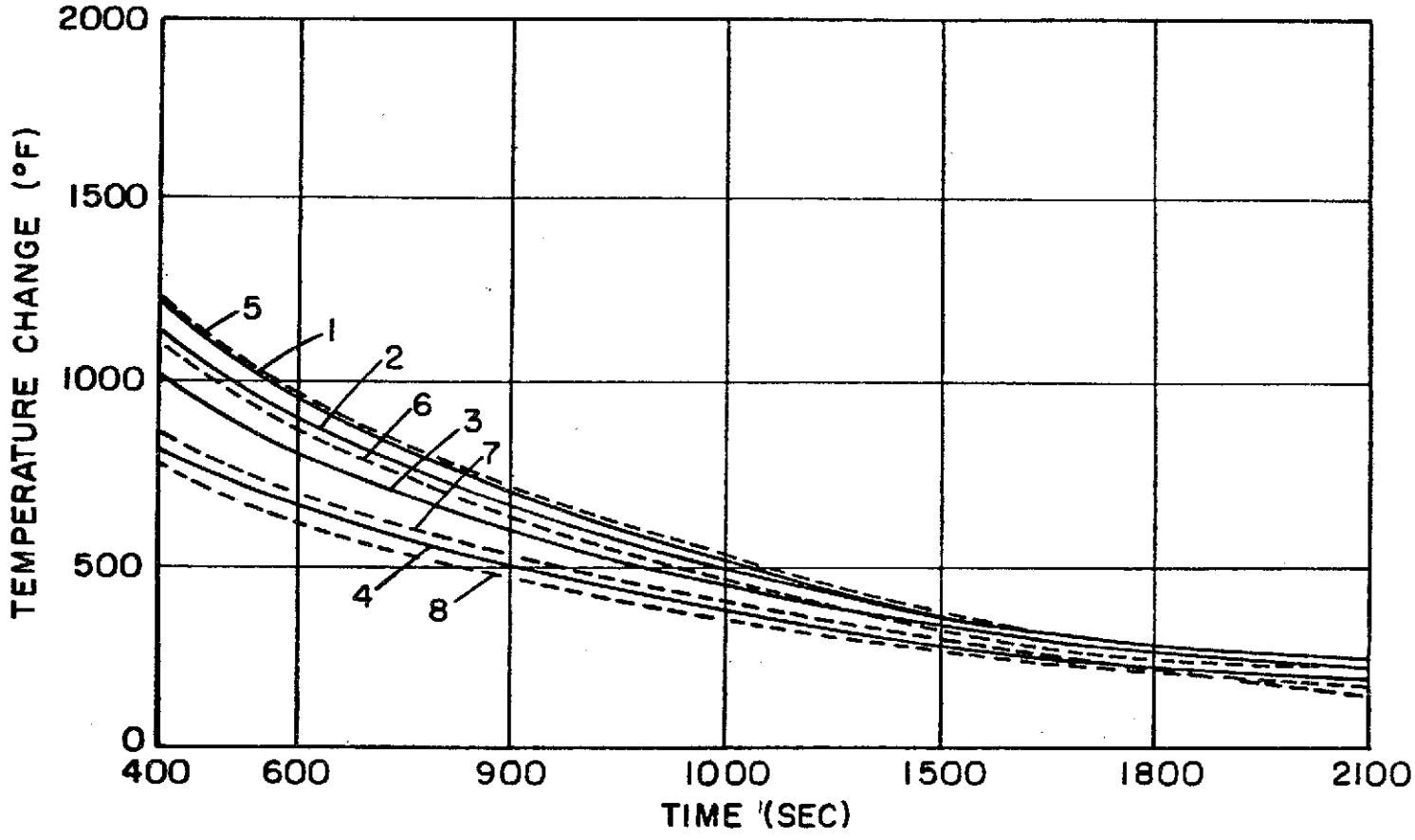

Note: Numbers on Curves Denote Thermocouple Numbers

FIGURE 25 Temperature Change Measured in Experiment 1

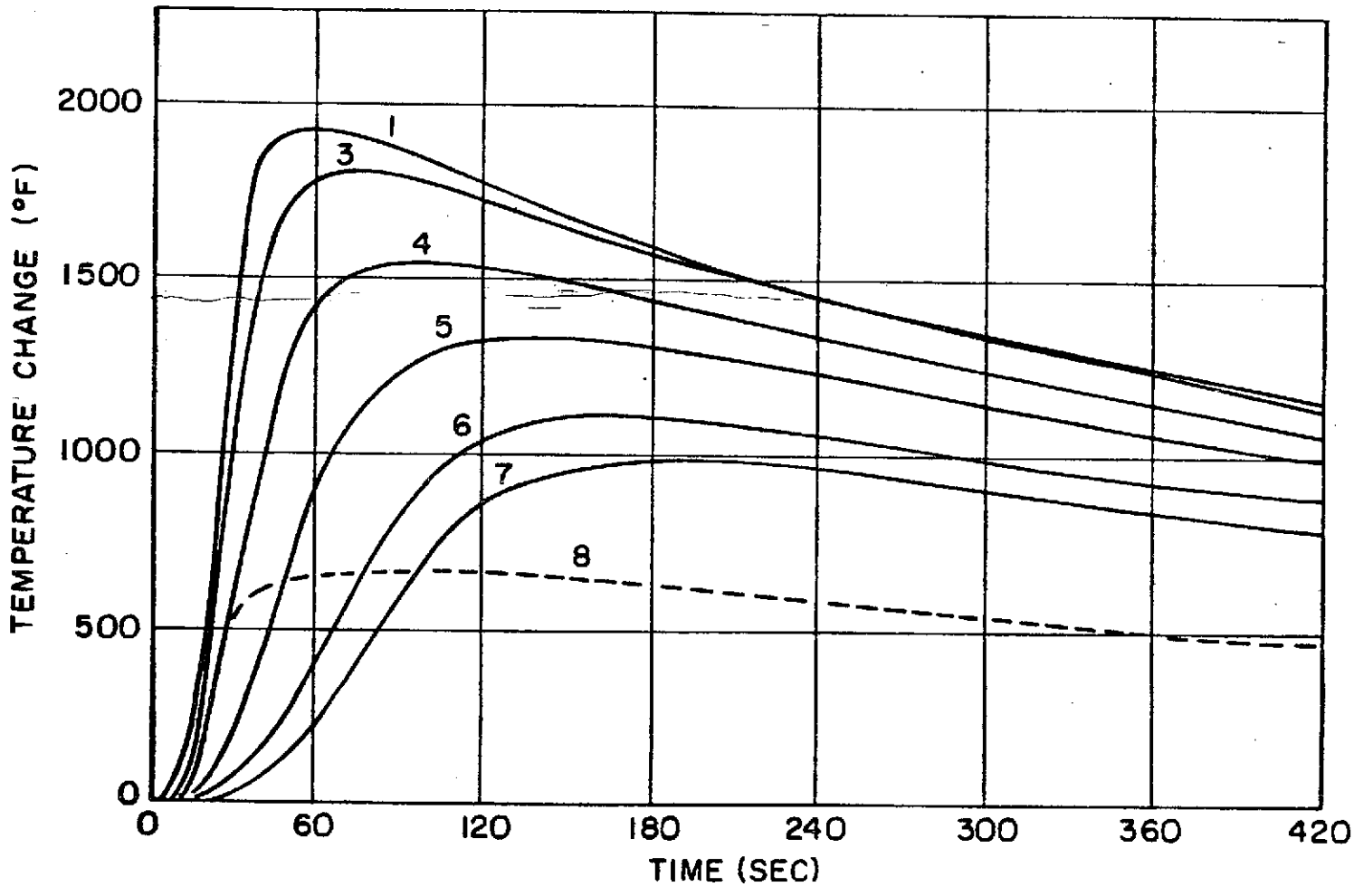

Note: Numbers on Curves Denote Thermocouple Numbers

FIGURE 26 Temperature Change Measured in Experiment 2

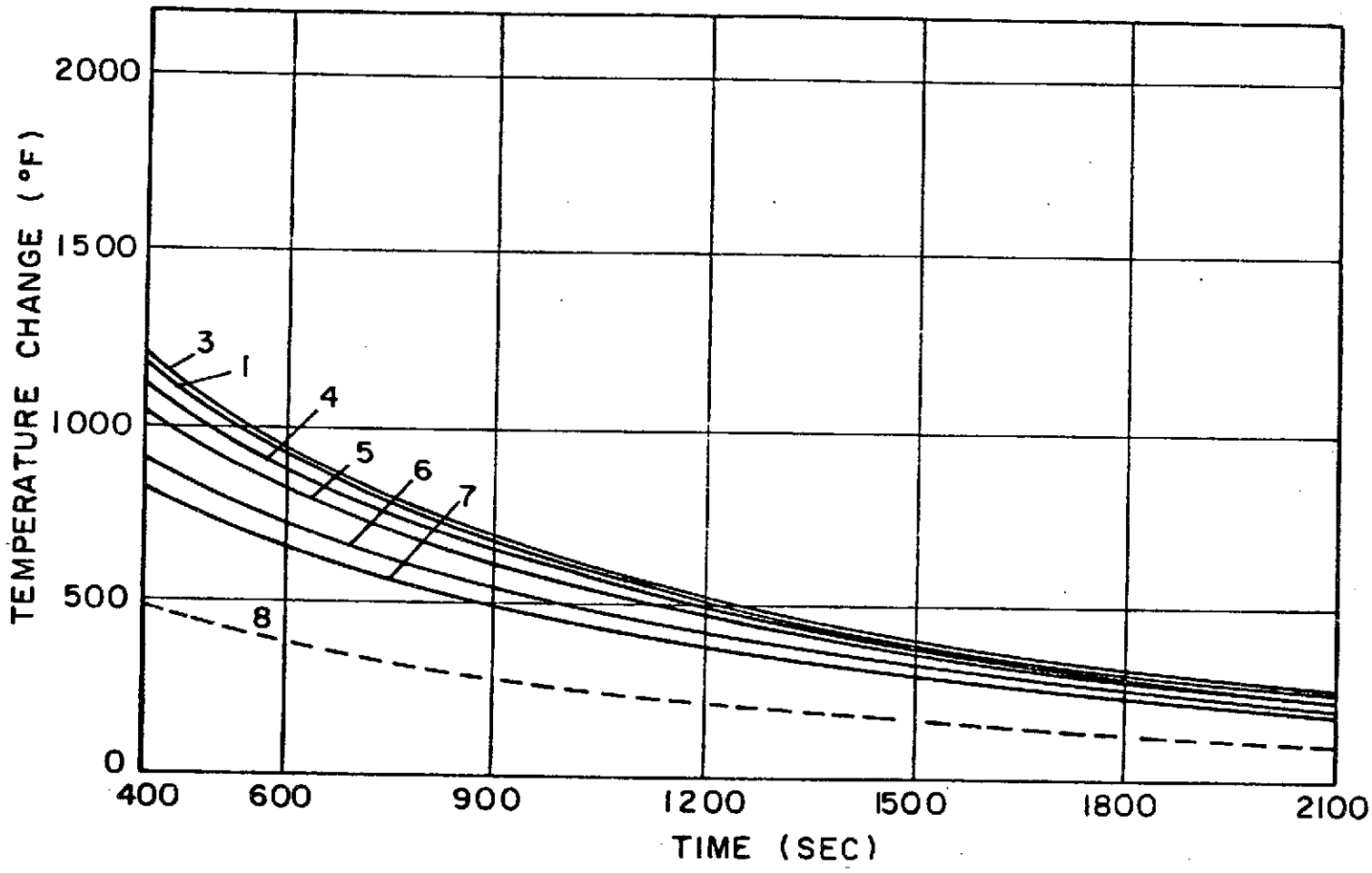

Note: Numbers on Curves Denote Thermocouple Numbers

FIGURE 27 Temperature Change Measured in Experiment 2

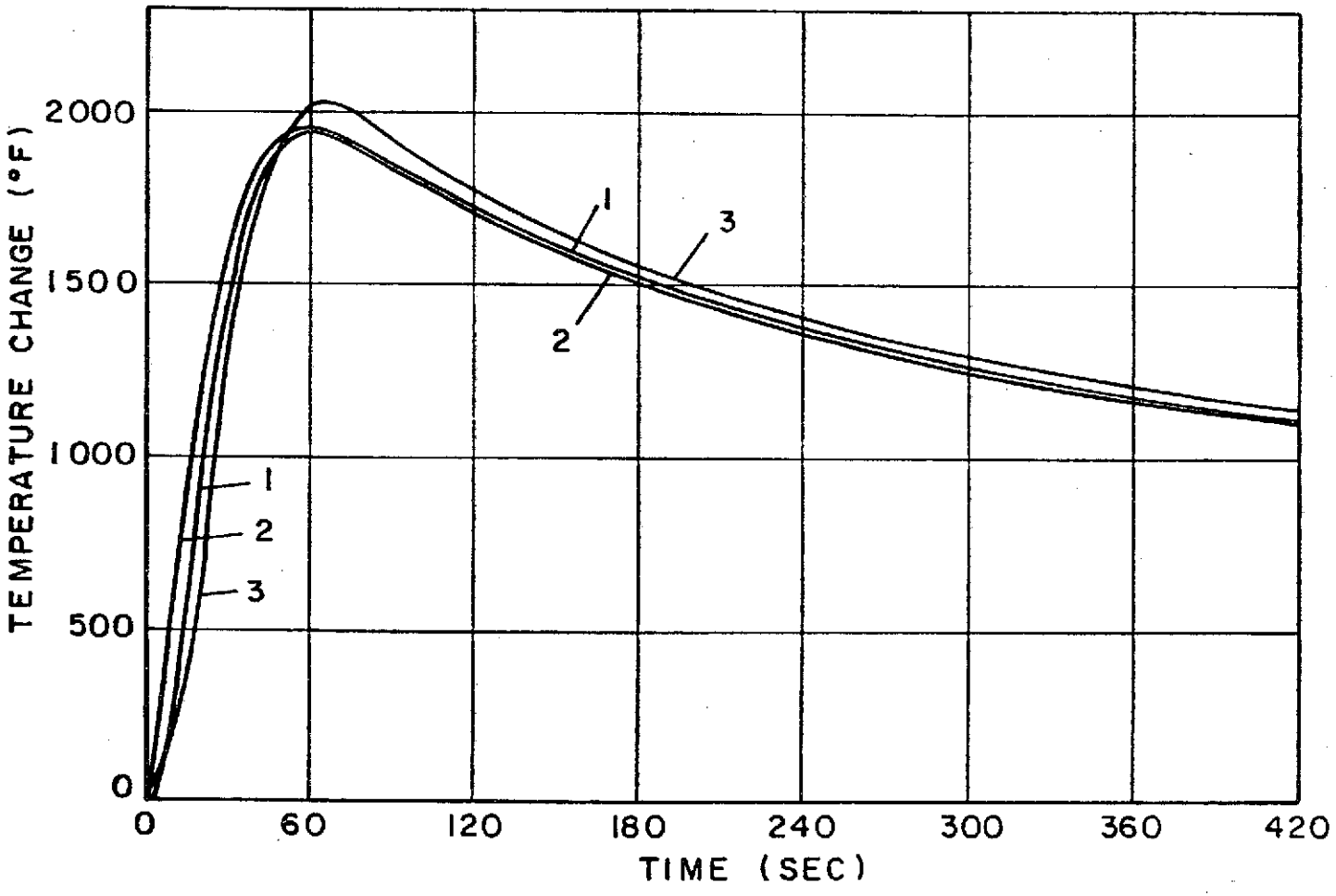

Note: Numbers on Curves Denote Thermocouple Numbers

FIGURE 28 Temperature Change Measured in Experiment 3

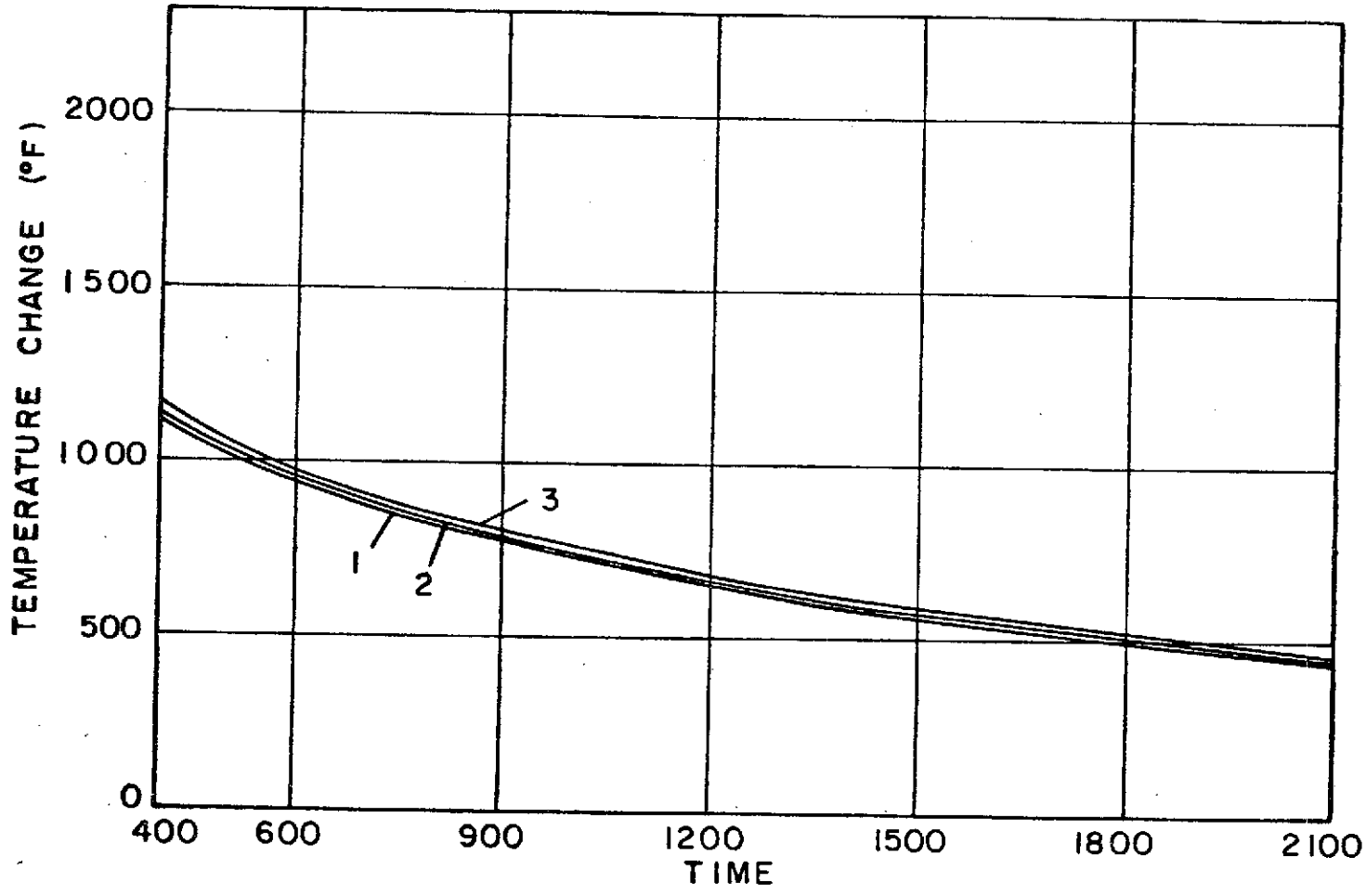

Note: Numbers on Curves Denote Thermocouple Numbers

FIGURE 29 Temperature Change Measured in Experiment 3

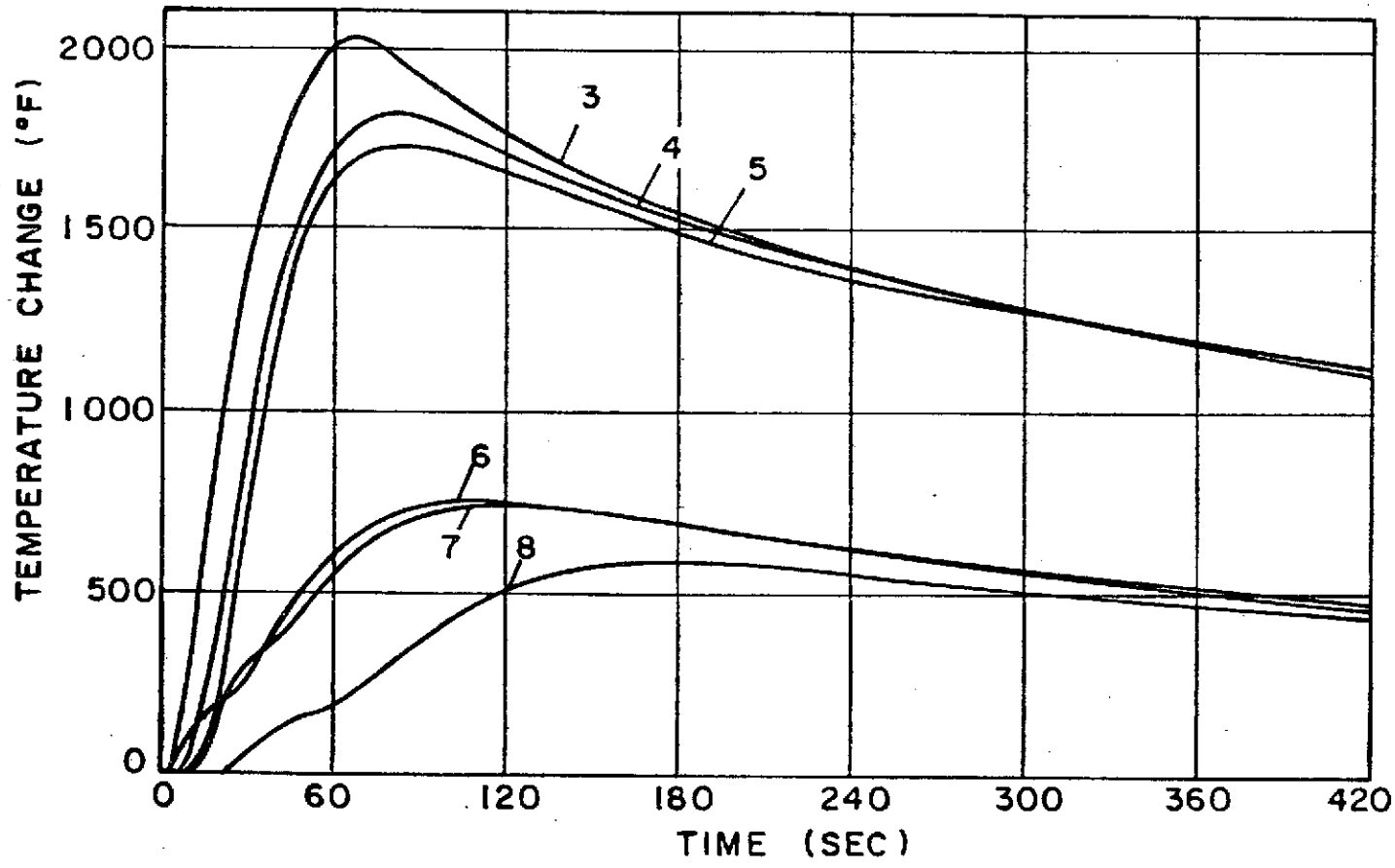

Note: Numbers on Curves Denote Thermocouple Numbers

FIGURE 30 Temperature Change Measured in Experiment 3

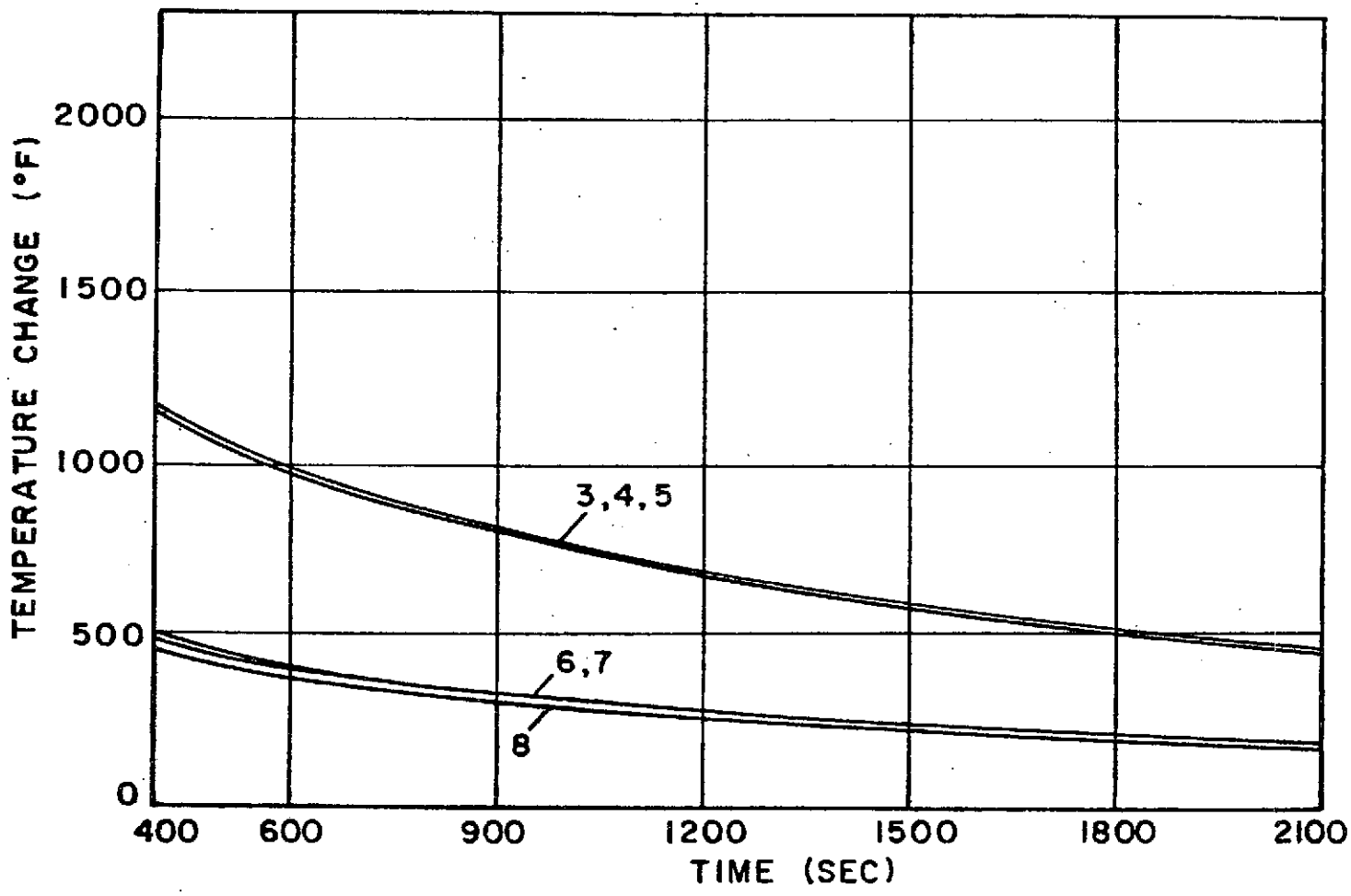

Note: Numbers on Curves Denote Thermocouple Numbers

FIGURE 31 Temperature Change Measured in Experiment 3

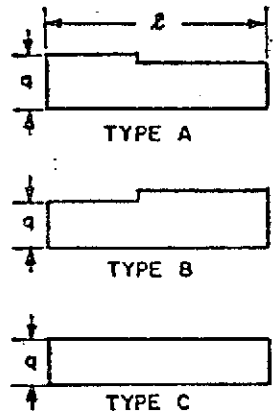

(a). Heat Distribution

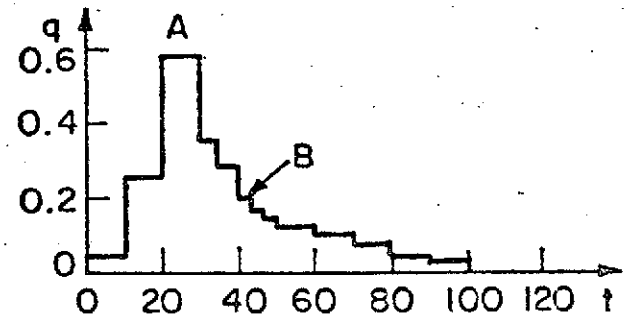

(b) Heat Intensity-Time Relation

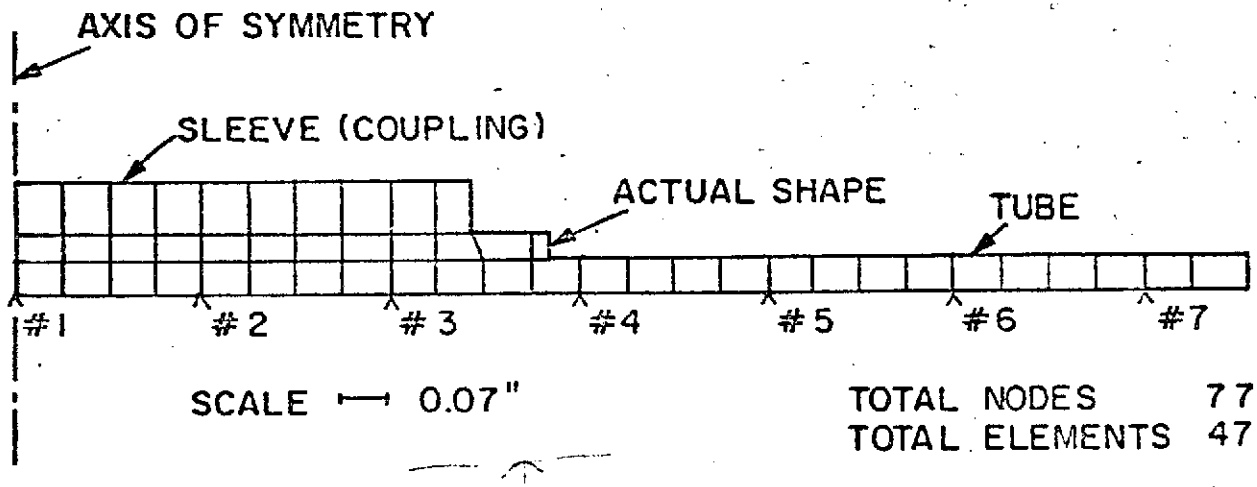

(C) Mesh pattern.

FIGURE 32. ANALYTICAL MODEL

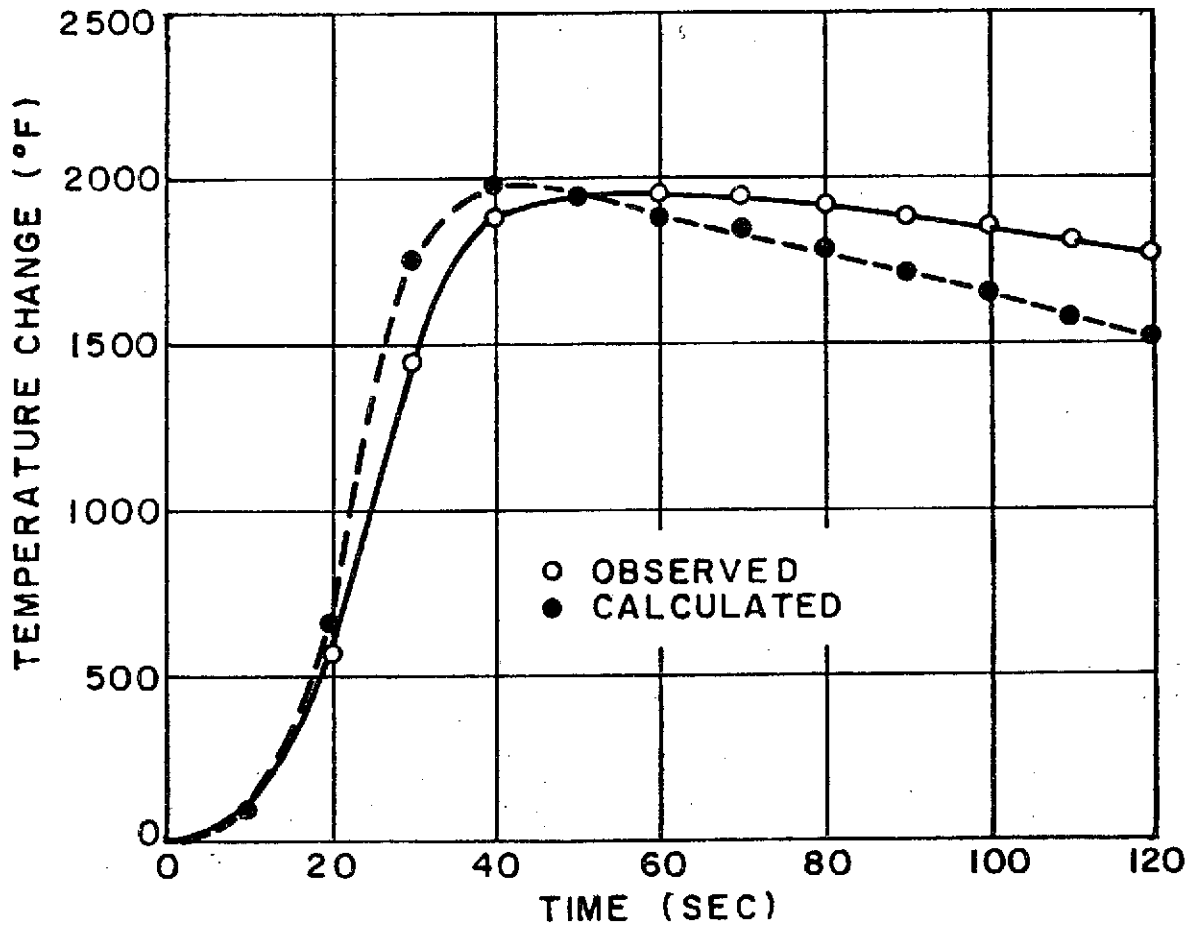

Note: —O—, Curve Observed from Experiment 2

FIGURE 33 Calculated and Observed Temperature Changes at Thermocouple 1

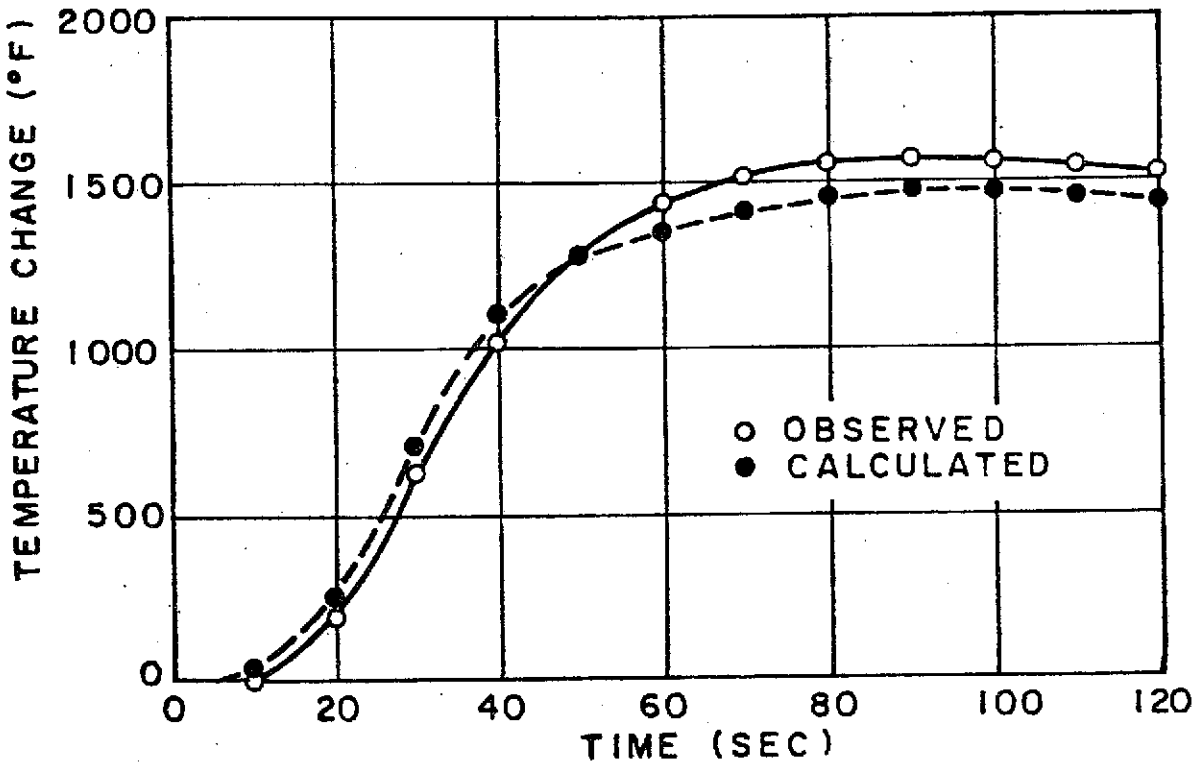

Note: —O—, Curve Observed from Experiment 2

FIGURE 34 Calculated and Observed Temperature Changes at Thermocouple 4

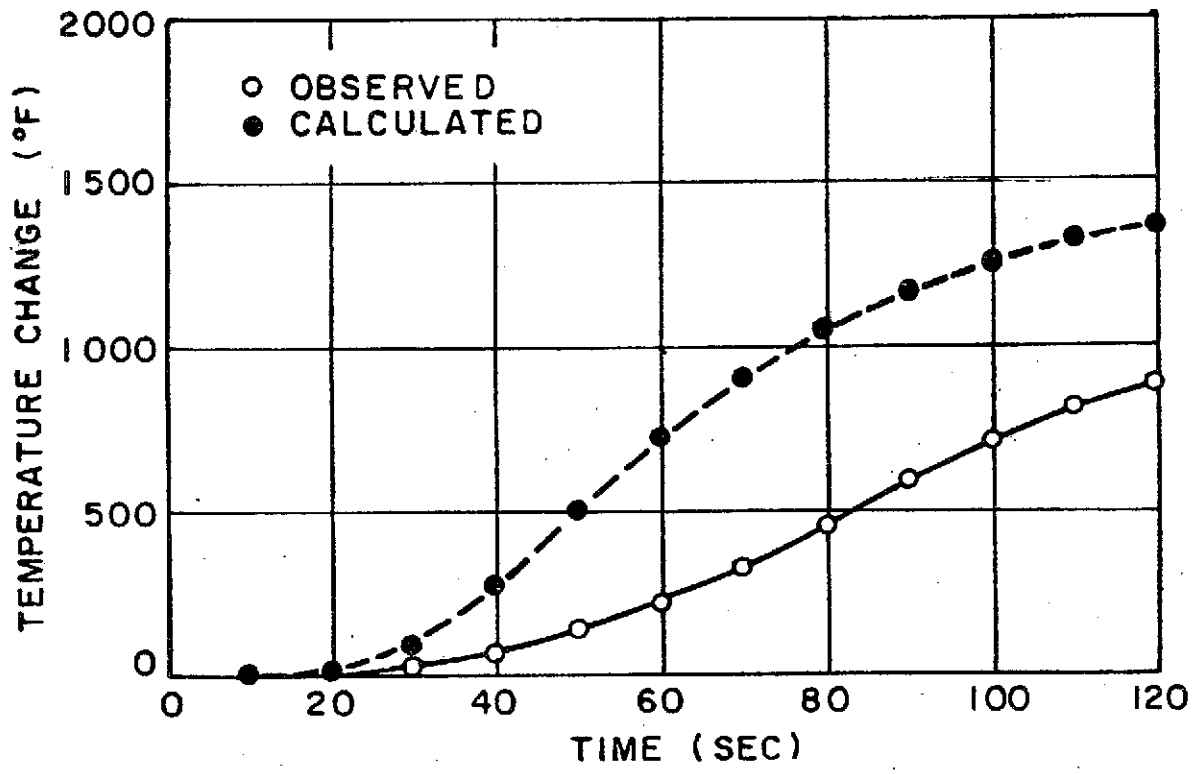

Note: —o—, Curve Observed from Experiment 2

FIGURE 35 Calculated and Observed Temperature Changes at Thermocouple 7

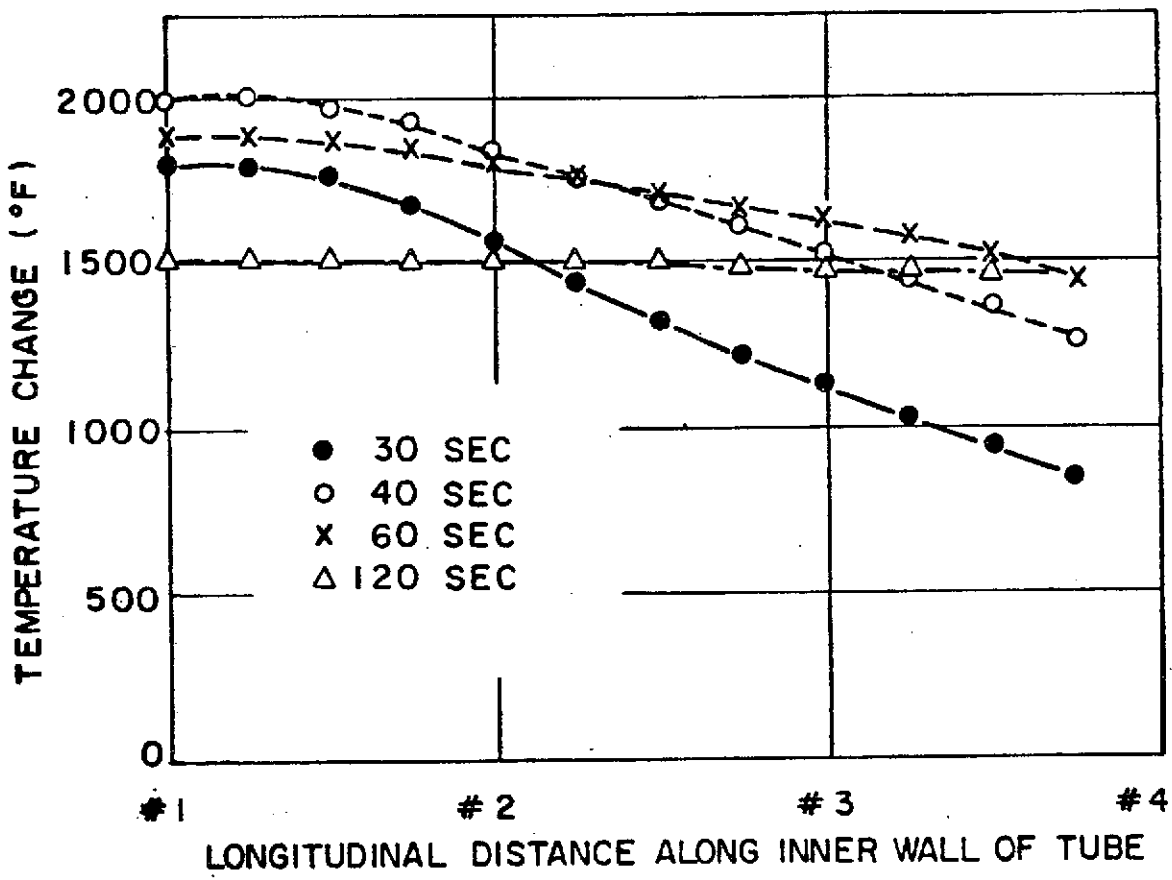

Note: #1, #2, #3, and #4 Correspond to These in Figure 32

FIGURE 36 Calculated Temperature Change Along Boundary Between Tube and Sleeve

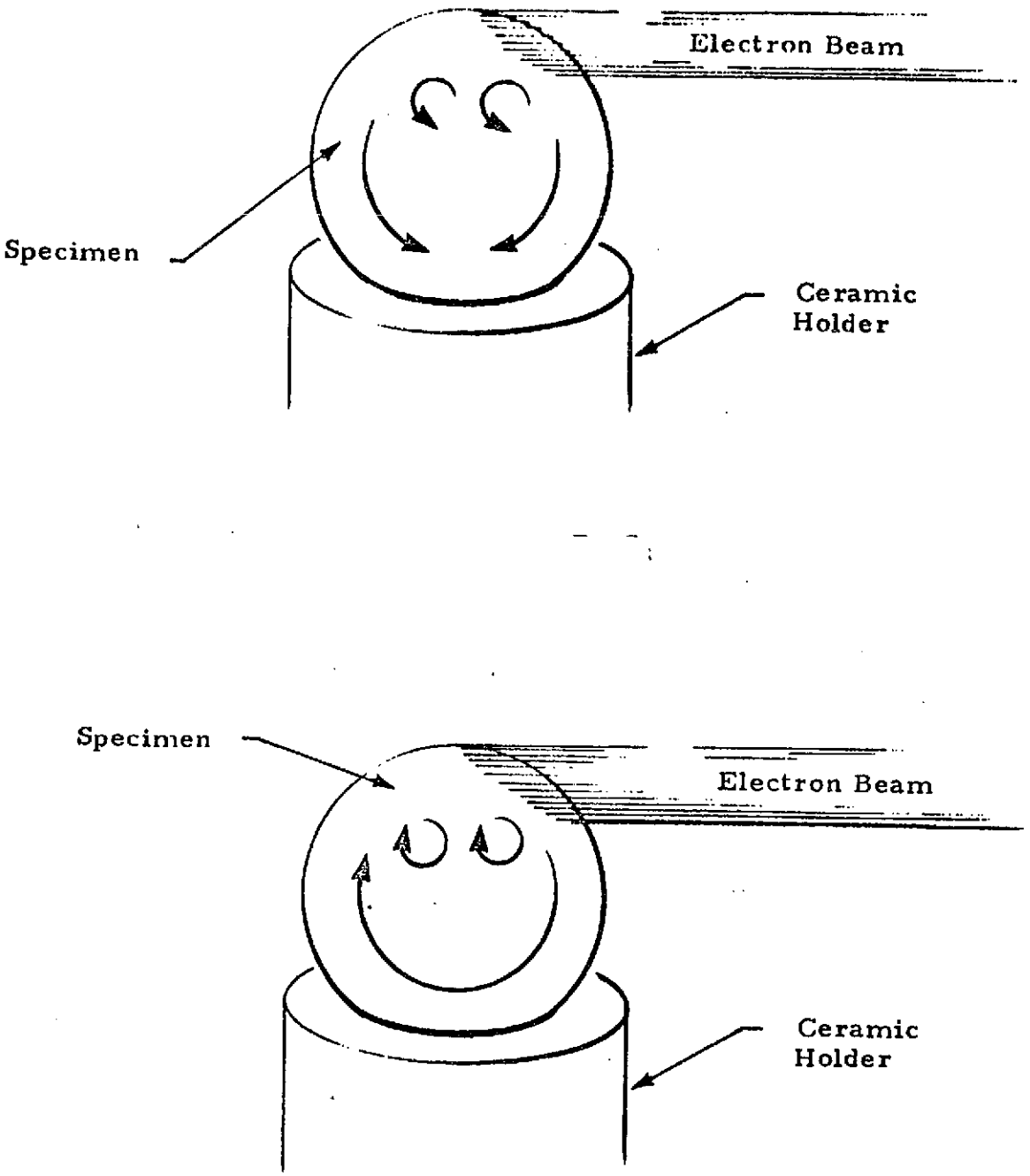

FIGURE 37. CONVECTIVE PATTERNS IN THE M553 SPECIMEN DURING MELTING

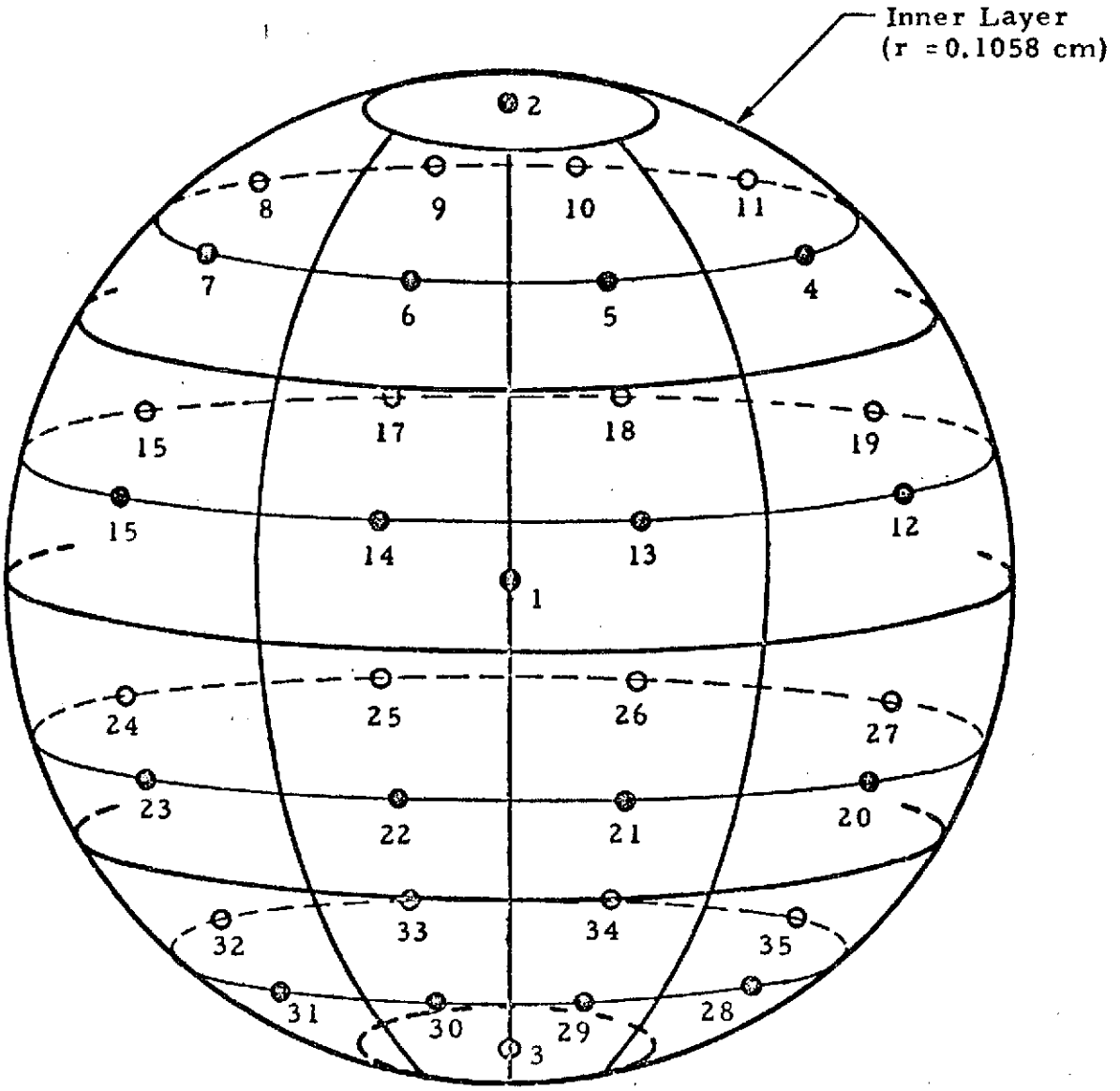

FIGURE 38 THERMAL MODEL FOR INNER LAYER

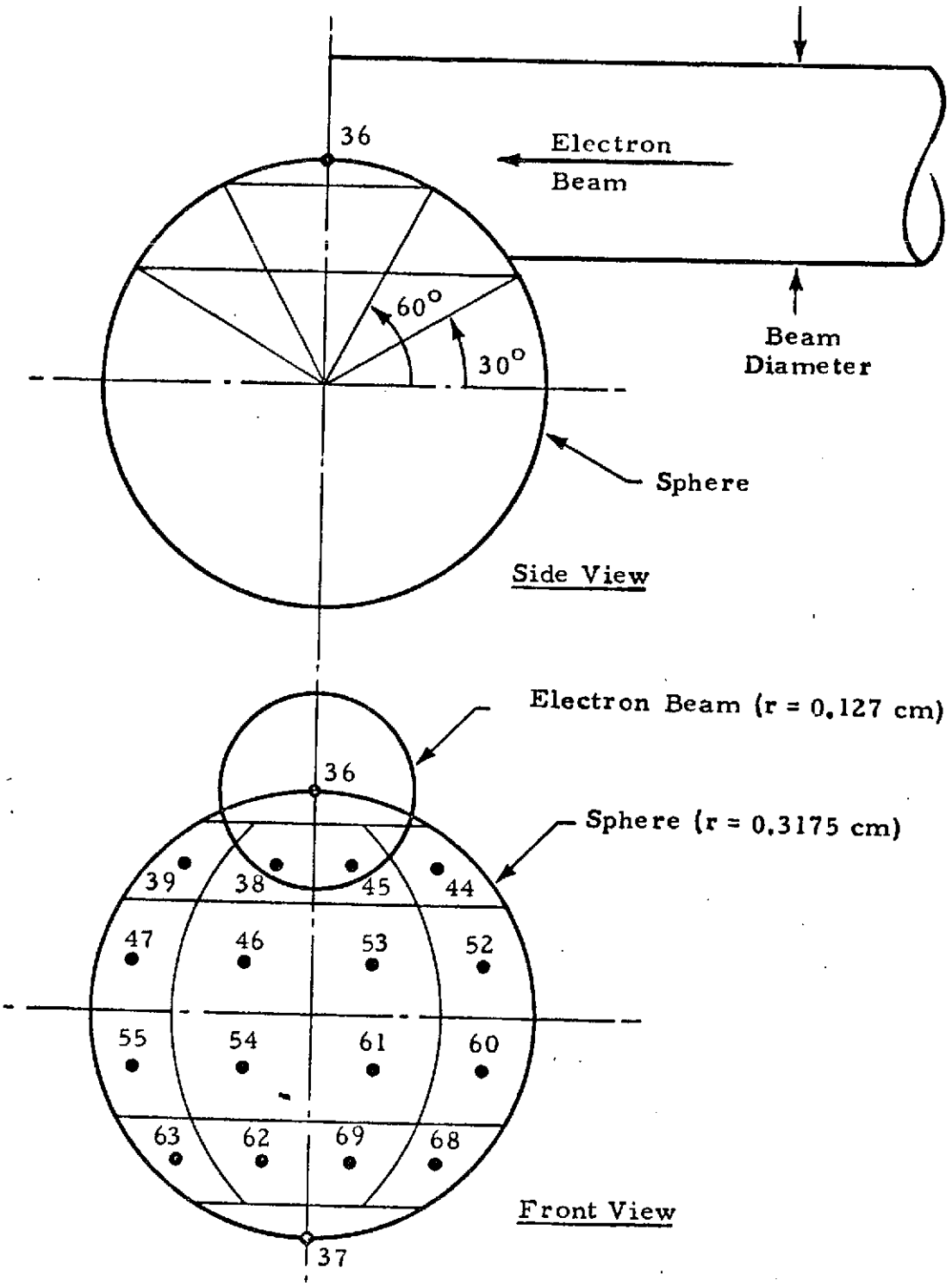

FIGURE 39 . THE RELATIVE POSITION OF ELECTRON BEAM TO SPHERE AND THERMAL MODEL FOR OUTER LAYER

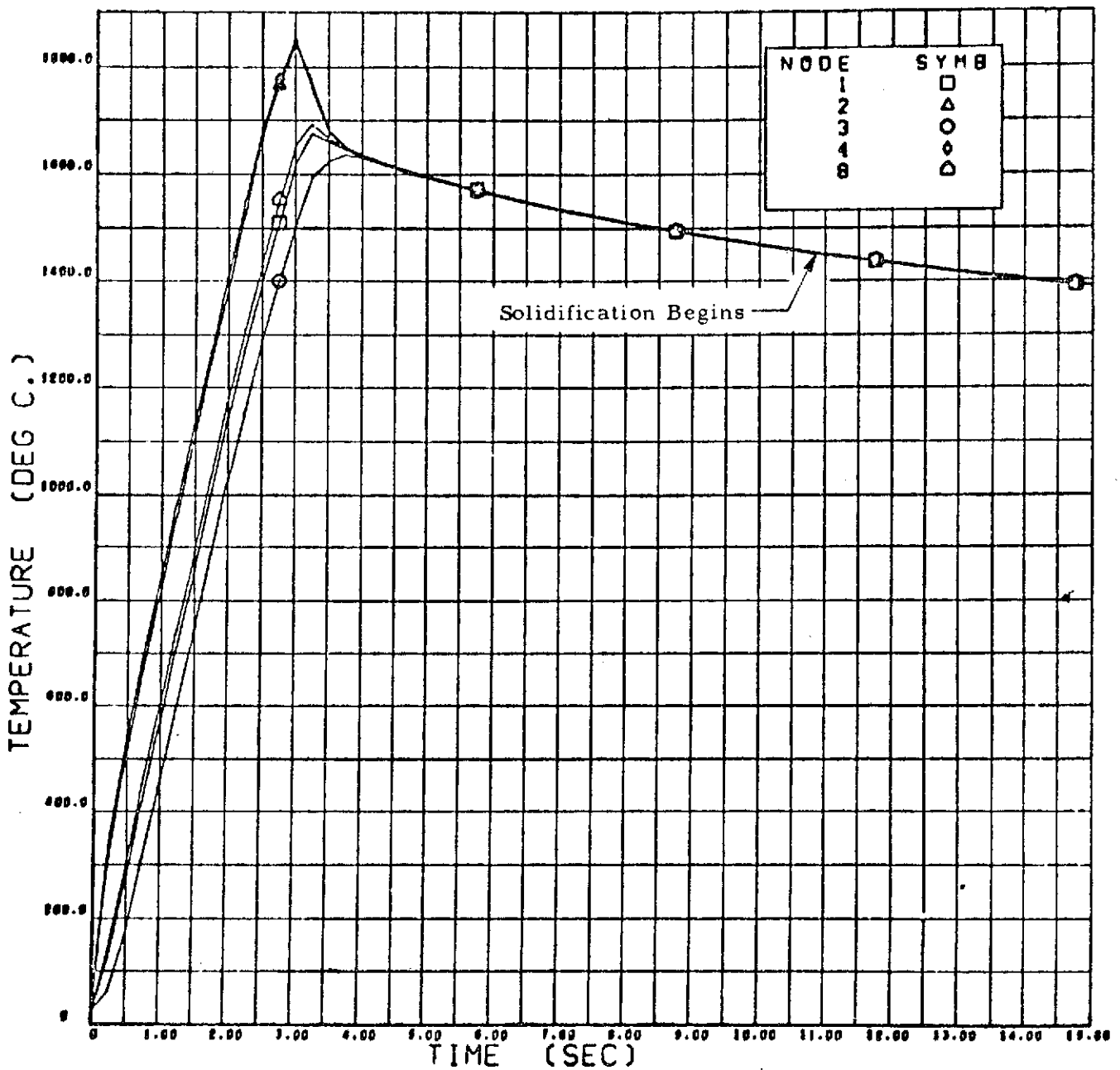

FIGURE 40 NICKEL TEMPERATURE HISTORY (NODES 1, 2, 3, 4 AND 8)

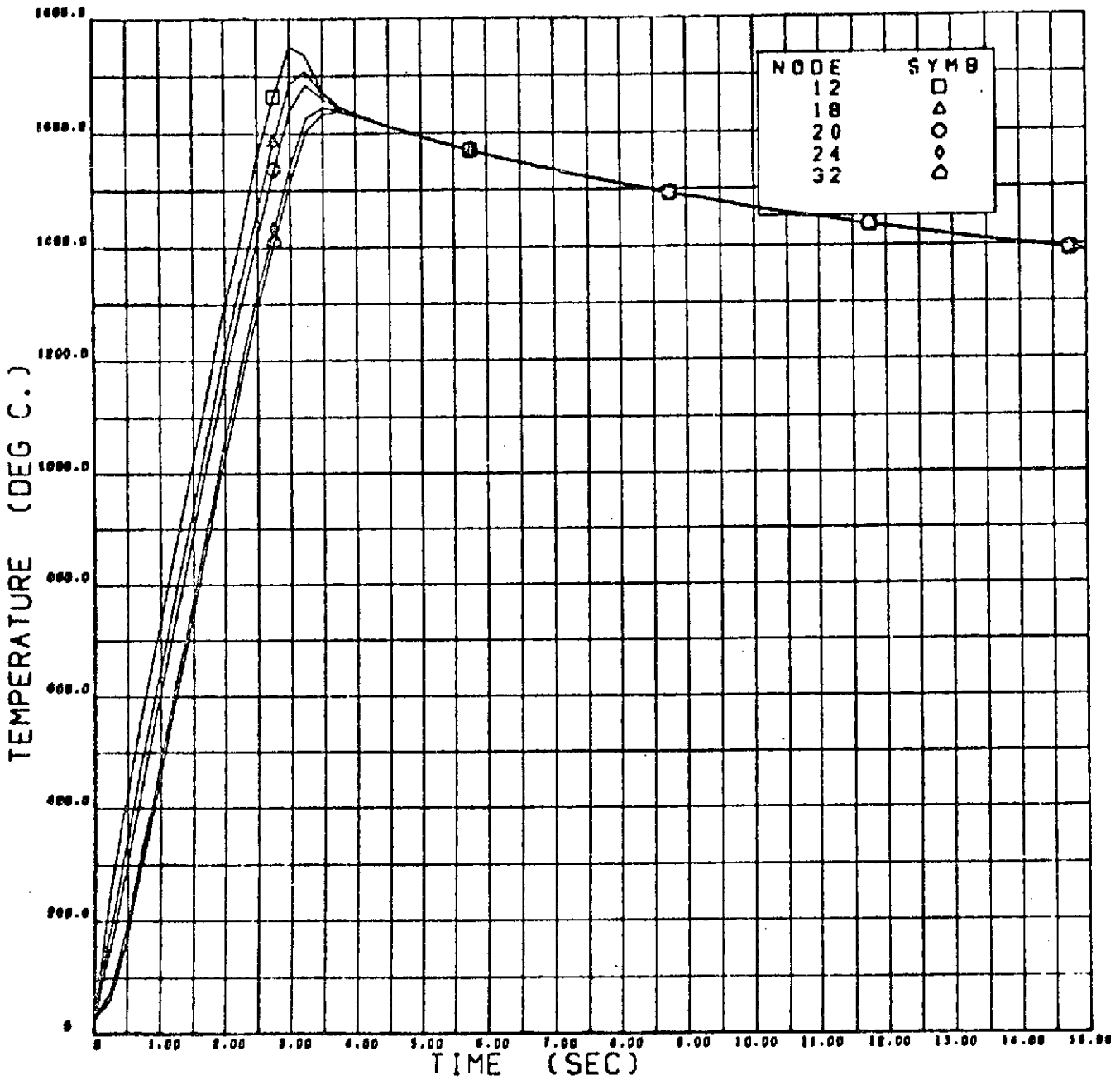

FIGURE 41 NICKEL TEMPERATURE HISTORY (NODES 12, 18, 20, 24 AND 32)

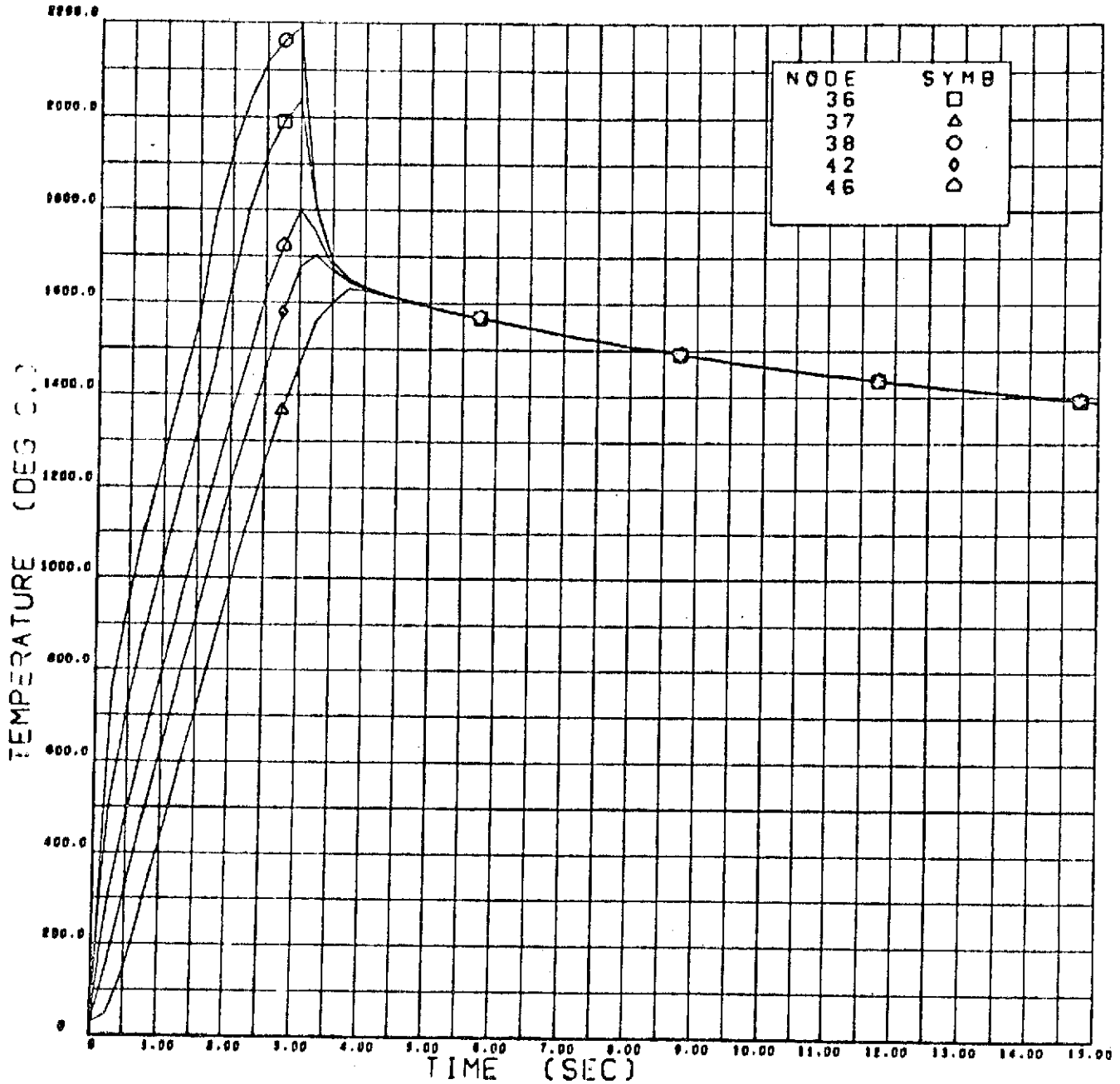

FIGURE 42 NICKEL TEMPERATURE HISTORY (NODES 36, 37, 38, 42 AND 46)

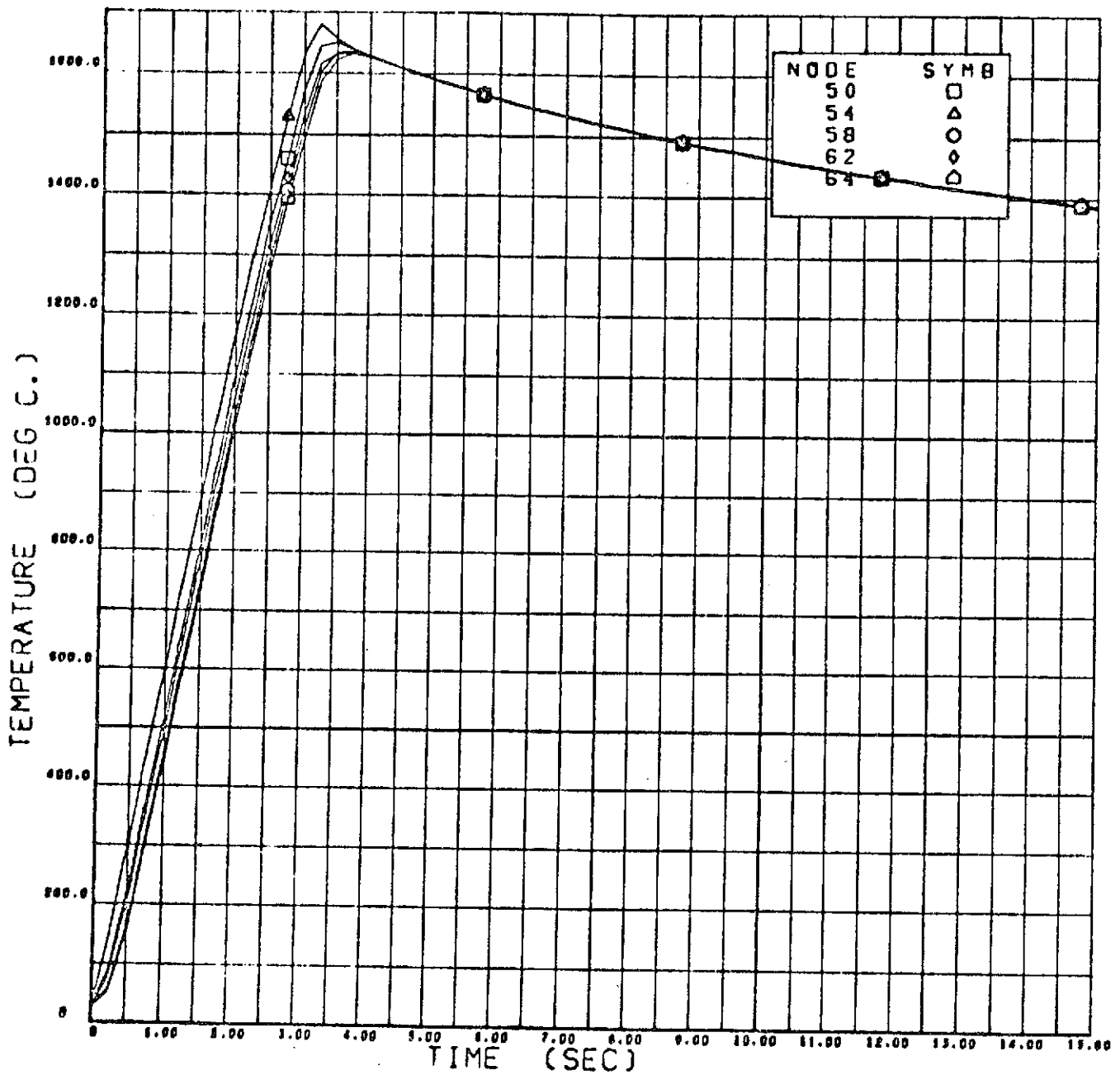

FIGURE 43 NICKEL TEMPERATURE HISTORY (NODES 50, 54, 58, 62 AND 64)

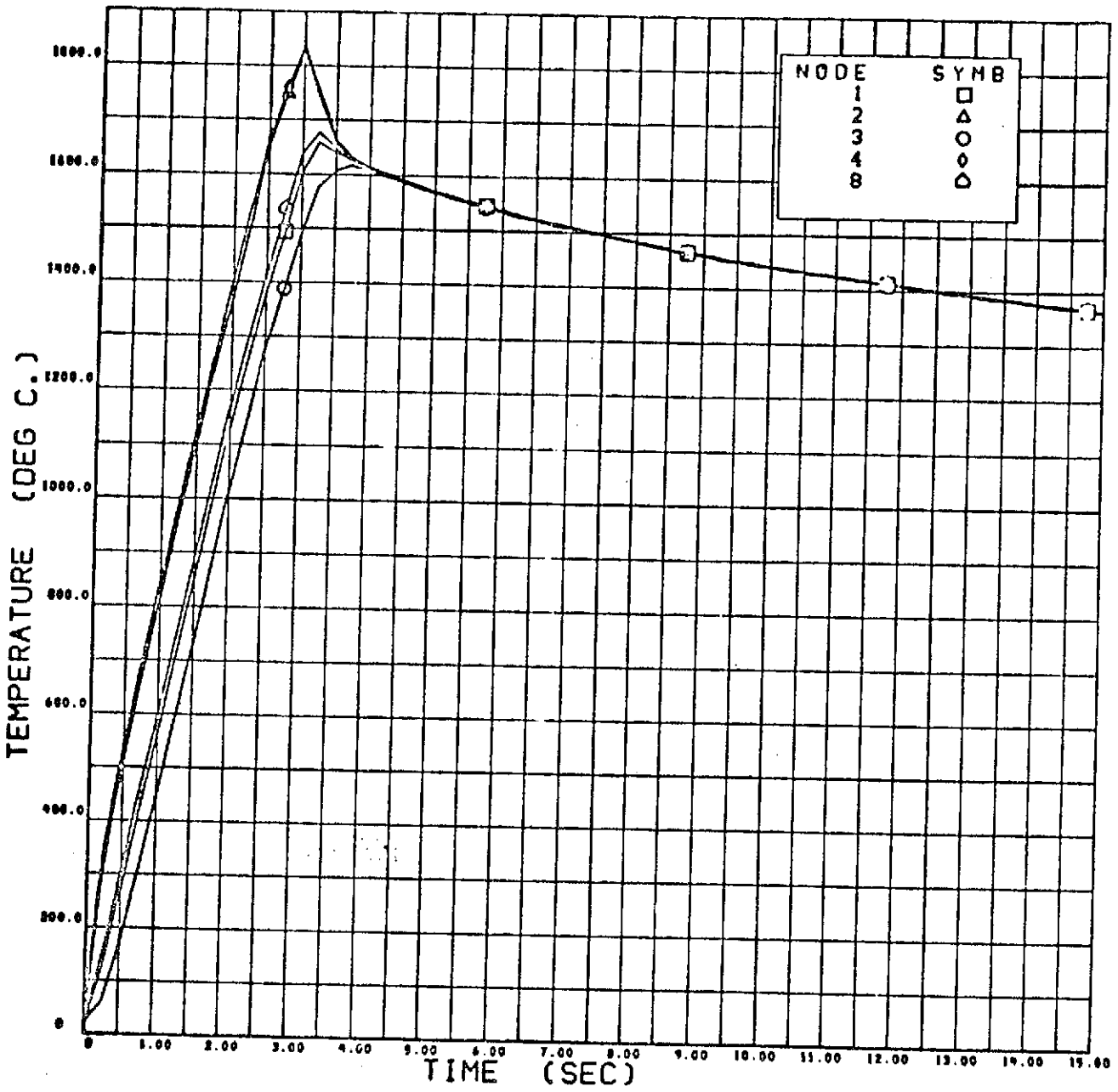

FIGURE 44 NICKEL-12% TIN TEMPERATURE HISTORY (NODES 1, 2, 3, 4 AND 8)

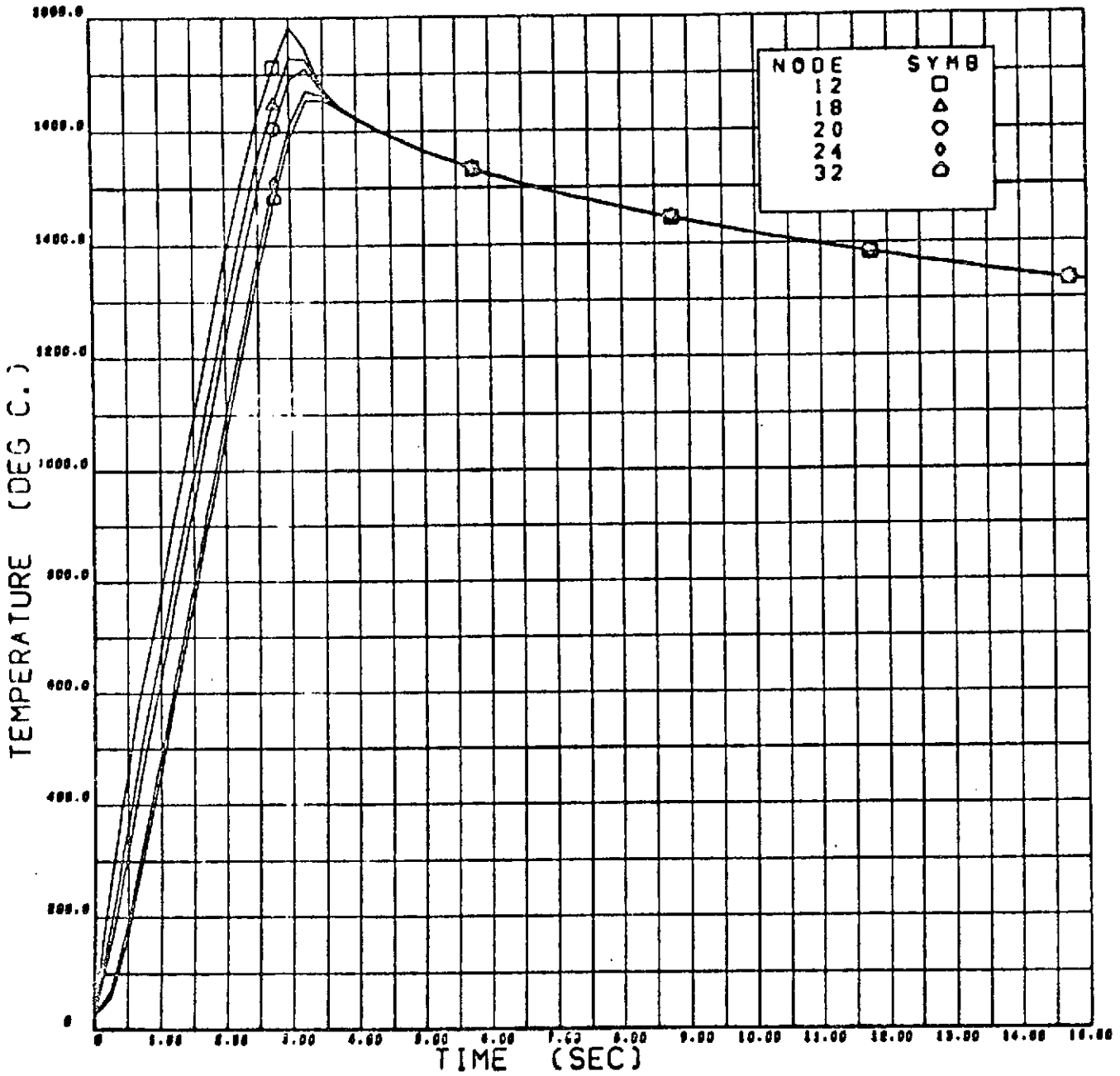

FIGURE 45 NICKEL-12% TIN TEMPERATURE HISTORY (NODES 12, 18, 20, 24 AND 32)

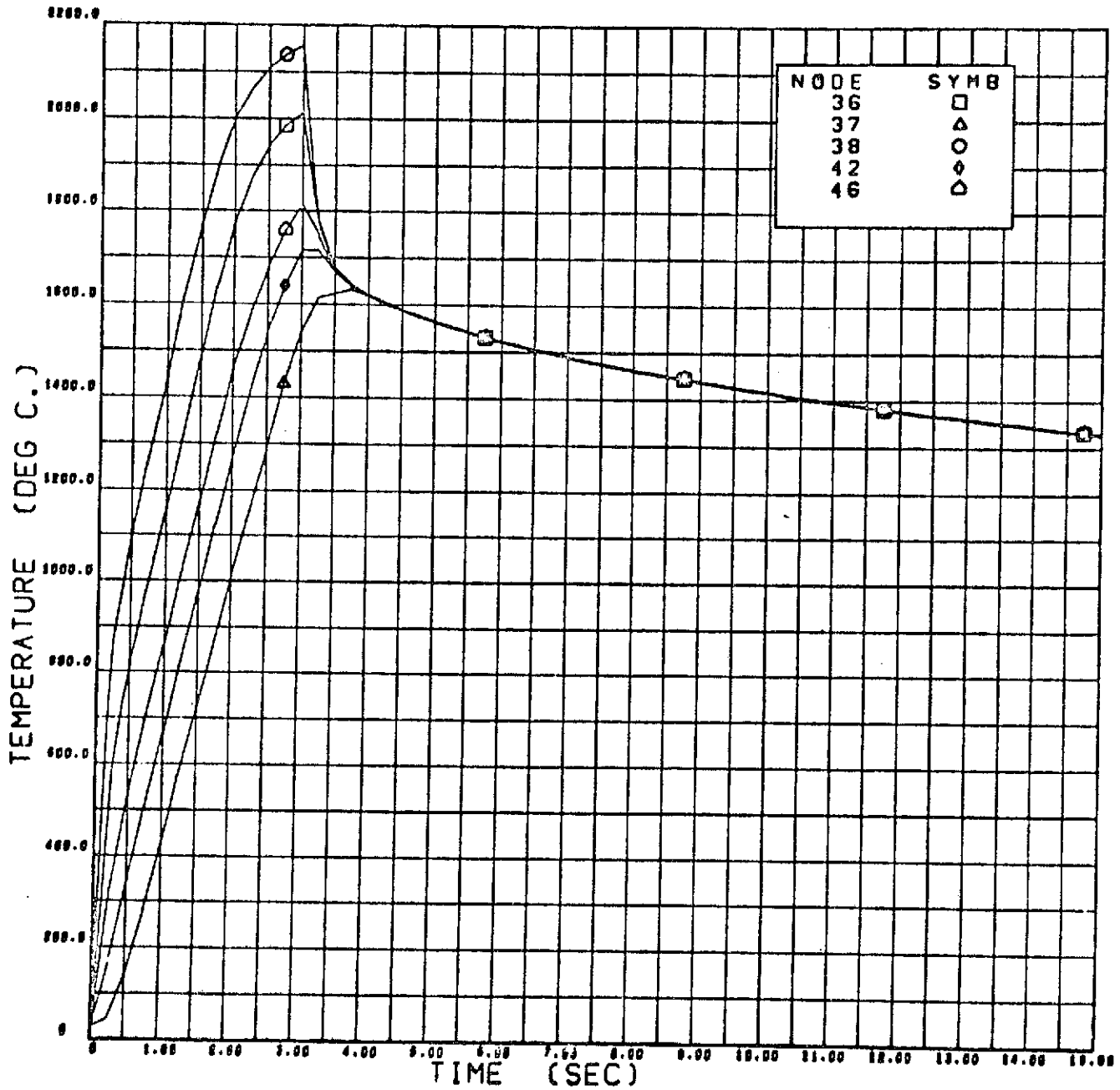

FIGURE 46 NICKEL-12% TIN TEMPERATURE HISTORY (NODES 36, 37, 38, 42 AND 46)

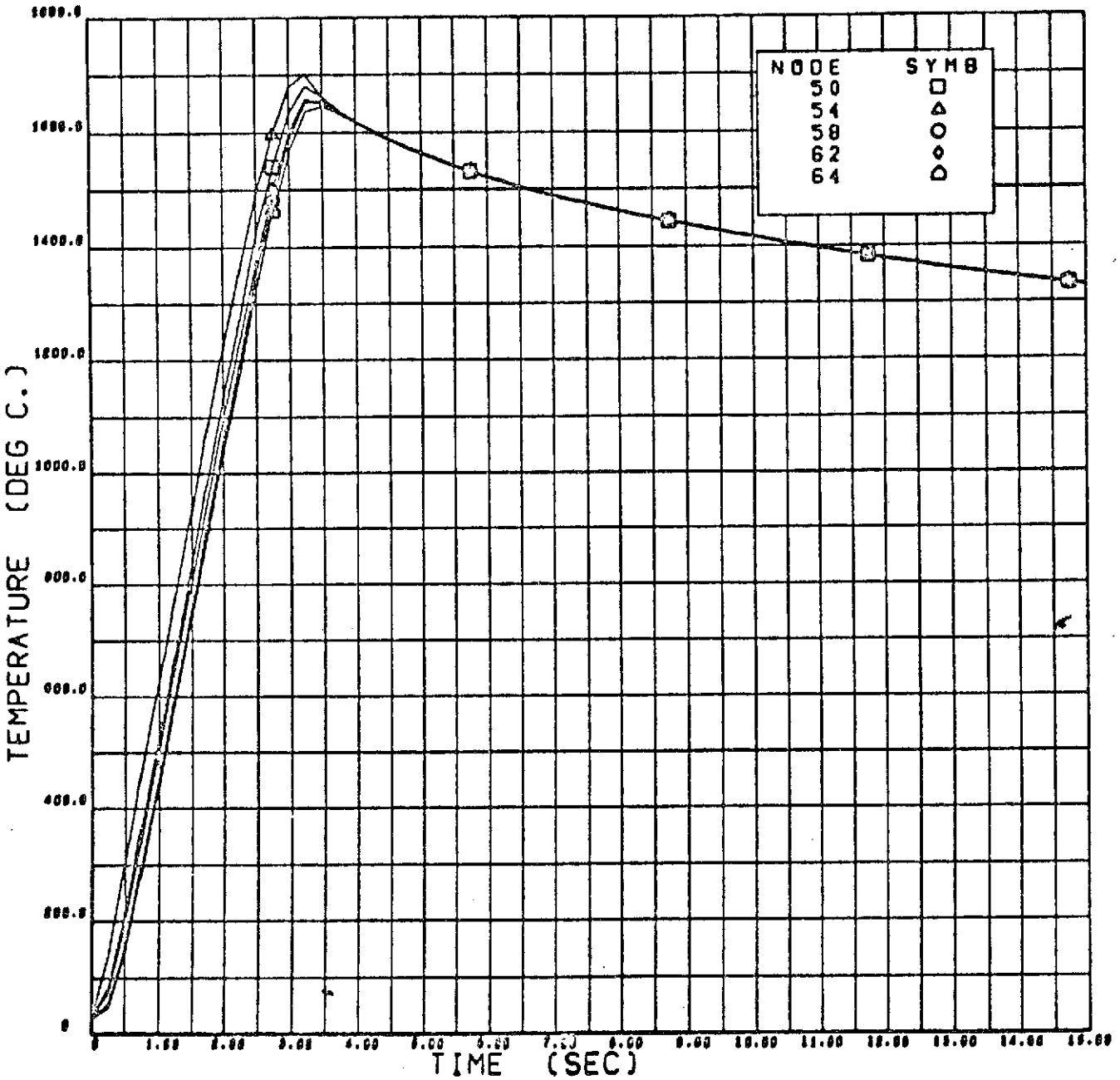

FIGURE 47 NICKEL-12% TIN TEMPERATURE HISTORY (NODES 50, 54, 58, 62 AND 64)

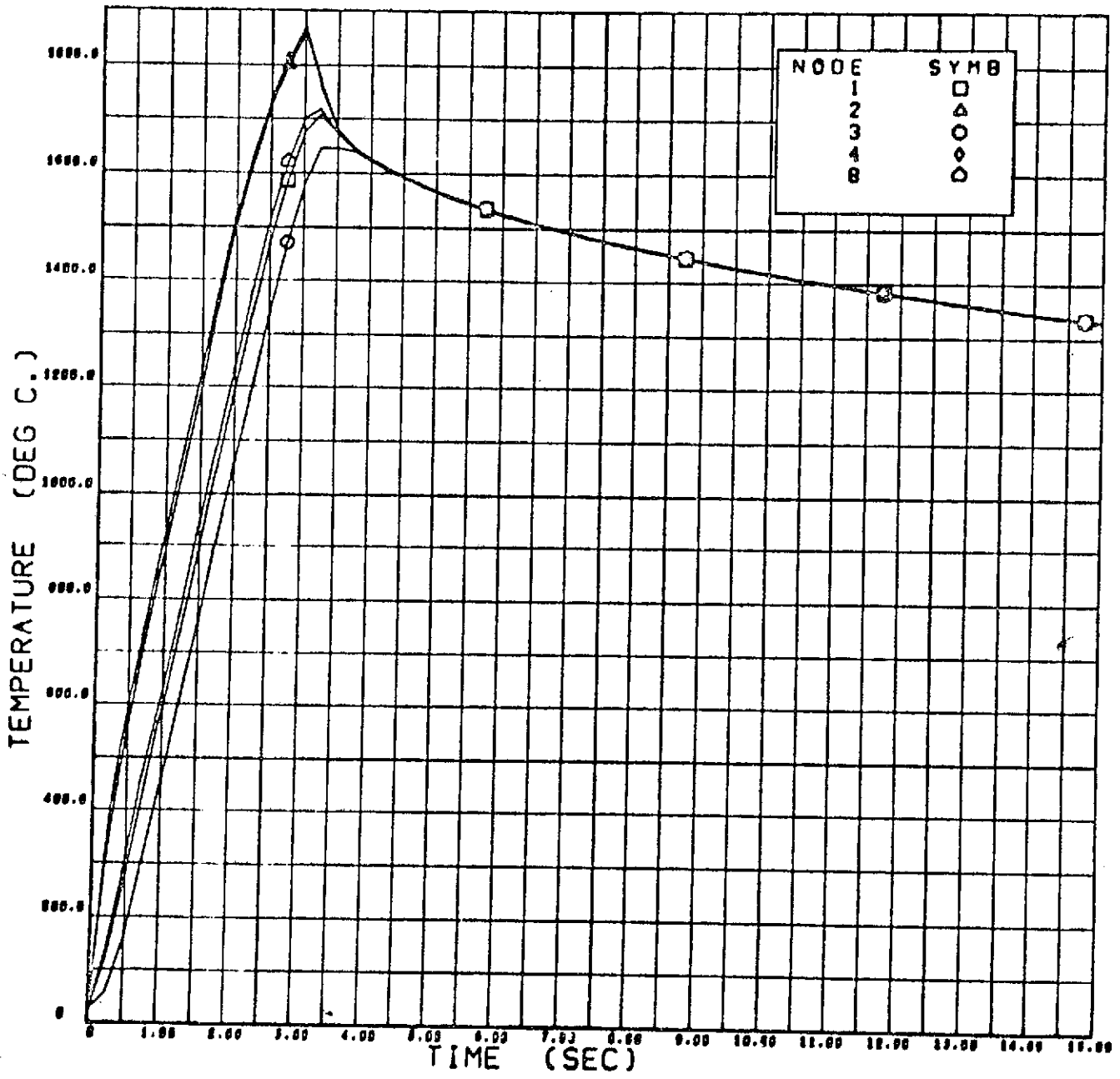

FIGURE 48 NICKEL-1% SILVER TEMPERATURE HISTORIES (NODES 1, 2, 3, 4 AND 8)

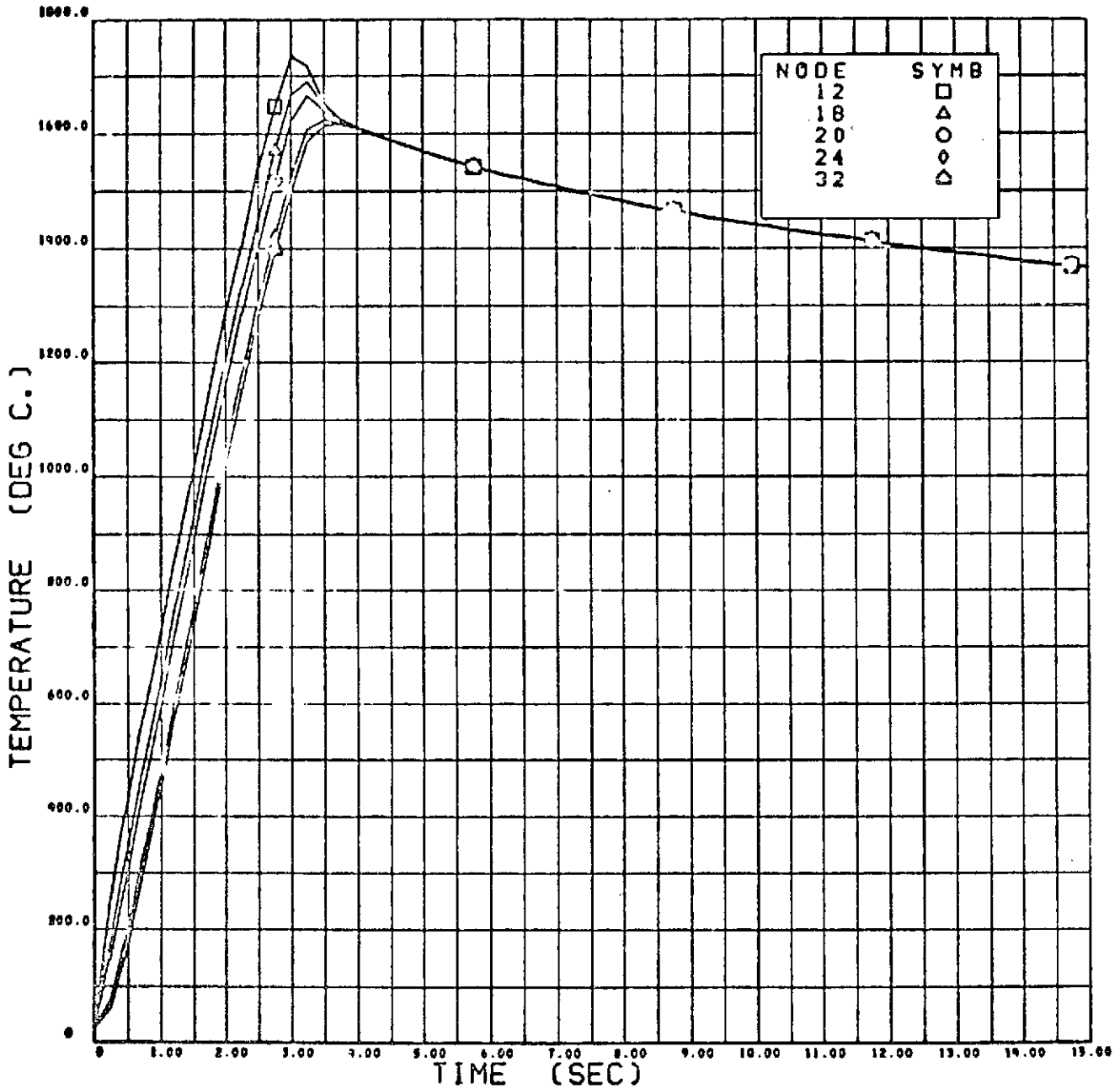

FIGURE 49 NICKEL-1% SILVER TEMPERATURE HISTORIES (NODES 36, 37, 38, 42 AND 46)

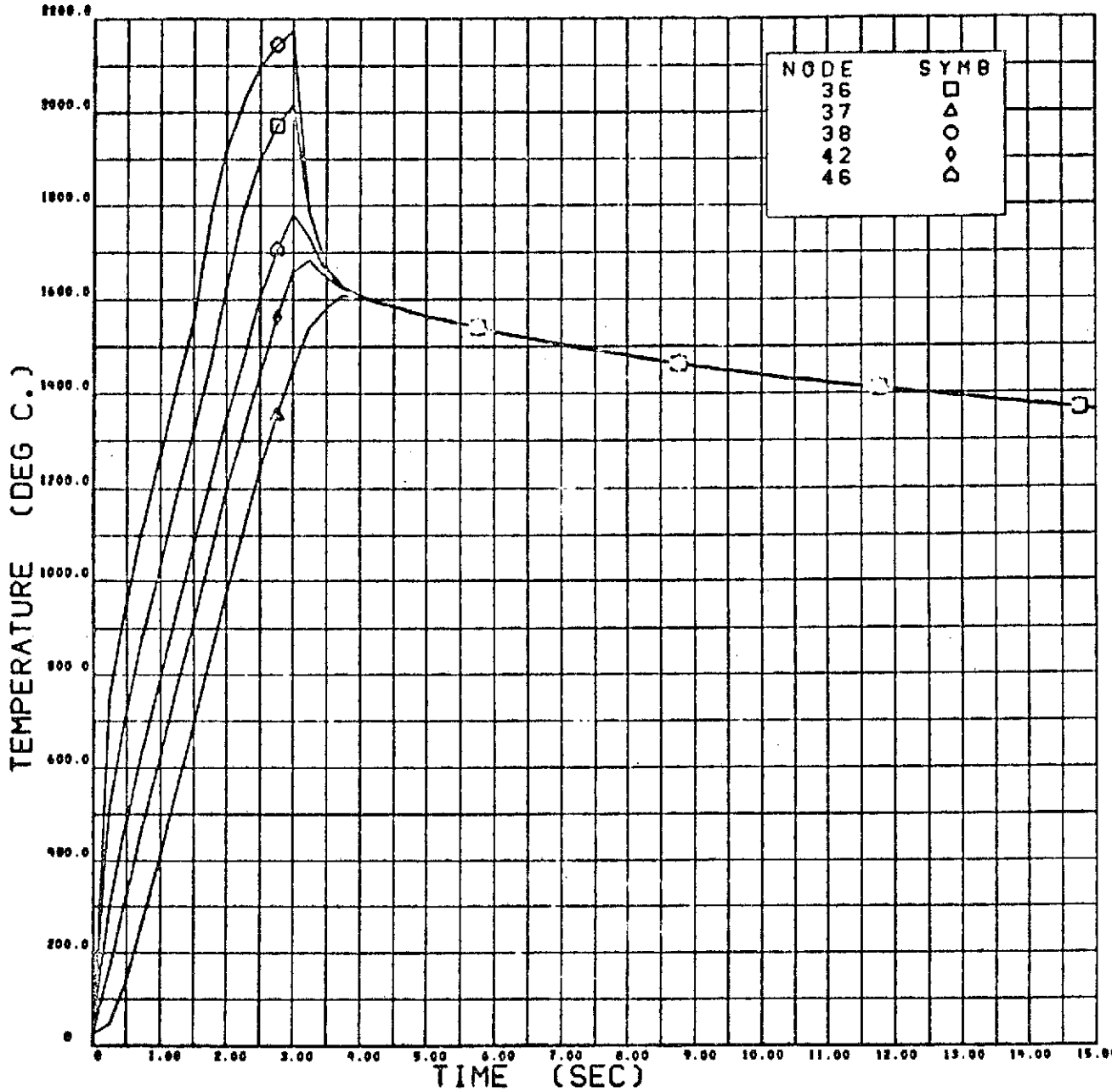

FIGURE 50 NICKEL-1% SILVER TEMPERATURE HISTORIES (NODES 36, 37, 38, 42 AND 46)

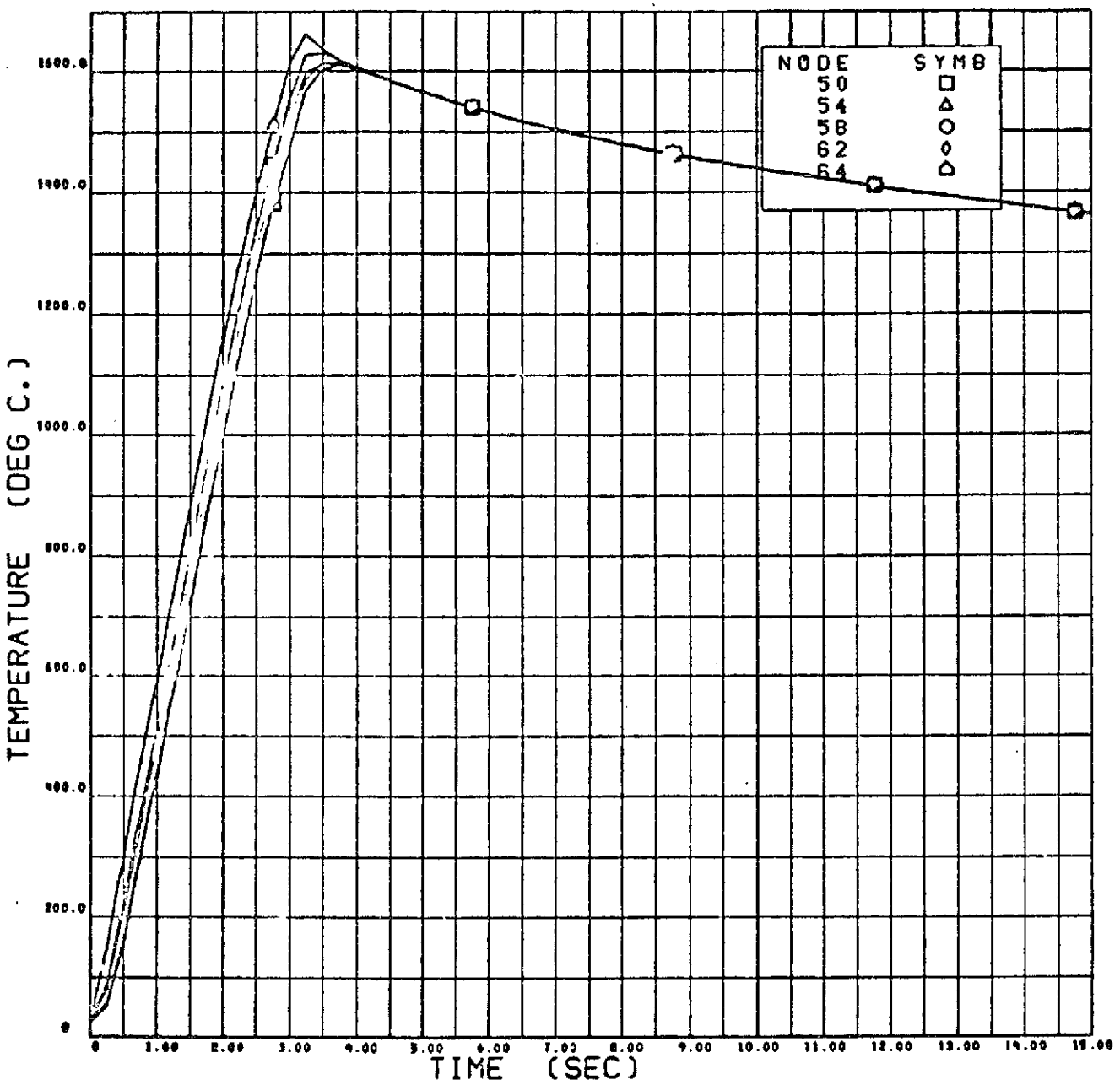

FIGURE 51 NICKEL-1% SILVER TEMPERATURE HISTORIES (NODES 50, 54, 58, 62 AND 64)

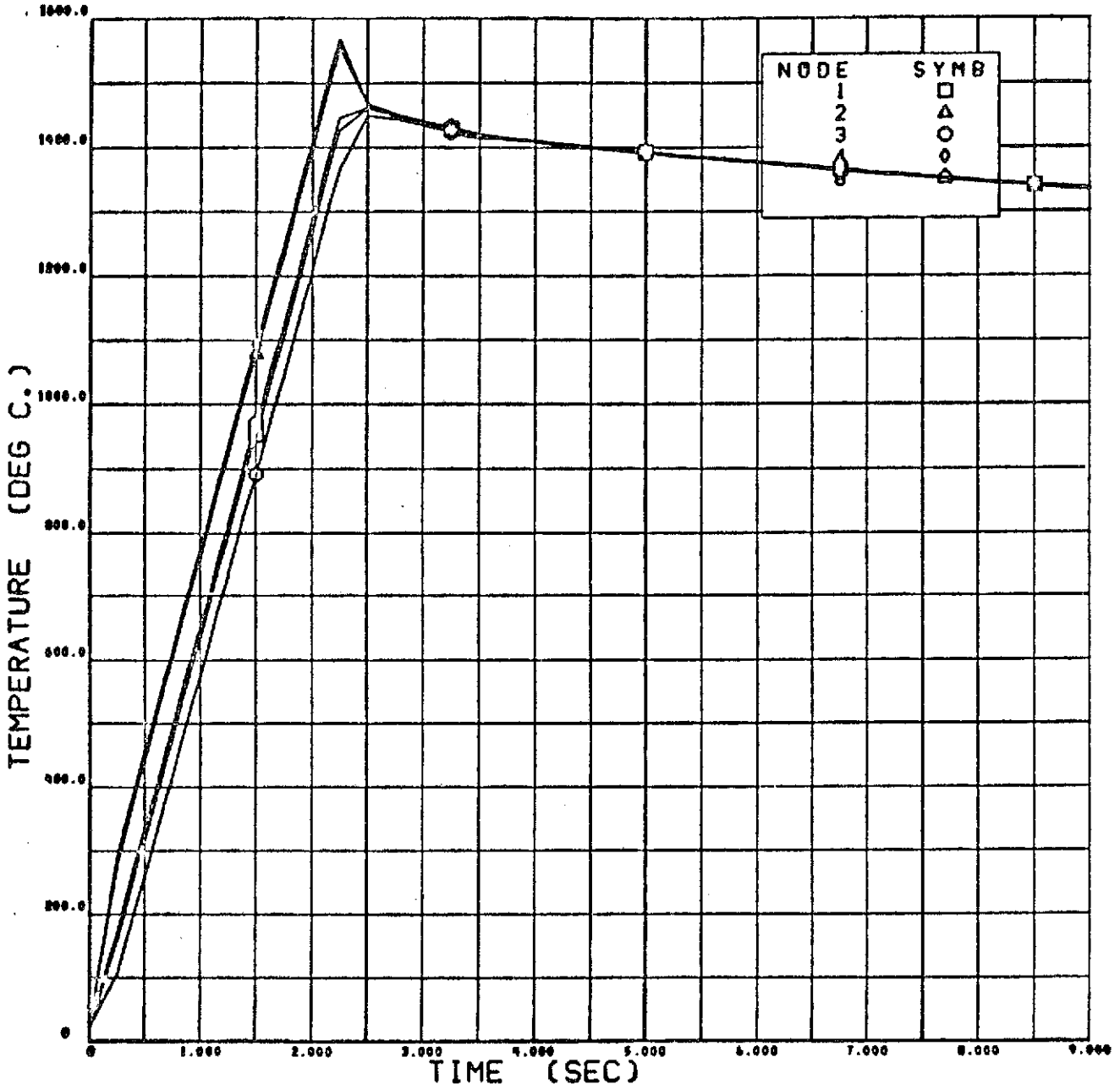

FIGURE 52 NICKEL-30% COPPER TEMPERATURE HISTORIES (NODES 1, 2, 3, 4 AND 8)

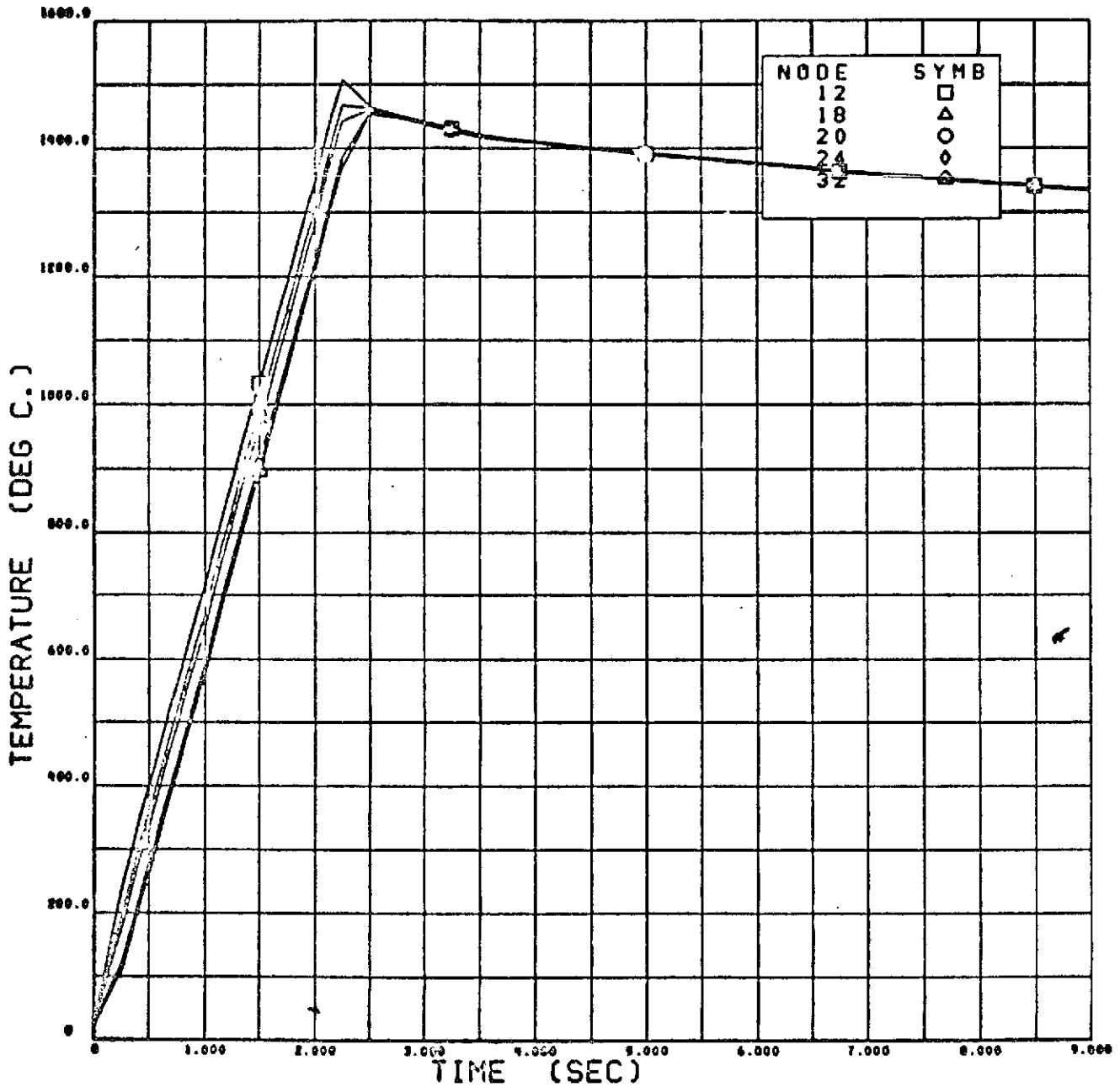

FIGURE 53 NICKEL-30% COPPER TEMPERATURE HISTORIES (NODES 12, 18, 20, 24 AND 32)

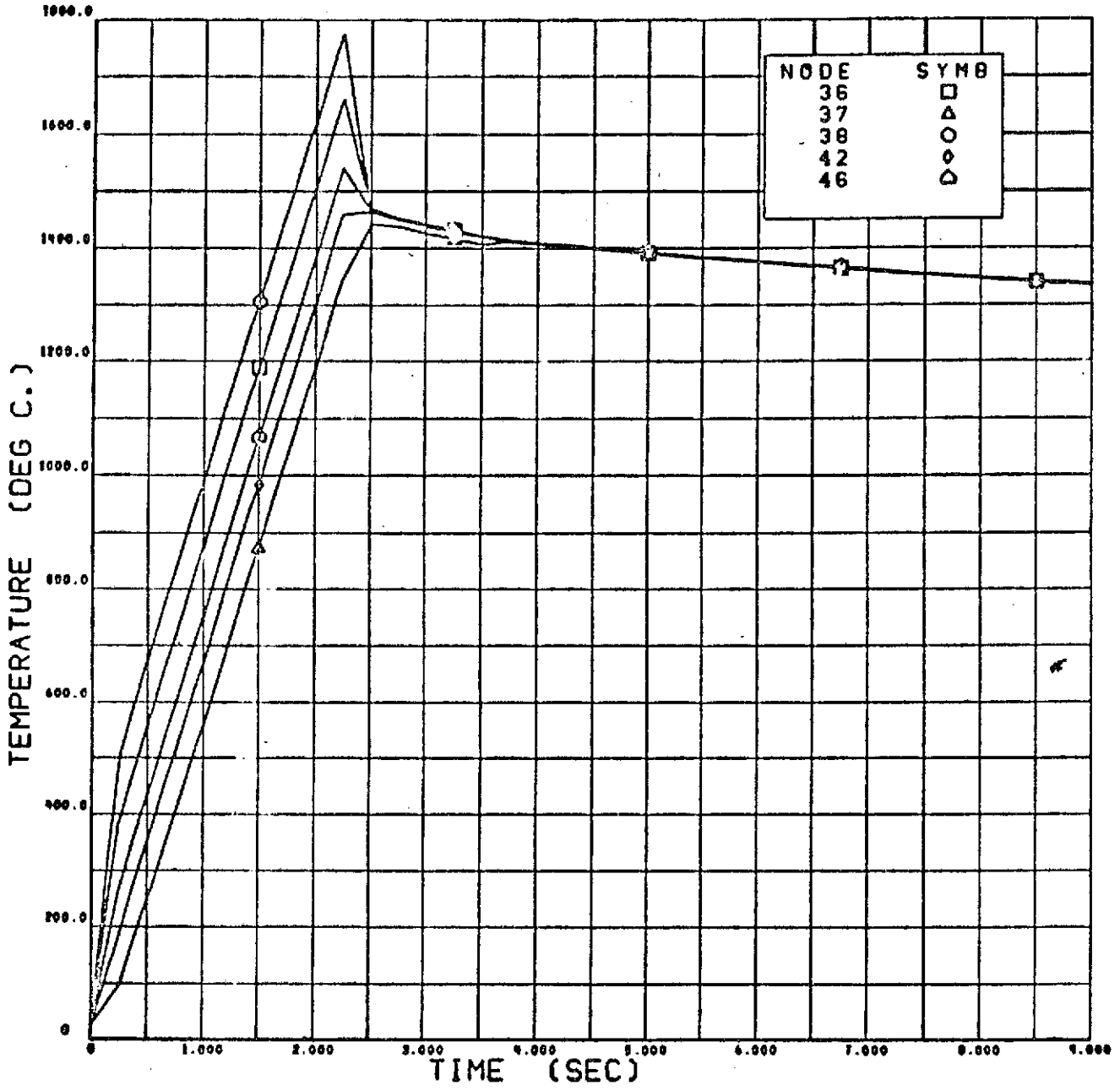

FIGURE 54 NICKEL-30% COPPER TEMPERATURE HISTORIES (NODES 36, 37, 38, 42 AND 46)

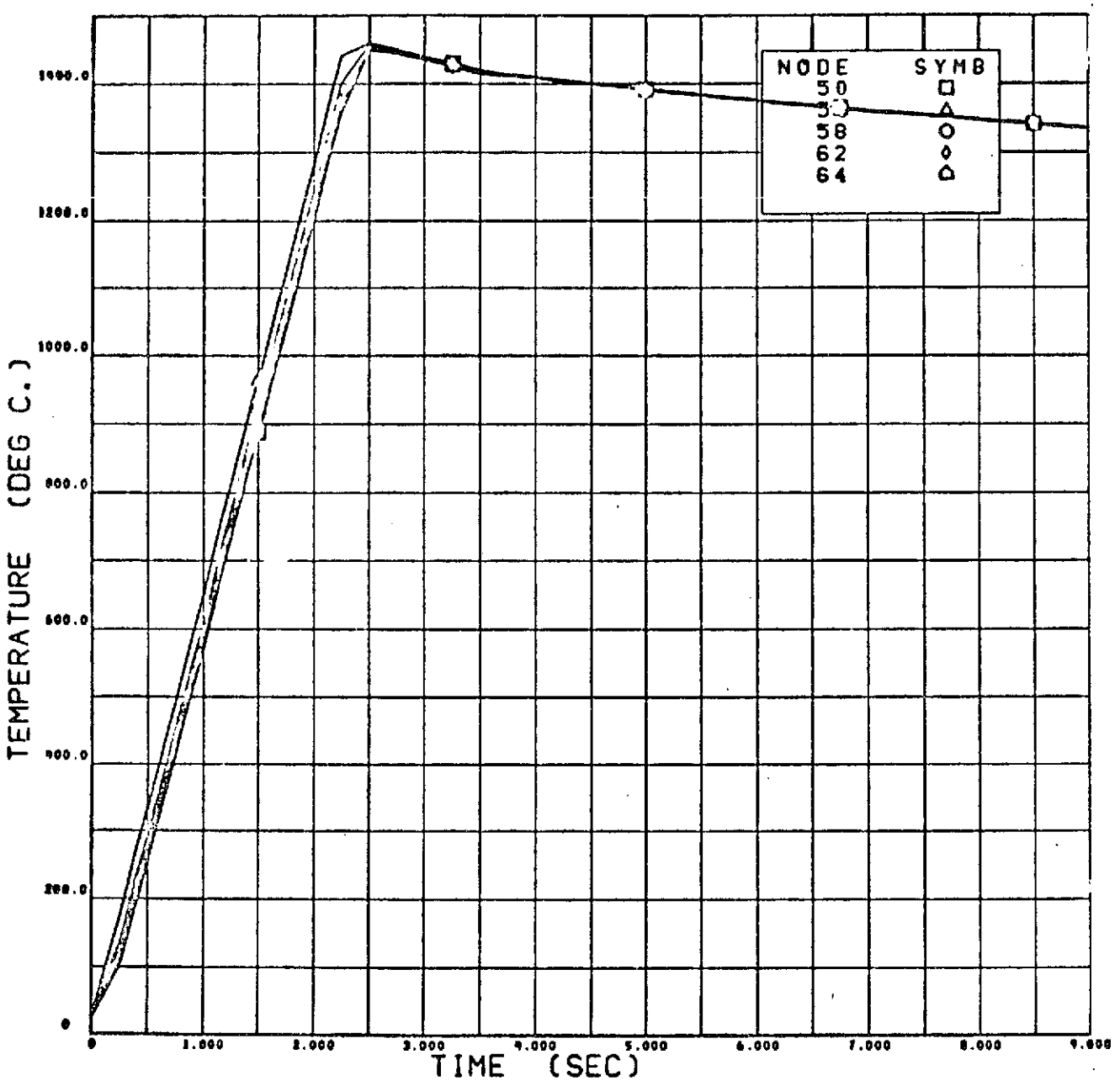

FIGURE 55 NICKEL-30% COPPER TEMPERATURE HISTORIES (NODES 50, 54, 58, 62 AND 64)

☆ U.S. GOVERNMENT PRINTING OFFICE 1974 – 640-448 / 154 REGION NO. 4